Physics of Fluids

Review of coating and curing processes: Evaluation in automotive industry

Cite as: Phys. Fluids **34**, 101301 (2022); https://doi.org/10.1063/5.0109376
Submitted: 12 July 2022 • Accepted: 14 September 2022 • Accepted Manuscript Online: 16 September 2022 • Published Online: 17 October 2022
Published open access through an agreement with Universidade da Beira Interior

Mohammad-Reza Pendar, Frederico Rodrigues, José Carlos Páscoa, et al.

Physics of Fluids REVIEW scitation.org/journal/phf

Review of coating and curing processes: Evaluation in automotive industry

Cite as: Phys. Fluids **34**, 101301 (2022); doi: 10.1063/5.0109376
Submitted: 12 July 2022 · Accepted: 14 September 2022 ·
Published Online: 17 October 2022

Mohammad-Reza Pendar,[1,a)] Frederico Rodrigues,[1] José Carlos Páscoa,[1] and Rui Lima[2]

AFFILIATIONS

[1]Department of Electromechanical Engineering, C-MAST (Center for Mechanical and Aerospace Sciences and Technologies), University of Beira Interior, and FCT (Portuguese Foundation for Science and Technology) Research Unit No. 151, Covilhã, Portugal
[2]CCEnergia Lda, Rio Maior, Portugal

[a)]**Author to whom correspondence should be addressed:** m.reza.pendar@ubi.pt. **Tel.:** +351925467631. **Fax:** +351275329972

ABSTRACT

The paint shop plant, as the largest energy consumer in the automotive manufacturing process, requires special attention to optimize energy efficiency and thermal management, reduce environmental impact and diminish the total costs to improve marketability. The current review covers the description of the automotive paint shop, recognition of the paint film layers, characterization of the paint spray applicators, evolution of their technology's advancement, explanation of the coating processes development, and investigation of the curing ovens thermal procedure in an automotive production stage. After systematically recalling pioneering studies dealing with the coating techniques and opening strategies, this paper focuses on reviewing recent findings conducted with improved modern methods in this subject area for higher sustainability and efficiency. Critical performance factors in developing surface durability, corrosion protectivity, paint material consumption, and environmental pollution are discussed. Focus is brought to the electrostatic spray-painting procedure flow physics understanding, particularly the complicated three-dimensional behaviors of paint droplets formation, distribution, control, and deposition on the body in constructed spray plums. Then, the baking and drying process of the produced film layer in the curing oven is precisely reviewed. The review additionally aids in the identification of knowledge gaps in the literature that should be addressed in future research.

NOMENCLATURE

BiW	Body in white
DMA	Dynamic mechanical-thermal analysis
DSC	Differential scanning calorimetry
dp	Paint droplet size
Di	Droplet diameter
D	Disk diameter
ED	Electro-deposition
EPA	Environmental protection agency
ERBS	Electrostatic rotary bell sprayer
FTIR	Fourier transform infrared
HVLP	High-volume low-pressure
HS	High solids
HVAC	Heating, ventilation, and air conditioning
IR	Infrared radiation
LES	Large eddy simulation
LIC	Line integral convolution
LPG	Liquefied petroleum gas
MW2DCS	Moving-window two-dimensional correlation spectroscopy
mi	Initial sample mass
mf	Mass after painting-drying
mout	Mass exits the nozzle
Ni	Droplet numbers
OEM	Original equipment manufacturer
PCA	Principal component analysis
PCW	Paint cure window
PDA	Phase Doppler anemometry
RTO	Regenerative thermal oxidizer
SMD	Sauter mean diameter
SDV	Shadow Doppler velocimetry
TAB	Taylor analogy breakup
TE	Transfer efficiency
TGA	Thermo-gravimetric analysis
TT	Transformed temperature
UBC	Underbody coating
UV	Ultraviolet

VOC	Volatile organic compound
VPS	Virtual paint simulation
VCup	Operating voltage of bell cup
VRing	Operating voltage of control ring conductor
$\dot{V}_L$	Fluid flow rate
V1	Inner recirculation zone
V2	Outer recirculation zone
μ_L	Viscosity of spray material
ρ	Liquid density
ρ_m^q	Charge-to-mass ratio
σ	Surface tension
ω	Bell cup rotary speed

I. INTRODUCTION

Automotive production is an energy-intensive and complicated process that consumes lots of energy, raw materials, and water. Paint film formation on the body in white (BiW) supplies vehicles with optical quality, aesthetic appeal, and physical features such as corrosion resistance, mechanical protection, and weather protection. In automotive manufacturing plants, the coating and curing processes are the most energy-intense stages, which use the most shares of energy to heat the booths and ovens. For that reason, deep consideration of the painting and curing line processes and features lead to a remarkable reduction in costs and energy (Roelant *et al.*, 2008; Galitsky and Worrell, 2008; Guerrero *et al.*, 2011; and Rivera and Reyes-Carrillo, 2014).

The summarized timeline taken up by the automotive industry toward progress and sustainability is depicted in Fig. 1. The revolution in automotive industries was sparked in the 1940s with vehicle mass manufacturing. A particular requirement to accelerate the painting and curing process and improve paint film performance to achieve higher durability and prevent corrosion was necessity by deployment of electro-coating in the 1960s resulted in lower volatile organic compounds (VOCs) values and dangerous air pollutants (Streitberger and Dossel, 2008). Followed by reducing vehicle emissions in the 1970s (Orsato and Wells, 2007) and the development of energy efficiency in the 1980s (Galitsky and Worrell, 2008), better resource management for recycling and remanufacturing in the 1990s and environmental legislation in the 2000s had occurred (Mayyas *et al.*, 2012), then manufacturing moved toward sustainability as the main topic in automotive original equipment manufacturers (OEMs). Finding new technologies, e.g., Nitrotherm electrostatic painting in the paint shop, improves the green footprint and the transfer efficiency (TE) of the process (Spang, 2014).

The following discussions provide a historical evolution of automotive painting and curing processes. Around a century ago, when the automotive industry first emerged, vehicles were painted with a varnish-like compound, then dried, sanded, and smoothed during the coating processes. For each vehicle, reapplying these operations to create several layers with shining surfaces required more than 40 days (Akafuah *et al.*, 2016). During the 1920s–1940s, using spray equipment and stoving enamels based on alkyd resins, as a transition in automotive painting technologies, significantly shortened coating and drying time to less than one week. In the 1920s, Ford Motor Company began employing nitrocellulose lacquer-based paints on automotive production lines, which had a considerably shorter drying time and better application for spray paint guns (Khanna, 2008). In the early 1930s, the development of "alkyd" enamel paints formed durable and resistant film due to their molecular bonding reactions after spraying and curing, which required less time to apply than lacquer systems (Standeven, 2006). In the 1960s, General Motors introduced new acrylic stoving enamels that were applied manually by spray gun and baked in an oven with high durability, glossy finishes, and corrosion-protective features, but uneven film thicknesses (Learner, 2000). In the mid-1970s, applying cathodic electrodeposition (ED) paints by dip coating operations (raised in the 1950s) resulted in greater corrosion protection, more coating deposition at lower current, and superior process reliability (Streitberger and Dossel, 2008; Besra and Liu, 2007). In a relatively short period, around 25 years ago, automotive painting processes and the paint liquid properties had evolved to reduce the average amount of paint consumption (the amount of 9–16 kg for reaching the thicknesses of ≈100–140 μm), increase durability, and improve quality (Prieto, 2010). Then, with the invention of the computer-controlled spray guns, the deposited paint-to-paint atomized ratio and the worker's safety were improved (Liu *et al.*, 2000). In recent years, the electrostatic painting method has been commonly implemented by using a high-speed rotary bell cup in automotive and other similar industries for painting, which will be considered in the present review comprehensively. The Nitrotherm electrostatic coating method is also started to be employed for its higher coating transfer

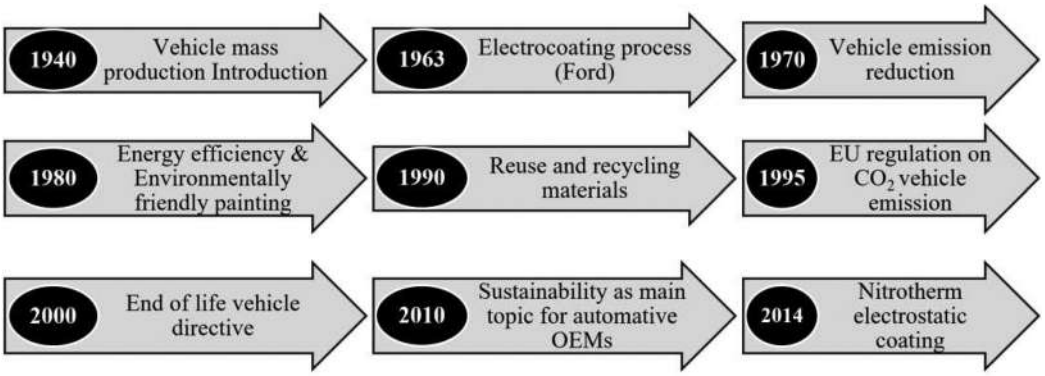

FIG. 1. The revolution in the automotive manufacturing industry since 1940.

efficiency (TE). Despite the improvements noted, the automotive paint shop plant still consumes 30%–50% of the product's total costs and is the most expensive section (Bensalah *et al.*, 2014). The majority of these costs go toward painting booths, paint drying ovens, working booths, pretreatment, heating, ventilation, and air conditioning (HVAC) controller, and volatile organic compounds (VOCs) removal systems. The removal of the over-sprayed paint particles and evaporated solvents from painting booths and the treatment of emissions caused by paint droplets, which are not deposited on target surfaces, are equally expensive (Galitsky and Worrell, 2008).

In the following two paragraphs, the availability of the review articles on automotive manufacturing with a particular focus on industrial coating and curing processes is considered to prove the necessity of conducting the present work. To date, a few reviews have been published that primarily focus on automotive manufacturing and coating procedures. Rivera and Reyes-Carrillo (2016) reviewed the environmental effect of various available painting technologies. Doerre *et al.* (2018) reviewed the automotive conversion coating in the aspect of the chemical interactions of material layers. Patel (2016) and Appah *et al.* (2019) presented a short review of using electrostatic spraying just in agriculture pesticides, emphasizing the optimum electrostatic parameters combination and the economic efficiency of the process, respectively. Mayyas *et al.* (2012) described the main topics related to the sustainability of the automotive industry, such as materials usage, manufacturing technologies, and recycling strategy.

Other reviews that have been published earlier are more concentrate on the automotive industry in specific aspects of analyzing technologies of thermal spray, use of sustainable materials and green composites (Koronis *et al.*, 2013), recycling infrastructure sustainability during the production process (Kumar and Sutherland, 2008), applying multifunctional materials (Salonitis *et al.*, 2009), technologies applied in automotive assembly (Michalos *et al.*, 2010) and energy consumption, management, and recovery during the automotive production (Chiara and Canova, 2013). According to the above evolution, there are almost no articles devoted to the electrostatic coating and the paint curing processes in the automotive paint shop plant.

The lack of the review paper's existence on the industrial coating and curing issue, with a particular look at the development of the electrostatic spray-painting method for researchers, is obvious. It is essential to recognize the optimum range for various factors in numerical studies of the electrostatic spray-painting process, such as the air–liquid flow rate, particle charge, droplets size distribution, and the breakup process, which will be covered by this work. Also, reviews in the experimental works yield an in-depth understanding of the techniques employed to capture the paint spray plum and surrounding air pattern. Addressing these issues that their absence is deeply felt is covered here as a database for satisfying the demands of researchers. As an introductory, the paint shop plant in automotive factories; the film paint layers' structure that is covering the vehicles; painting apparatus evolution were reviewed.

The structure of this paper is as follows: Sec. II presents the general description of the paint shop plant. Section III provides a detailed explanation for automotive paint film layers recognition. Section IV describes all available conventional spray-painting methods in detail. Section V supplements the review of the electrostatic spray-painting technique and strategies to reach energy efficiency sustainability in this method. Finally, Sec. VI explains the automotive oven thermal curing procedure.

II. AUTOMOTIVE PAINT SHOP PLANT DESCRIPTION

The automotive manufacturing plants are typically divided into four major areas: the press shop, body shop, paint shop, and final assembly. In the paint shop, the car body is cleaned, coated, and finally cured. Pretreatment, conversion coating, electro coat, oven, base coat 1 and 2, flash off zone, clear coat, and final oven are the stages in which the BiW traverses through a typical painting and curing line at the paint shop, as shown in Fig. 2. Finally, five coating layers with various functions and thicknesses cover the surface of the final products.

In the paint ovens, the wet paint-coated surfaces are converted to a dry film, which consumes significant energy for air heating and circulation. Each of the five coating stages aforementioned involves the curing or drying process (Gerini Romagnoli, 2016). The vital convection ovens components are insulated walls and roof, heater boxes and supply ducts that are nourished through the fans.

A. Automotive paint shop plant thermal energy consumption

Figure 3(a) compares the share of energy consumption for each area of a conventional automotive manufacturing plant (Oh and Hildreth, 2016). However, these values are influenced by outdoor environmental conditions and various production process typologies adopted for manufacturing (Kiliç *et al.*, 2018). The paint shop that provides corrosion protection and a pleasant appearance to the BiW consumes the largest portion of energy, ≈36%, during vehicle manufacturing operations. In the paint shop, during the paint film deposition and curing processes, the components of painting booths, ovens, working booths, pretreatment, and VOCs removal system, in order to consume the most portion of energy based on the Dürr's analysis (Gerini Romagnoli, 2016), as shown in Fig. 3(b). The paint shop in terms of energy management is handled by dedicated companies due to its complexities, e.g., Taikisha, Eisenmann, Dürr, etc. (Streitberger and Dossel, 2008). Figure 4 exhibits an evaluation of a conventional automotive manufacturer's electricity and natural gas usage. The most natural gas is utilized to generate the necessary hot air and hot water for the spray booth, oven, and pretreatment [Fig. 4(a)]. A small amount is also used to eliminate VOCs that were created during the painting process. Electricity energy power is mainly used to operate the fan motors, compressing air for atomizer, paint booths, ovens, and secondary energy sources production. Additional electricity usage, with a share lower than 5%, includes lighting, conveyors, pumps, chiller, etc. [Fig. 4(b)] (U.S. Department of Energy, 2008; Gerini Romagnoli, 2016).

B. Energy efficiency improvement strategies

Innovative strategies that were implemented to reduce the painting process complexity have been discussed here. As one of the best approaches, the primer coating booth and curing oven are eliminated by reformulating paint to reduce the paint shop energy consumption, as shown in Fig. 5. An actuator is added to the base coat layer that adopts for ultraviolet (UV) barrier and chip resistance for the E-coat layer. Around 30% of the capital cost is saved when this strategy is implemented (Streitberger and Dossel, 2008). Changes to the oven's

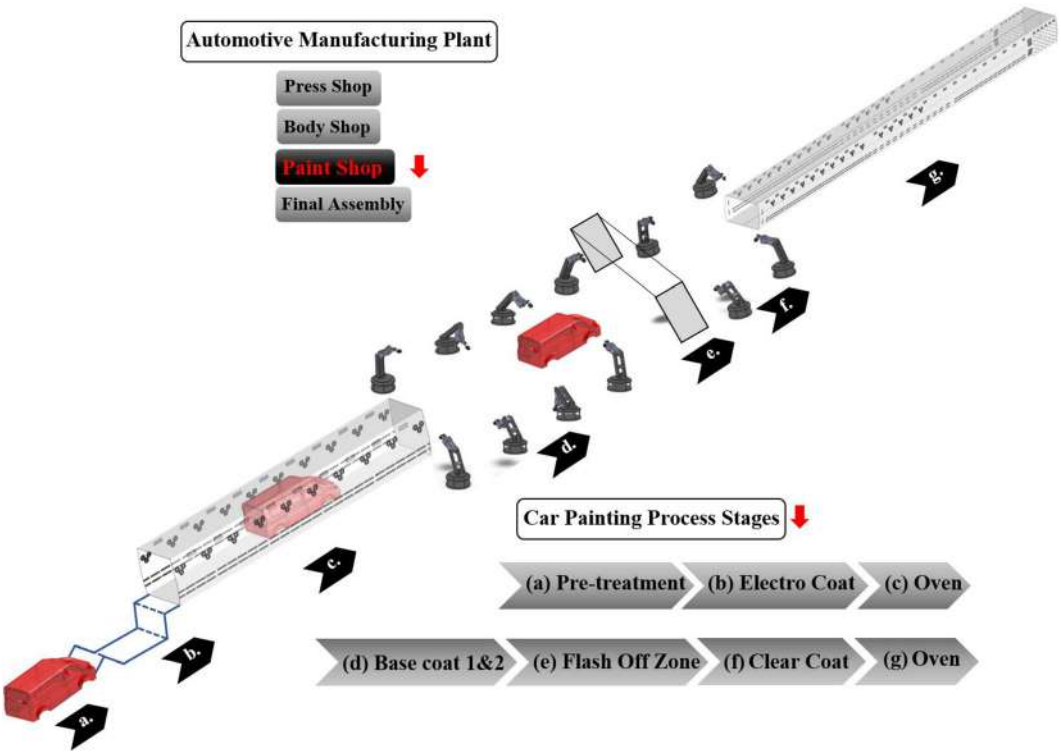

FIG. 2. Schematic illustration of the conventional automotive manufacturing paint shop plant.

characteristics or design have also been suggested as viable energy-saving measures.

Also, coating on a wet paint surface, the wet-on-wet (2-wet) method, as an effective strategy, can eliminate the curing process among paint film layers coating (BMW, Volkswagen, Seat), significantly reduce the energy consumption and CO_2 and VOC and emissions. In recent years, an innovative approach based on wet-on-wet-on-wet (3-wet) painting, using only one curing process after

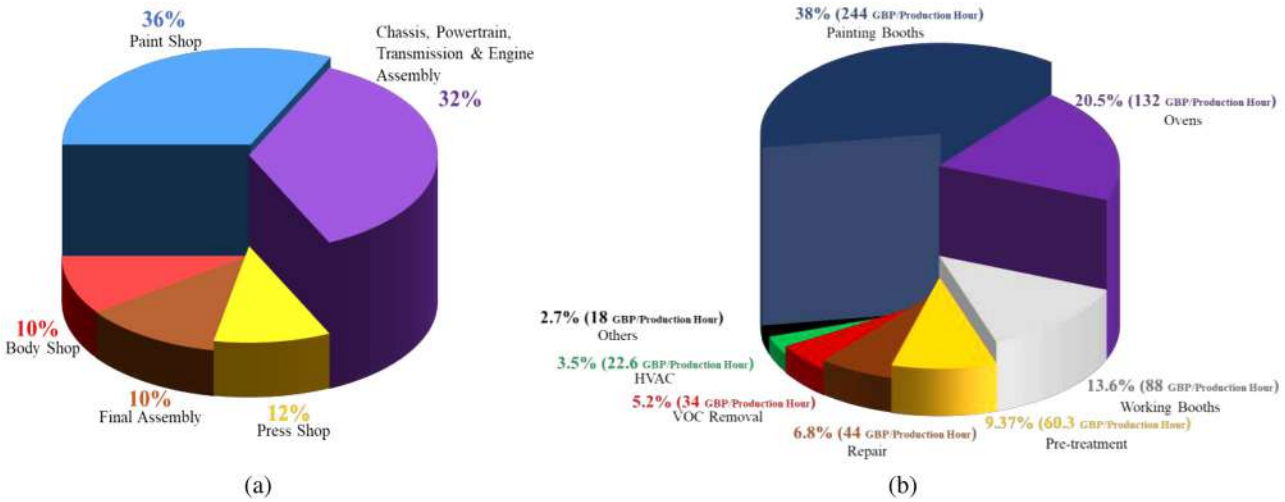

FIG. 3. Energy consumption for (a) an overall conventional automotive manufacturing plant components and (b) paint shop facilities. Adapted from Giampieri *et al.*, "A review of the current automotive manufacturing practice from an energy perspective," Appl. Energy **261**, 114074 (2020). Copyright 2020 Author(s), licensed under a Creative Commons Attribution (CC BY) License.

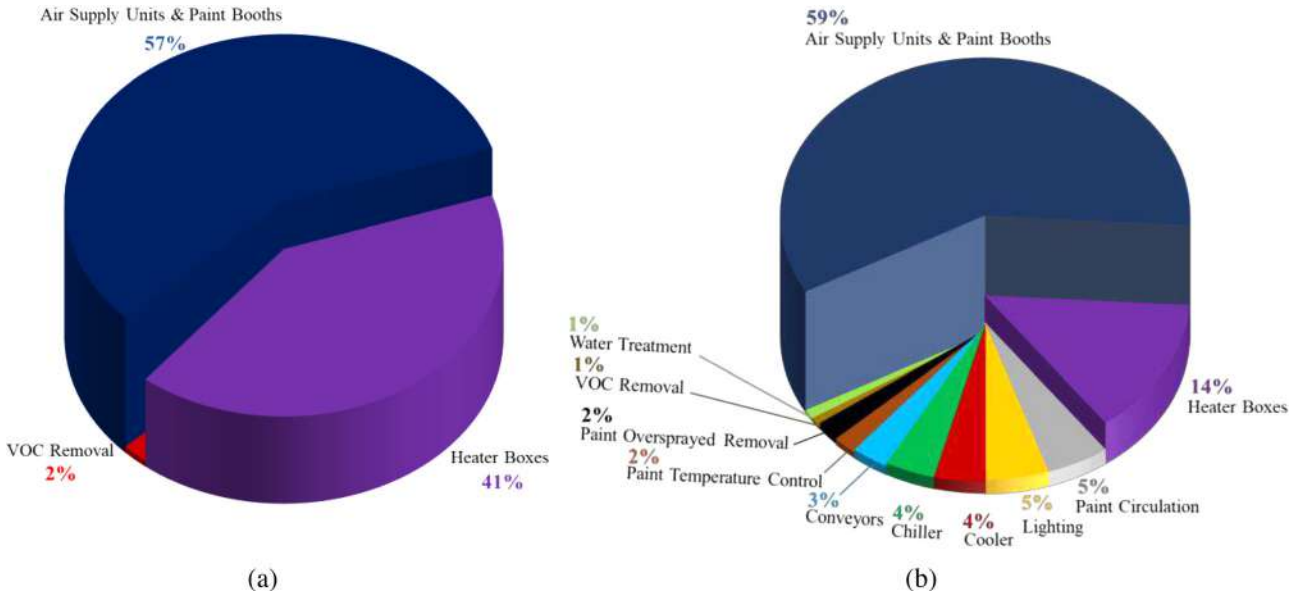

FIG. 4. Analysis of (a) natural gas and (b) electrical power consumption distribution in an automotive paint shop plant. Adapted from Giampieri *et al.*, "A review of the current automotive manufacturing practice from an energy perspective," Appl. Energy **261**, 114074 (2020). Copyright 2020 Author(s), licensed under a Creative Commons Attribution (CC BY) License.

three layers deposition, was introduced via Ford and Mazda (Akafuah *et al.*, 2016) [Fig. 5(d)]. Also, in Fig. 5(e), the values of emitted VOC and CO_2 during these innovative strategies are compared. In comparison to solvent-based paint, water-based paint emits higher CO_2 and less VOC due to higher energy usage during the extended drying period. But, the 3-wet method resulted in the best environmental performance.

Alternative techniques of the infrared radiation (IR) due to speeding up and the ultraviolet (UV) due to lower time and temperature requirement during curing are used as a substitute for conventional curing techniques. Currently, UV curing is mainly utilized for the painting of the vehicle's plastic parts (Galitsky and Worrell, 2008). The cost of the IR curing method is less than the UV curing approach, which gives a 50% reduction in energy consumption. A hybrid of the

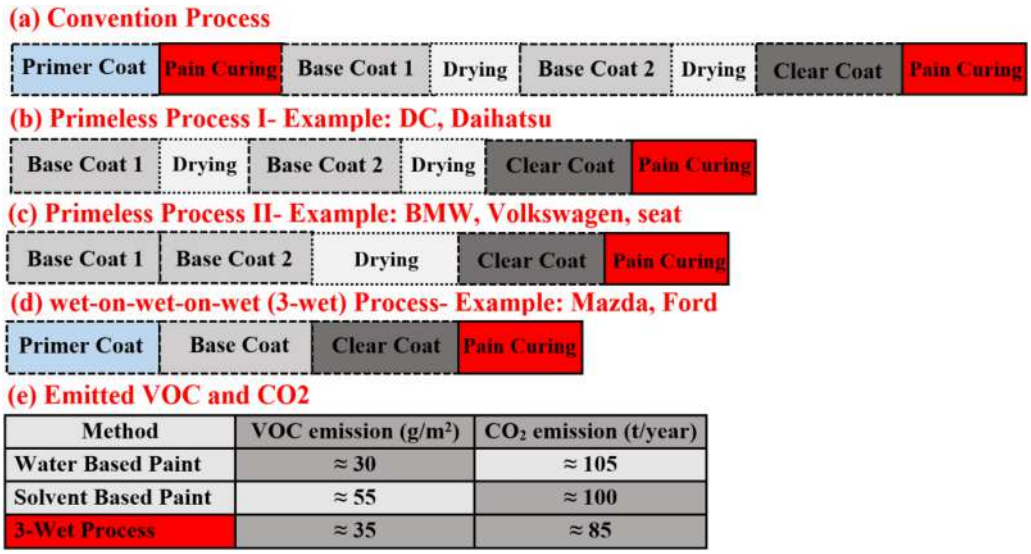

Method	VOC emission (g/m^2)	CO_2 emission (t/year)
Water Based Paint	≈ 30	≈ 105
Solvent Based Paint	≈ 55	≈ 100
3-Wet Process	≈ 35	≈ 85

FIG. 5. Evolution of different methods of the automotive painting process, as well as their impact on VOC and CO_2 volume emissions. Adapted from Giampieri *et al.*, "A review of the current automotive manufacturing practice from an energy perspective," Appl. Energy **261**, 114074 (2020). Copyright 2020 Author(s), licensed under a Creative Commons Attribution (CC BY) License.

TABLE I. Introduction of the renewable energy resources employed in automotive manufacturing plants.

Renewable energy	Manufacturers example
Solar photovoltaic	Seat, Martorell facility (8 MW photovoltaic plant) (SEAT al Sol, 2018)
	Nissan (4.75 MW solar plant)
Solar thermal	Dürr, Eco+Paintshop (Zahler and Iglauer, 2012)
Wind	Nissan Mexico, Sunderland (6.6 MW) and Aguascalientes facility
	BMW, Leipzig facility (20% of the energy required) (BMW, 2010)
	Ford, Dagenham facility, two turbines with capacity of 3.6 MW.
Hydroelectric	Volkswagen, Chattanooga
	BMW, Moses Lake facility
Geothermal	Audi, Gyor: 60%–70% of the plant requirements energy (82 GW h/y produced)
Landfill gas	GM, four facilities in the USA: Use of landfill gas as energy source of power plant boilers
	Nissan Mexico, Aguascalientes facility
	BMW, Spartanburg facility

IR and convection ovens for heat-up and hold-on zones, respectively, can be used as an efficient strategy for reducing energy consumption and reaching a higher clear-coat quality (Giampieri *et al.*, 2020).

During the spraying process, for suctioning the over-sprayed paint, using a "dry scrubber" technology reduces energy consumption and CO_2 emission (Akafuah *et al.*, 2016). The newly introduced technique works with cardboard EcoDry filters (Dürr, 2018) or high voltage (Swoboda *et al.*, 2015) for the over-sprayed paint separation process. The adoption of a more energy-efficient combustion process is one of the energy-efficient solutions for VOC elimination (Trinh and Mok, 2016).

Despotovic and Babic (2018) developed the curing ovens performance by the evolution of the influencing operating parameters. The effective management of energy efficiency can be obtained in curing ovens by the reduction of supplied airflow during downtime (Feng, 2019) or based on the required production (Taikisha, 2018). These advancements resulted in significant economic saving in electric and thermal energy by avoiding unnecessary heating and reducing the fan speed (Feng *et al.*, 2016).

C. Substitution of renewable energy resources

Recently, various renewable energy resources, such as solar thermal and photovoltaic, wind, hydroelectric, geothermal, and landfill gas, have been employed during automotive manufacturing for thermal and electrical production (Oh and Hildreth, 2016; AMS, 2018). The use of these resources drastically reduces harmful gas emissions. Table I lists the ranges of the produced energy by the mentioned renewable energy resources, noting the companies in which they have been used.

Figure 6 schematically describes the heat cascade of the solar thermal used in the paint shop plant. The usage of solar thermal technology in the paint shop by Dürr effectively reduced the energy cost (Zahler and Iglauer, 2012). By using the Fresnel collector's system, the superheated water (400 °C) for delivery to curing ovens is produced (Zahler and Iglauer, 2012). The oven is powered by superheated water (220 °C), and the hot exhaust air (180 °C) from the oven is transported to the regenerative thermal oxidizer (RTO) to burn the VOCs. The stack heat of RTO is then warmed water for intermediate ovens (110 °C) or preheated fresh air (115 °C) for the paint booth. A combination of the linear Fresnel collectors and micro-gas turbine technology (Iglauer and Zahler, 2014) introduced innovative and efficient heat and electric power generator resources for the painting process. Furthermore, the usage of produced electricity by the gas turbine resulting in a 35% reduction in fuel combustion (Iglauer and Zahler, 2014).

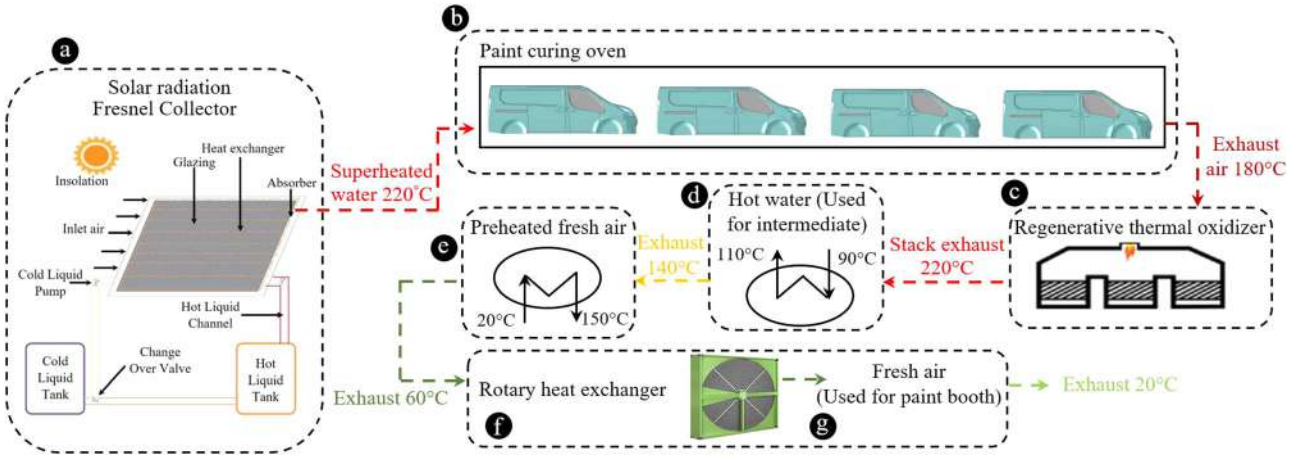

FIG. 6. Schematic visualization of the solar thermal (Fresnel collectors) technology employed in the paint shop plant. Adapted from Giampieri *et al.*, "A review of the current automotive manufacturing practice from an energy perspective," Appl. Energy **261**, 114074 (2020). Copyright 2020 Author(s), licensed under a Creative Commons Attribution (CC BY) License.

In addition, the RTO's secondary heat recovery is used to heat or cool air supply units.

III. AUTOMOTIVE PAINT FILM LAYERS RECOGNITION

Deposition of the paint film layers during the coating process, as one of the main operations of automotive production, accounts for roughly 10% of the entire cost, with energy usage accounting for 50% of the total cost (Clément *et al.*, 2014). The paint deposition procedures are a surface-based chemical reactions consequence. The paint layers are sandwiched among the base metal and cover surface. As shown in Fig. 7, the paint coverage on the modern automotive coated surface includes five primary layers of conversion coat (mainly made up of phosphates layer), electro-deposition (ED), underbody coat (UBC) film, primer coat, and topcoat (base coat and clear coat). Each of these paint layers has its own set of properties and thickness, as well as finishing and protection functions (Ansdell, 1980), which will be explained in Subsections III A–III E in detail. Before starting the coating process, the zinc film layer, which has the capability to promote adhesion on the sheet metal and also provide corrosion resistance, covers the sheet of the BiW.

A. Conversion coating process

The BiW, after entering to the paint shop, cleaning and rinsing, being immersed primarily in degreasing and conditioning liquid, then dipped in the phosphate salts and phosphoric acid dilute solution for insoluble crystalline phosphates layer formation (Chang, 2011; Akafuah *et al.*, 2016; and Doerre *et al.*, 2018). These sequences, as shown in Fig. 8, are called the pretreatment process. An appropriate setting of parameters in pre-phosphating stages, viz., dip-cleaning, degreasing, de-rusting, and surface activation have a significant impact on the morphology, uniformity, quality, and coating weight of the phosphate deposited layer. The degreasing solution includes trisodium phosphate, caustic soda, and sodium carbonate, consisting of knock-off-degrease and dip sequence steps. The formed phosphate layer on the metal provides corrosion resistance for the body, which is highly dependent on the bath factors being in the recommended range (Akafuah, 2013).

B. Electro-deposition (ED) procedure

In the electro-deposition process, the electrically charged paint droplets are deposited on the car body that was dipped in the coating solution tank. Nowadays, in industries, the cathodic configuration for the body due to providing exceptional resistance is used (Streitberger and Dossel, 2008). The vehicle body is grounded in this configuration, while the bath gains a DC positive charge through the electrodes that regulate the coating film thickness. The positively charged paint droplets migrate toward the cathode (vehicle). In modern automotive manufacturing, ED with SCGA solution (90% Zn–10% Fe) is commonly utilized (Akafuah *et al.*, 2016). The electrocoat film, a firm adherence and solids content layer with a thickness of around 20 μm in most current automotive industries, covers the body (Sankara Narayanan, 2005). It must be mentioned that the ED stage as an environmentally friendly process uses just 0.5% of solvent solution (Loop, 1978). Reducing the solution water caused the formation of hydroxyl ions and charged paint droplets neutralization and precipitated them to the vehicle (Nichols and Tardiff, 2016). Finally, the body, after the pretreatment and ED processes, is sent to the curing oven. The steps mentioned above can be followed in Fig. 8.

C. Underbody coating (UBC) film cover

Recently, acryl-urethane and polyvinyl chloride sealants have been employed as a dampening coat stage to impart vibration

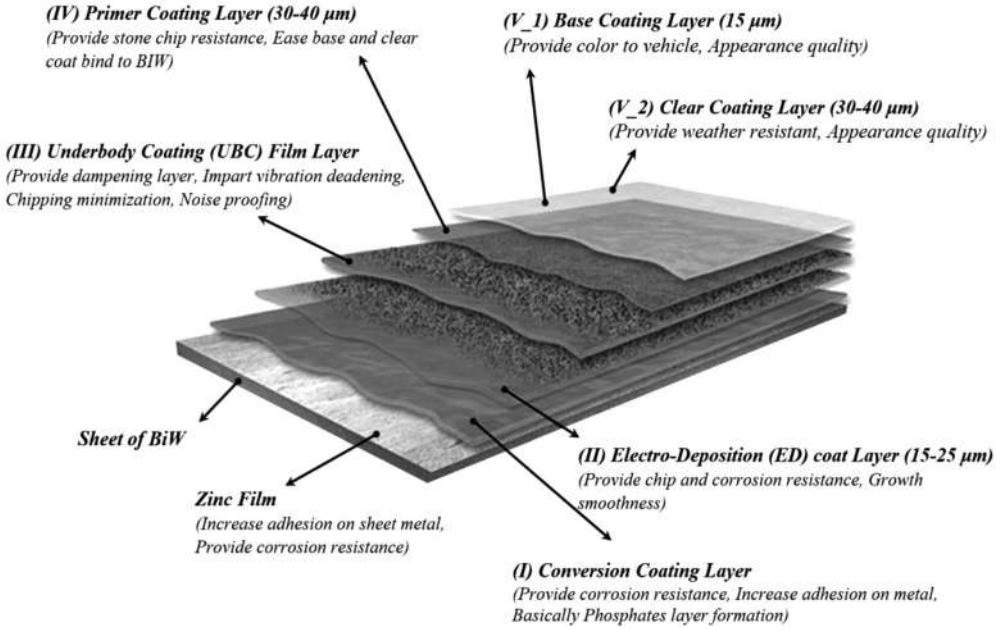

FIG. 7. Schematic description of the paint layers with their thicknesses in the automotive coating operation.

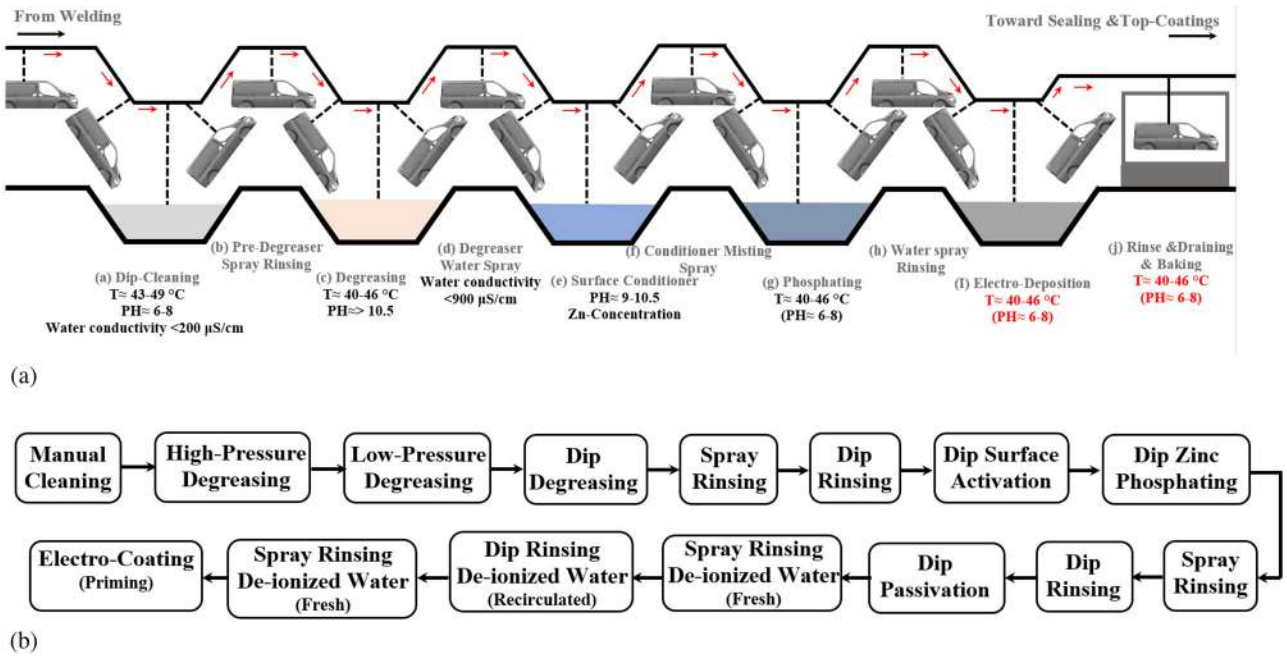

FIG. 8. Representation of the pretreatment and ED sequences for the BiW in (a) typical and (b) modern automotive paint shop plants. Adapted from Doerre *et al.*, "Advances in automotive conversion coatings during pretreatment of the body structure: A review," Coatings **8**, 405 (2018). Copyright 2018 Author(s), licensed under a Creative Commons Attribution (CC BY) License.

deadening, chipping minimization and noise proofing (Tomalino and Bianchini, 1997). These sealants are primarily applied in the hood, surrounding and inside the doors, trunk, metal joints, and the back wheel area of the car body. The underbody coating (UBC) that is generally accomplished with robot arms supplies chipping prevention and anti-corrosion (Tomalino and Bianchini, 1997).

D. Primer coat layer

The other three remaining paint layers of primer, base, and clear are sprayed using the electrostatic rotary bell sprayers (ERBSs) or pneumatic atomizer. The primer coat layer, which improves paint appearance, weather resistance and chipping protection, can be solvent-borne, water-borne, or powder (Moore, 2017). The primer coat layer promotes adhesion between the body surface and the basecoat. Recent improvements in water-borne primers have resulted in their widespread adoption. They cause considerably lower VOC emissions, thermoplastic properties improvement, durability increment and a finish harden (Poth, 2008). The primer coat's hardness, elasticity, and adhesive properties (among ED lower and base coat lower layer) are usually controlled (Misev and Van der Linde, 1998). The primer coating operations consist of the interior and exterior coating that are usually implemented via the manual operator and Robot arms, respectively. The interior and exterior primer coat layer thickness are 20 and 25–40 μm, respectively. This process typically operates at 140 °C for around 30 min.

E. Topcoat layers: Basecoat and clearcoat

The final topcoat layer consists of two layers of basecoat and clearcoat. The clearcoat layer protects the body from corrosion, fading by the UV light and environmental impacts and provides a smooth and unblemished layer with esthetic appeal film (Akafuah, 2013). The topcoat layers can be implemented in two methods of wet-on-wet (with a middle short flash-off stage) or separate process (with a middle curing oven stage). The typical time and temperatures needed for implementation of this step are around 30–40 min and 125 °C, respectively (Wu *et al.*, 2014). Three different basecoat forms that are used can be named as the medium solids (MS) solvent-borne, high solids (HS) solvent-borne, and water-borne (Pfaff, 2008). Because of the environmental advantages, the waterborne type is preferred in the U.S. car manufacturing industry. Up to now, 40 000 base coat colors are known and around one thousand new colors also are added each year (Streitberger and Dossel, 2008). The UV radiation absorption and scratch-resistance of clearcoats are two crucial factors affecting long-term car surface appearance. The UV radiation with wavelengths ranging from 290 to 400 nm can be absorbed (Gerlock *et al.*, 2001). The clearcoat of 1 K-acrylic melamine is utilized commonly in the automotive industry due to its low cost, higher resistance, lack of need for hardening and performance balance (Noh *et al.*, 2012; Dutt *et al.*, 2013).

IV. EVOLUTION OF COATING SPRAYERS TECHNOLOGY

The anti-chip, primer, base, and clear coat layers are applied by spraying technique during the modern coating process. Therefore, recognition and advancement of the current employing atomizers are crucial. Atomization is defined as the liquid disintegration to the different distribution of droplets (Liu, 2001) through a variety of causes, e.g., aerodynamic, electrostatic, mechanical, or ultrasonic forces. During the spraying system, droplets are immersed in a continuous

gaseous phase (Lefebvre and McDonell, 2017). Better atomization performance is directly linked with a narrower droplet size dispersion (Lee *et al.*, 2012). The liquid breakup into droplets phenomena occurs when the liquid and air impingements due to dominant centrifugal forces in rotary atomization, electrostatic fields in electrostatic atomization, electromagnetic fields in electromagnetic atomization, or rapid vibrations established by a piezoelectric transducer in ultrasonic atomization. The terms (I) transfer efficiency (TE), (II) Sauter mean diameter (SMD), (III) overspray capturing efficiency, (IV) spray plume pattern dimensions, (V) atomization ratio, and (VI) paint film thickness on target, as prominent criteria, are now taken into consideration while evaluating the sprayer's performance. The transfer efficiency (TE) is expressed by dividing the deposited paint amount on the workpiece after spraying by the total injected paint from the sprayer. The Sauter mean diameter ($SMD = \sum N_i D_i^3 / \sum N_i D_i^2$) as a meaningful parameter for droplet fineness is defined as a droplet diameter with a similar volume ratio to surface area for the entire spray (Lefebvre, 1989). D_i and N_i denote the droplet diameter and numbers in the i-th size range, respectively. Also, the ratio of overspray captured to overspray entering the capturing system is called "overspray capturing efficiency."

Recently, in the automotive industry, high-speed rotary bell sprayers or air spray guns are two main types of applicators used for the coating. Both of these apparatuses can work in electrostatic or non-electrostatic modes. However, the electrostatic rotary bell sprayer (ERBS) is more common due to more efficient operation and higher TE (Corbeels *et al.*, 1992).

The overall purpose of the automotive coating is to achieve the following desirable characteristics (Fettis, 1995):

(I) maximized coating TE without harming the appearance of the paint film, (II) fast, robust and reliable performance while applying a paint film in a short time (Arikan and Balkan, 2006), (III) a superclean operation for minimizing defection of the paint on the surface, e.g., sags, mottle, solvent popping, and craters (Love *et al.*, 2001). Optimizing the sprayer's technology leads to satisfying the above performances to reach the uniform film, maximum overspray capturing efficiency, and the highest TE with maximum production rate. A strong demand exists to increase the overspray capturing efficiency to reach less energy consumption, lower operational cost and minimum environmental pollution because of, for instance, wet scrubbing and water washing (Salazar *et al.*, 1997; 2000). A comprehensive review of the different sprayers in the industry can be beneficial in achieving the intended goals during the spraying. Here, characteristics of the paint spray applicators that includes conventional air sprayer, high-volume low-pressure (HVLP) sprayer, air-assisted airless sprayer, airless pressure sprayer, rotary bell sprayers, and electrostatic rotary bell atomizers are described in detail.

A. Conventional air sprayers

Conventional air atomizers include high-volume low-pressure and two-fluid sprayers. Despite producing a paint film that is acceptable, these sprayers have a low TE and a high paint usage rate. Numerous research had been implemented to recognize the atomization control mechanisms and effective parameters for conventional air sprayers (Kim and Marshall 1971; Kumar and Lakshmi Prasod, 1971). Early contributions to investigate conventional air sprayers were implemented by Nukiyama and Tanasawa (1939). They suggested an empirical expression for the droplet size relation with liquid properties and gas and liquid flow rates. Their work showed that liquid and gas flow rates, viscosities and densities are the most influential factors affecting the droplet size. More recent research has also confirmed these findings, e.g., the thesis of Corber (2009). Janna (1976) published one of the first research articles on design of the spray gun and droplet atomization process. The shutter airless spray nozzle was used to spray latex paint, water–glycerine mixtures, and water liquid. The impact of nozzle size, paint surface tension, and viscosity, as well as hydrostatic pressure, was analyzed. According to the developed empirical equations, an increase in the wall shear stress, liquid density and volumetric flow resulted to a reduction in median droplet diameter. However, a rise in the surface tension and viscosity of paint obtained a larger median diameter.

Based on the produced various spray patterns, nozzles in conventional sprayers are classified into different categories, such as flat spray, full cone, or hollow cone. Full-cone nozzles produced the largest size distribution of droplets, followed by flat-spray and hollow-cone nozzles at the same rate of air and liquid (Andrade *et al.*, 2012). The size of the droplets is usually increased when the liquid flow rate increases and reverses (Schick, 2006). Also, the droplet size has an inverse relation with the air pressure. Similarly, droplet size and spray angle are inversely proportional; a higher spray angle results in a smaller droplet size dispersion (Schick, 2006; Lefebvre and McDonell, 2017). The air velocity is undoubtedly the most critical component influencing the Sauter mean diameter (SMD) value in conventional air sprayers. Lefebvre and McDonell (2017) for pre-filming nozzles estimated that the SMD was proportional to the air density to the power of 0.6. For the liquids with low viscosity, the air velocity is inversely proportional to the SMD, emphasizing the need to work at the highest possible air velocity (Lefebvre and McDonell, 2017). However, due to decreasing the TE by growing the air pressure, determining the optimum air pressure value is required. Evaluating the interactions among influential parameters is essential to achieve thorough conclusions on conventional air sprayers.

1. Twin-fluid atomizer air sprayers

Figure 9(b) illustrates a typical cap within the primary functions of an air spray atomizer. These air sprayers contain a paint orifice, primary and secondary air orifices and shaping air holes that affect the atomization mechanism (Hicks, 1995). The liquid that exits from the paint nozzle ($V \approx 5$ m/s) is encountered the air orifices in two directions. The different orientations of primary and secondary orifices cause twice disintegration happening for droplets during the spraying. These spray guns generally operate at the liquid and air pressure of up to 0.5 and 0.3 MPa, respectively. The shear layer close and on the surface of the target induced an overspray phenomenon [Fig. 9(a)], which prevented small droplets with low axial momentum from adhering to the surface in this sort of sprayer. Although this air sprayer type produces a smooth finish, but it has a low TE rate (≈20%) when compared to other sprayers (Plesniak *et al.*, 2004).

Kim and Marshal (1971), in their experiment for the twin-fluid atomizer, by using the curve-fitting method, obtained the correlation for droplet size. The correlation among various parameters after the improvement of the nozzle design was discussed. Hicks and Senser (1995) developed a numerical model for the prediction of trajectory

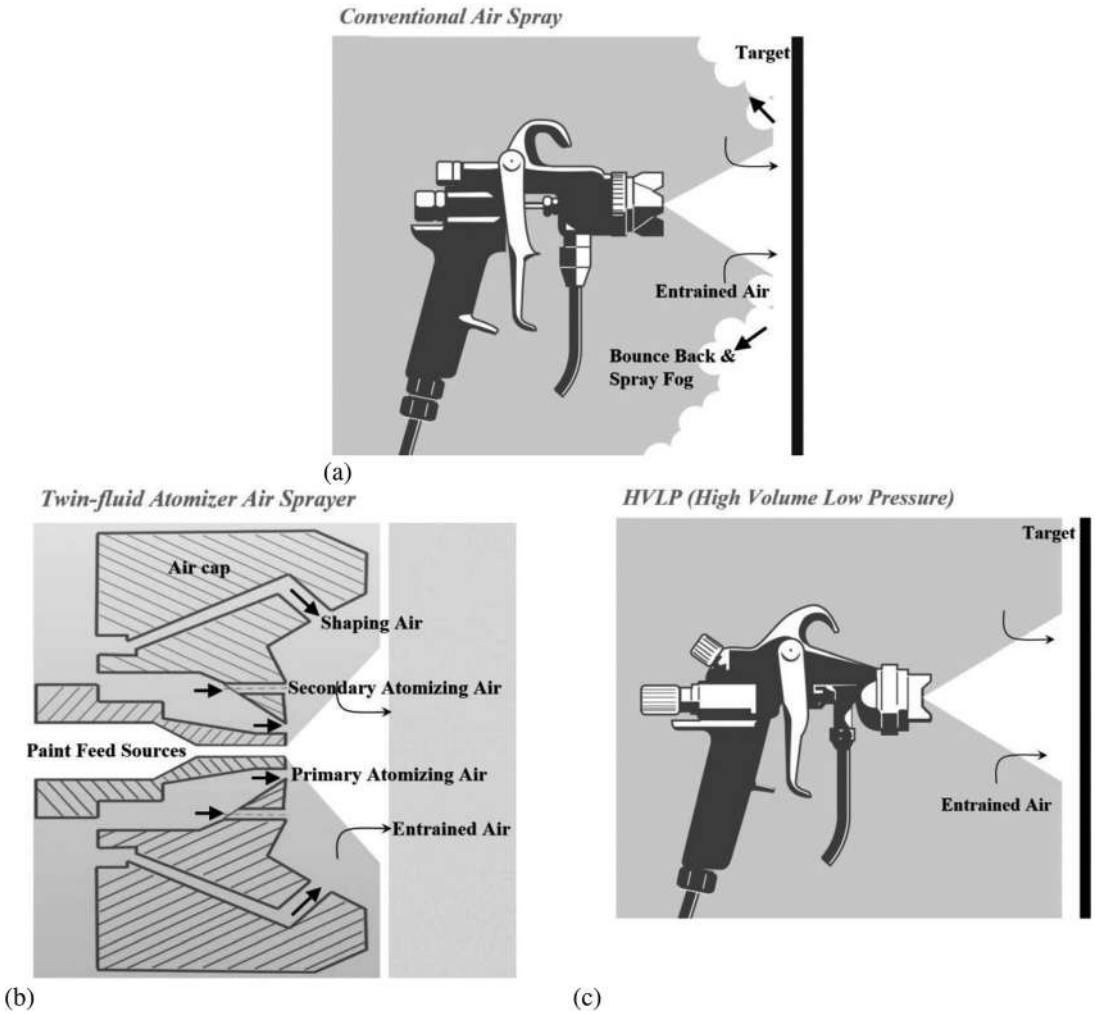

FIG. 9. Typical sprayer's structure: (a) conventional air sprayers, (b) twin-fluid atomizer air sprayers, and (c) HVLP devices.

and deposition of paint droplets generated by the air sprayer. They assessed the velocity of turbulent air effect on the trajectories of the droplets and TE. They concluded that the droplets with a size range smaller than 120 μm induced a meager TE rate. Domnick *et al.* (1994), Morikita and Taylor (1998), and Kwok (1991) employed the phase Doppler anemometry (PDA), shadow Doppler velocimetry (SDV) and hot wire and a pitot tube technique in their experiments, respectively, to assess the spray gun and air cap design effect on droplet velocities, spatial distributions and size. Flynn and Sills (2001) modeled paint droplet breathing-zone concentrations. However, they were unable to predict the TE and paint particle size distribution. To fitting the size distribution of droplets in the mentioned experimental during various operational conditions, the Rosin–Rammler, log kernel, or Nukiyama–Tanasawa distributions were employed in numerical modeling (Movahednejad *et al.*, 2010). Ye *et al.* (2002) described the air flow among the nozzle and target by consideration of the air and droplet interaction. The initial conditions of droplets and air enabled the spray cone pattern determinations over the pneumatic atomizer and the produced film. Computational fluid dynamics (CFD) was also used by Fogliati *et al.* (2006) to predict paint droplet trajectories and deposition distributions on rectangular target plates. Recently, Li *et al.* (2019) investigated the shaping air holes pressure and intersection in pneumatic atomizers as the two most important parameters. They found that an increase in the distance between the intersection and the paint hole causes the droplet size becomes larger and leads to more overspray. Also, by growing shaping air hole pressure, the spray distribution on the target became narrow, and the ovality pattern increased.

2. High-volume low-pressure devices

In comparison to the sprayers stated above, high-volume low-pressure (HVLP) devices direct paint to target at lower air pressure. This performance of these sprayers resulted in a lower

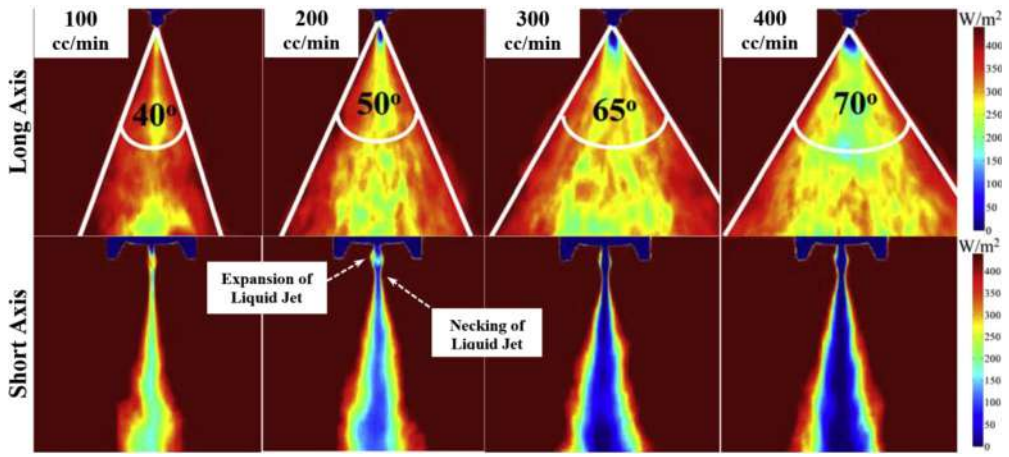

FIG. 10. Infrared thermographic images of the HVLP atomizer, with growing liquid flow rate at a constant air pressure of 0.4 MPa. Expansion and necking explanation along the short axis. Reproduced with permission from Akafuah *et al.*, "Infrared thermography-based visualization of droplet transport in liquid sprays," Infrared Phys. Technol. **53**(3), 218 (2010). Copyright 2010 Elsevier.

overspray phenomenon [Fig. 9(c)]. Darroch (1997) introduced air conversion spray guns and turbine-driven systems as two types of HVLP devices. HVLP spraying technology leads to higher TE and produces a finish with higher quality, but operating of coating process by it is not easy. In HVLP systems, low air inertia causes uneven finish, higher paint usage, and more time-consuming with a lower rate of production. In 2002, the low-volume medium-pressure spray was invented to solve the issues of HVLP and provide a faster finishing time with a higher TE (Shilton *et al.*, 2002). Figure 10 presents the infrared thermographic visualization of the spray generated by the HVLP sprayer, reported in reference Akafuah *et al.* (2010). They announced that by increasing the liquid flow rate from 100 to 400 cc/min, the spray angle opens up, the SMD linearly grows, and a progressively denser core is obtained.

B. Airless pressure sprayers

Airless pressure sprayers are utilized for a wide range of coating applications due to their higher TE, which is the result of high fluid pressure. The paint is atomized when the paint is pushed through a tip with a diameter of ≈0.18–1.2 mm at very high pressure (8.0–52 MPa). However, airless pressure sprayers generally form a sharp edge with a fan-shaped spray pattern, enabling precise spray targeting rarely utilized in automotive industries [see Fig. 11(a)]. Settles (1997) provided a basic understanding of ligament and droplet formation over airless pressure sprayers by considering a flow as quasi-two-dimensional. Xing *et al.* (1998) investigated the correlation between the orifice diameter and the SMD in airless pressure applicators. They found that when paint viscosity increased, the size and distribution of droplets widened. Airless pressure sprayers are mostly employed in

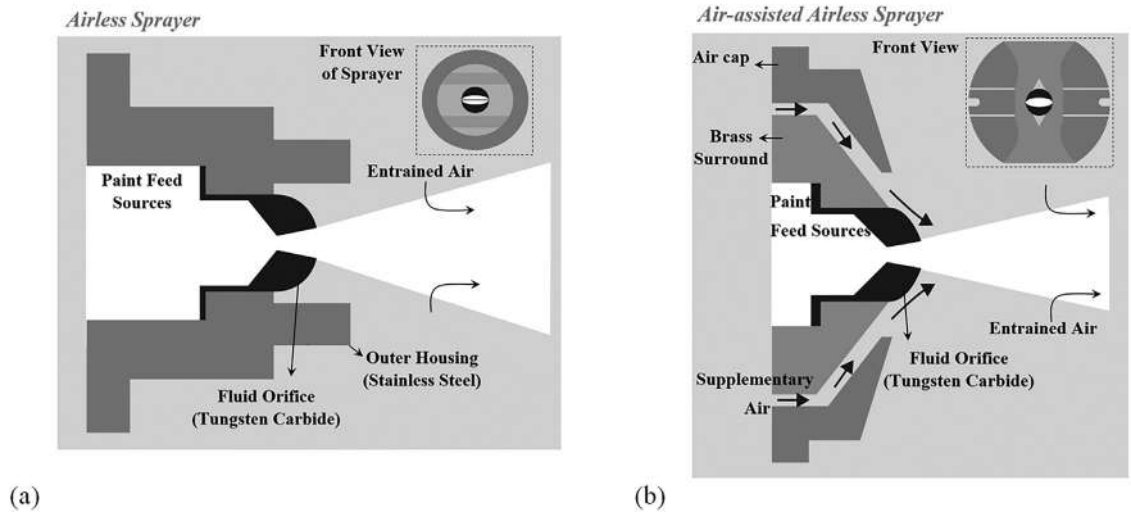

FIG. 11. Structure of conventional (a) airless pressure sprayers, and (b) airless sprayers with air assistance.

applications that require huge volumes of a coating, such as automotive undercoating (Plesniak *et al.*, 2004). Plesniak *et al.* (2004) considered the influential critical factors on the airless pressure sprayer's TE. They reported the TEs between 70% and 95% for this sprayer. Ye *et al.* (2013) numerically and experimentally investigated the operating parameters on ship painting with an airless pressure sprayer by focusing on the droplet's integral sizes and velocities, using the PDA method. They reported the TE values of 55% for the longest painting distance. The airless pressure sprayer's problems include coarse atomization, overspray wastage, operating hazards, and nozzle clogging. Nevertheless, airless pressure sprayers are still commonly utilized in industrial coatings applications, especially for waterborne paints.

C. Air-assisted airless sprayers

Developing sprayers with the combination of them to reach higher TE, less paint usage, and compliance with US Environmental Protection Agency (EPA) regulations started in the 1970s (Love, 2001). Air assisted airless sprayer is the combination of an HVLP and airless pressure sprayers that have the best features of high TE and high production rate [see Fig. 11(b)]. The pressurized paint is injected by an airless pump and complemented by a small quantity of air injection from an air nozzle horns. The liquid paint and assistant air pressures are in the ranges from 4.8 to 6.2 MPa and 0.10 to 0.20 MPa, respectively. These sprayers provide a smooth finish, medium production rate range, and higher spray TE due to lower overspray. Among the scarce literature about these sprayers, Ye *et al.* (2015) reported numerical and experimental results on a basecoat material to evaluate the TE on a dynamic target while changing the assisting airflow. The airless gun's numerical and experimental results for TEs were 86% and 88%. However, for the air-assisted gun, these values are 78% and 77%, respectively. Ye and Pulli (2017) tested a complex geometry workpiece and an inclined atomizer alignment while spraying by the pneumatic atomizer.

Then, Qian *et al.* (2018) designed a new sprayer in combination with a multi-orifice nozzle to produce uniform ultrafine coatings. Figures 12 visualized the velocity contours (frame I) and spatial droplet spray pattern (frame II) between sprayers with single-hole nozzle spray [Fig. 12(b)] and multi-orifice nozzle spray [Fig. 12(c)], which are compared in their studies. The modification in the total spray pattern for the multi-orifice case is evident. The multi-orifice nozzles of fan gas and auxiliary gas are able to distribute the droplets in a wider area, decrease the central pressure, and overspray phenomenon alleviation, especially in the central spray. Also, Chen *et al.* (2019), by their multi-orifice spray nozzle, examined the created film quality on the spherical and flat surfaces. They found that a spherical surface has a higher paint deposition rate with more expansive paint film and as well as lower film thickness. Recently, Wang *et al.* (2020) designed a novel double-nozzle air spray gun structure that works based on the double jet Coanda effect. The double-nozzle obtained an 85.7% increase in the effective coating width compared to the single-nozzle air spray gun,

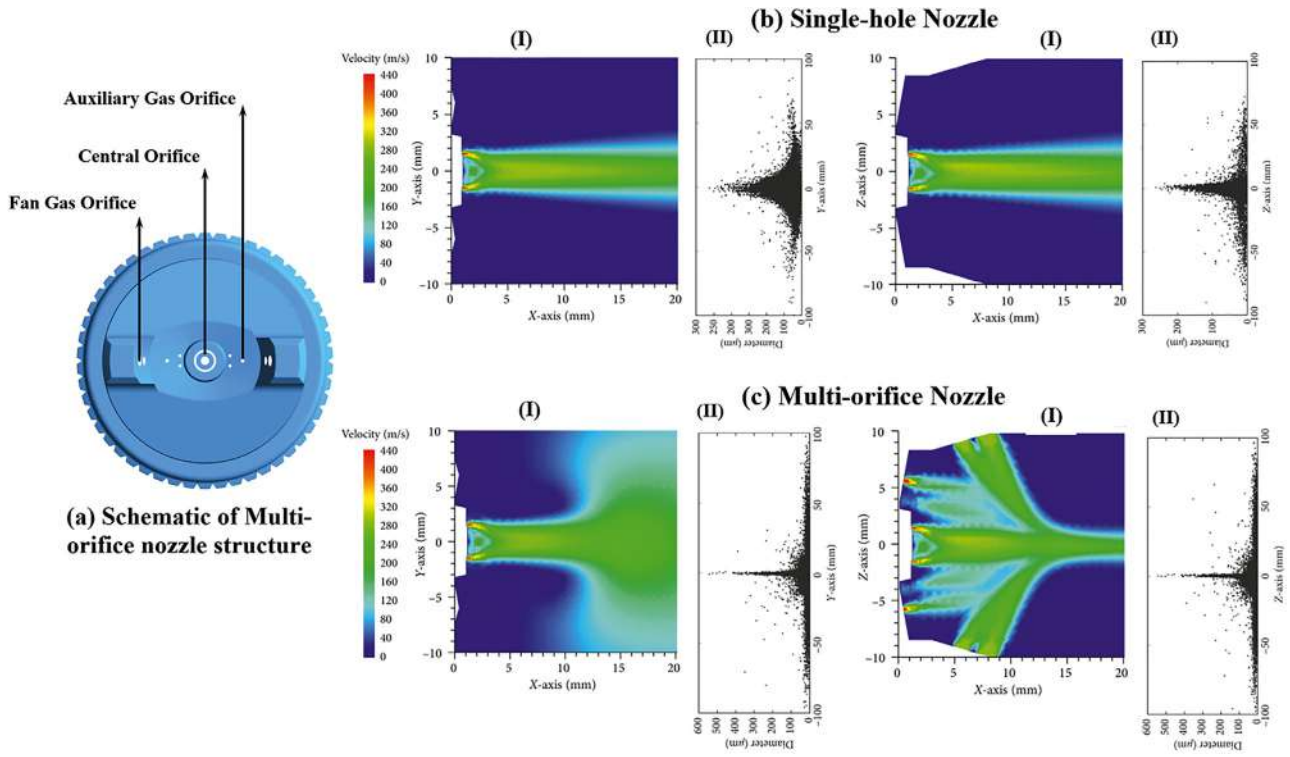

FIG. 12. (a) Schematic of multi-orifice nozzle structure. Comparison of velocity contours (frame I) and droplets spatial distributions (frame II) for the air-assisted airless sprayer with (b) single-hole nozzle and (c) multi-orifice nozzle [X-Y plane (left), X-Z plane (right)]. Reproduced with permission from Qian *et al.*, "A new spray approach to produce uniform ultrafine coatings," J. Nanotechnol. **2018**, 8978541. Copyright 2018 Author(s), licensed under a Creative Commons Attribution (CC BY) License.

considerably enhancing the spraying efficiency. The small and large values of L (distance among the centers) and θ (angle between the axes) of two paint holes cause more concentrated paint in the central area (rhombus shape) and side regions (concave shape), respectively.

D. Rotary bell sprayer

The rotary bell sprayer's introduction and development was a revolution in paint shops to reach a higher production rate (Toda *et al.*, 2012). Because of the higher TEs, lower paint-air consumption, and more consistent spray pattern, they preferred the air spray atomizer. The original rotary bell sprayers were only used for primer coatings due to poor atomization efficiency (Fig. 13), but the electrostatic or Nitrotherm electrostatic generation of these sprayers are used in a wide range of applications. Figure 14 reveals the significant differences in the infrared thermographic images of the spray directions around the ERBS by increasing the bell rotational speed and shaping airflow rate (Darwish Ahmad *et al.*, 2018). The strong effect of these two critical parameters is apparent, and a dramatic reduction in the radial divergence of the spray plum pattern is evident during the growth of the mentioned parameters. The bell rotational speed, shaping airflow rate, high voltage setting, and liquid flow rate can be specified as the four key operating factors while using the ERBSs. The efficient operation of the ERBSs depends on the many parameters that will be described and analyzed in detail in Sec. V A, as the main subject of this review focuses on it.

E. Coating sprayers transfer efficiency (TE) range

The transfer efficiency (TE) is defined by dividing the deposited paint amount on the workpiece after spraying by the total injected paint from the sprayer and formulated as a $TE = (m_f - m_i) \times 100/m_{out}$, where m_i, m_f, and m_{out} are the initial sample mass, mass after painting-drying, and the mass exits the nozzle, respectively (Pendar and Páscoa, 2019a). Figure 15 shows the range of the TE for the various discussed spraying system. However, the TE is so sensitive to the following items (Lee *et al.* 2012): (I) operating parameters, e.g., speed and distance of target (Plesniak *et al.*, 2004; Tan, 2001), shaping airflow pressure, bell cup rotational speed for a rotary atomizer (Pendar and Páscoa, 2019a; 2020a; 2021), (II) technologies of finishing

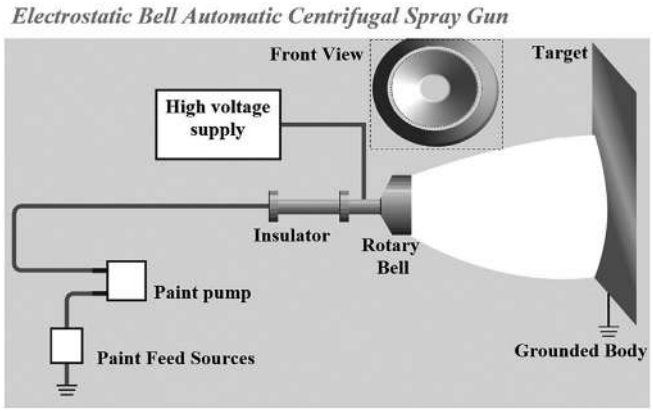

FIG. 13. Typical structure of common rotary bell sprayer.

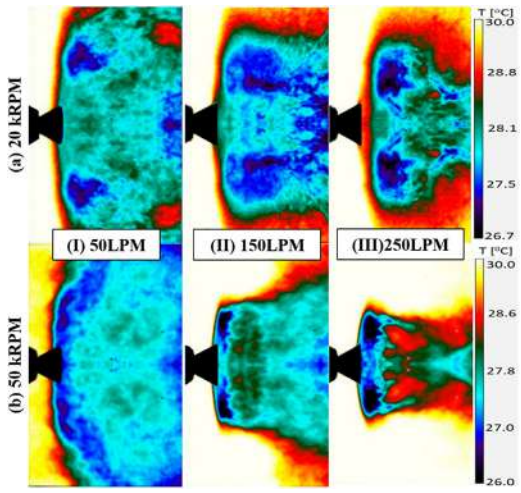

FIG. 14. Infrared thermographic images of the ERBS Spray at various bell rotational speeds of (a) 20 kRPM and (b) 50 kRPM, for a fixed paint flow rate of 0.1 LPM and different shaping air flow rates of 50, 150, and 250 LPM. Reproduced with permission from Darwish Ahmad *et al.*, "Schlieren visualization of shaping air during operation of an electrostatic rotary bell sprayer: Impact of shaping air on droplet atomization and transport," Coatings **8**, 279 (2018). Copyright 2018 Author(s), licensed under a Creative Commons Attribution (CC BY) License.

spray, (III) characteristics of the body surface, (IV) air conditions of spray booth (relative temperature, velocity and humidity), and finally (V) characteristics of liquid paint coating. For instance, the TE percentage is being reduced during the coating of complex and small bodies due to the growth of the overspray phenomenon.

Based on the discussion conveyed by an expert in the automotive painting industry (Ye *et al.*, 2003), the values of actual TEs are substantially lower than what is reported in published literature. In Fig. 15, according to the literature data, the TE for the ERBS, which is appropriate for the automotive coating, has the highest value, ≈55%–95%. However, other literature states that for a real coating, this value scarcely approached 60% (Poozesh *et al.*, 2017). Finding a solution for increasing the TE, while maintaining a high-quality finish to avoid the

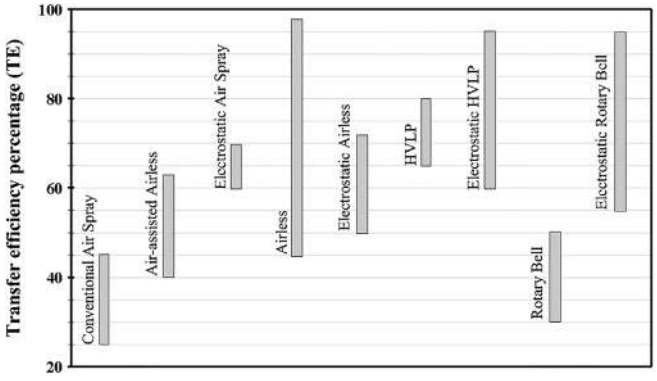

FIG. 15. Approximate transfer efficiencies (TE) for different paint spraying technologies. Data collected from Toda *et al.* (2012); Plesniak *et al.* (2004); Tan (2001); Ye *et al.* (2015); Tricou and Knasiak (2005); and Poozesh *et al.* (2017).

economic burden, environmental pollution, VOC emissions, paint sludge produced, and overspray is vital. A one percent increment in the TE can save millions of dollars per year in paint shop material utilization costs.

F. Summary for coating sprayers operational features

Table II classified the operational parameters, spray and film features for different types of coating atomizers considered in the current work. As is obvious, there are several appropriate alternatives to conventional air sprayers, which allow to achieve significantly higher transfer efficiency percentages with better film quality. Sprayers based on the rotary bell or airless pressure technologies may present transfer efficiencies ≈96% and they are followed by other atomization technologies, such as the high-volume low-pressure devices and the air-assisted airless sprayers, that are able to reach transfer efficiencies ≈90% (see Table II). However, we should keep in mind that the transfer efficiency is quite sensitive to the operational variables, such as the distance between the spray nozzle and target, and the reported transfer efficiencies usually lack a standardized method or a clearly defined procedure for its calculation (Poozesh *et al.*, 2018). It is interesting to note that, independently of the sprayer technology usage, the spray booth conditions are similar, with low air velocities below 1 m/s and temperatures close to room temperature (≈20–25 °C).

Most of these sprayers use low working pressures, commonly less than 1 MPa, except the airless pressure atomizer systems, which contrarily operate with such high values of ≈52 MPa. Furthermore, the conventional air sprayers are associated with painting film thicknesses

TABLE II. Classification of the operational parameters, spray and film features for various coating sprayers considered in this study.

Atomizer	Typical operational parameters in different studies
Conventional air sprayers	• Transfer efficiency: 20%–40% in Heitbrink *et al.* (1996); 25%–45% in Poozesh *et al.* (2017) • Spray booth air velocity: 0.5 m/s in Poozesh *et al.* (2017) • Air pressure: 0.2–0.4 MPa in Poozesh *et al.* (2017) • Spray booth temperature: 21–23 °C in Poozesh *et al.* (2017) • Liquid flow rate: 600–800 cm^3/min in Poozesh *et al.* (2017) • Application viscosity: 210–240 mm^2/s in Poozesh *et al.* (2017) • Range of droplet size distribution: larger than 100 μm in Andrade *et al.* (2012); 100–400 μm in Corber (2009) • Film thickness: 240–400 μm in Lefebvre and McDonell (2017)
Twin-fluid atomizer air sprayers	• Transfer efficiency: 15%–20% in Poozesh *et al.* (2017) • Air pressure: 0.101–0.507 MPa in Lefebvre (1992); up to 0.3 MPa in Poozesh *et al.* (2017) • Liquid pressure: up to 0.5 MPa in Poozesh *et al.* (2017) • Gas flow rate: 0.83–5 cm^3/min in Ochowiak *et al.* (2018) • Spray booth temperature: 26.85 °C in Fogliati *et al.* (2006) • Liquid flow rate: 180 cm^3/min in Fogliati *et al.* (2006); 166.67–833.33 cm^3/min in Ochowiak *et al.* (2018) • Application viscosity: 30–80 mm^2/s in Broumand *et al.* (2022) • Range of droplet size distribution: 50–200 μm in Lefebvre (1992) • Film thickness: 100–300 μm in Lefebvre (1992)
High-volume low-pressure devices (HVLP)	• Transfer efficiency: at least 65% in Heitbrink *et al.* (1996); 65%–87% in Gatano (1997) • Spray booth air velocity: 0.11–0.15 m/s in Heitbrink *et al.* (1996) • Air pressure: 0.24–0.4 MPa in Poozesh *et al.* (2017); up to 0.4 MPa in Adornato (2015); 0.05–0.63 MPa in Akafuah *et al.* (2009) • Liquid pressure: up to 0.4 MPa in Adornato (2015) • Liquid temperature: up to 50 °C in Adornato (2015) • Liquid flow rate: 200 cm^3/min in Adornato (2015); 86–162 cm^3/min in Flyyn *et al.* (1999) • Application viscosity: 40–93 mm^2/s in Flynn *et al.* (1999) • Range of droplet size distribution: 40–150 μm in Adornato (2015) • Film thickness: 25.4–30.48 μm in Joseph (2009); 8–14 μm in Luangkularb *et al.* (2014)
Airless pressure sprayers	• Transfer efficiency: 72%–97% in Plesniak *et al.* (2004); 70%–97% in Poozesh *et al.* (2017) • Spray booth air velocity: 0.1 m/s in Ye *et al.* (2013); 0.7 m/s in Poozesh *et al.* (2017) • Air pressure: 10–20 MPa in Plesniak *et al.* (2004); 8.0–52 MPa in Poozesh *et al.* (2017) • Liquid pressure: 8.0–52 MPa in Poozesh *et al.* (2017) • Liquid flow rate: 300–1500 mm^3/min in Poozesh *et al.* (2017)

TABLE II. (*Continued.*)

Atomizer	Typical operational parameters in different studies
Air-assisted airless sprayers	• Application viscosity: 50–500 mm^2/s in Poozesh *et al.* (2017) • Range of droplet size distribution: 65–85 μm in Ye *et al.* (2013) • Film thickness: 10–75 μm in Ye *et al.* (2013) • Transfer efficiency: ≈78% in Poozesh *et al.* (2017) • Spray booth air velocity: 0.3 m/s in Ye *et al.* (2015) • Air pressure: 0.10–0.20 MPa in Poozesh *et al.* (2017) • Liquid pressure: 4.8–6.2 MPa in Poozesh *et al.* (2017) • Liquid flow rate: 122.39–164.88 cm^3/min in Ye *et al.* (2015)
Rotary bell sprayer	• Application viscosity: 150–900 mm^2/s in Felstein and Lum (1993) • Range of droplet size distribution: 10–15 μm in Ye *et al.* (2015) • Film thickness: 12.7–25.4 μm Felstein and Lum (1993); 8–35 μm in Ye *et al.* (2015) • Transfer efficiency: 76%–96% in Guettler *et al.* (2017) • Spray booth air velocity: 0.3 m/s in Mark *et al.* (2013) and Guettler *et al.* (2017); 0.2 m/s in Poozesh *et al.* (2017) • Air pressure: 0.06–0.20 MPa in Poozesh *et al.* (2017) • Spray booth temperature: 23 °C in Guettler *et al.* (2017) and Poozesh *et al.* (2017) • Liquid flow rate: 100–400 cm^3/min in Akafuah *et al.* (2009); 150–300 cm^3/min in Poozesh *et al.* (2017) • Application viscosity: 150–360 mm^2/s in Poozesh *et al.* (2017) • Range of droplet size distribution: 10–50 μm in Akafuah *et al.* (2009); 4–100 μm in Guettler *et al.* (2017) • Film thickness: 15–40 μm in Guettler *et al.* (2017); 5–50 μm in Mark *et al.* (2013)

considerably larger when compared with other more sophisticated atomizers. However, we verify that the more advanced atomizers are able to produce paint films with very low thicknesses in ranges of only a few tens of micrometers.

In addition to the factors presented in Table II, an additional aspect that should be considered in the painting process is the pollutants emission to the adjacent atmosphere. Independently of the type of atomizer, any automotive coating process is associated with pollutants emissions, commonly called volatile organic compounds (VOCs) (Li *et al.*, 2013). During the coating process, VOCs easily evaporate and are released into the atmosphere, mainly originating from the organic solvent commonly used to dilute the paint (Yano *et al.*, 2019). The downdraft airflow, which originates from the spray booth ventilation system, presents an essential role in VOCs removal, transporting the paint particles and VOC contained air into the drain system (Li *et al.*, 2013). To reduce the solvent content of the paints and, in consequence of that, reduce the VOCs emission, studies have been performed to develop water-based paints and powdered paints (Kim, 2011). Although waterborne paints are not fully organic solvent-free, they are a type of coating that can easily be implemented in conventional air sprayers, airless and air-assisted airless systems, electrostatic and HVLP spraying devices, and are associated with low VOC emissions (McMinn *et al.*, 1993).

V. ELECTROSTATIC SPRAY TECHNIQUE

In this section, the electrostatic spraying method and its application in various areas will be reviewed in detail. In the 1940s, Ransburg was the first to introduce the electrostatic coating technique in the United States (Tilney, 1953). Currently, various types of electrostatic sprayers, including air sprayers, airless sprayers, air-assisted sprayers, and rotary sprayers, are available for using in different applications. One of the advantages of the electrostatic spraying method is the ability to wraparound round-shape and complex geometries. Several patents and investigations, such as Roger and Sames Machines Electrostatiques (1962), Hines (1966), Demeter and Villamos Automatika Intezet (1970), and Bienduga and Wagner Systems, Inc. (1995), have proved the ease with which paint particles are applied to vehicles by using this coating approach. During the electrostatic spraying process, the electrically charged droplets leave the nozzle's output, facing a provided electric field between the spray gun and the target that compelled them toward their final destination. As a result, a uniform film layer with a high TE and significant paint savings formed on the surface.

The theories of the electrostatic spraying procedure and its various applications were described in references Kelly (1994) and Okuda and Kelly (1996), respectively. Hayati *et al.* (1987), Jaworek and Krupa (1999), and Jaworek (2007) were among the first who described the electrostatic spraying mechanisms and followed formed jet, microparticle and nanoparticle. The usage of the electrostatic spraying method in the automotive and aerospace industries, agriculture practices, disinfection processes, and pharmaceutical companies for equipment product finishing, pesticide and crop dusting, saliva-disease-carrier droplets removal and pill covering, respectively, have been progressively expanded in recent years (see Fig. 16).

Electrostatic spraying is used in agriculture to protect crops from pest infestation and increase production [see Fig. 16(b)] (Martin and

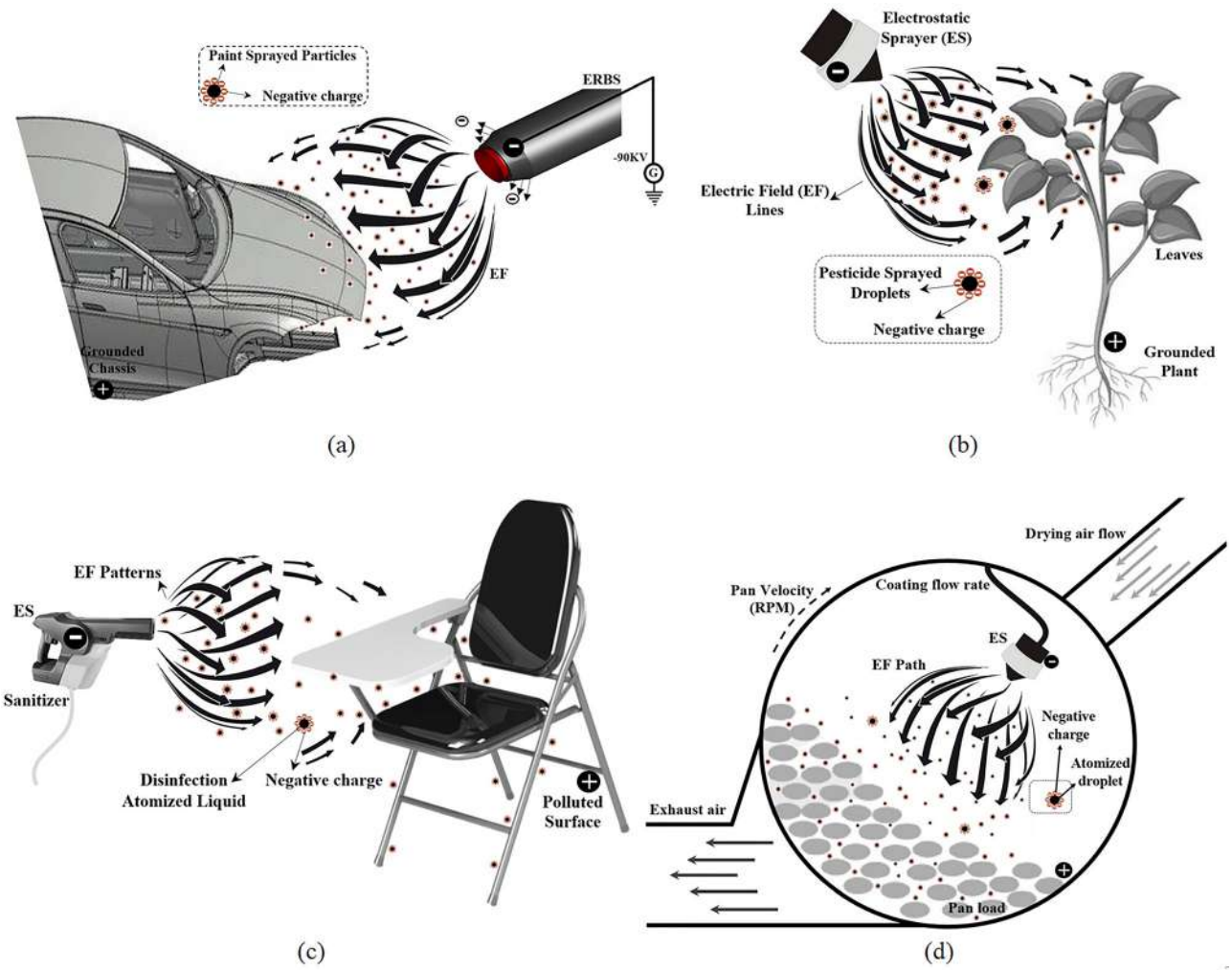

FIG. 16. Different applications of the electrostatic spraying technology: (a) automotive industries: charged paint droplets are harmonized and form a high-quality uniform film on the body, (b) agriculture practices: charged droplets adsorption on the leaf surface, (c) disinfection processes: spreading sanitizer on the polluted surface, and (d) Pharmaceutical companies: covering film coats on tablet surface.

Latheef, 2017; Patel *et al.*, 2015). Recently, system parameters investigation has been analyzed suitably, implementing the droplets charging process for the influential impact of pesticides on substrates (Appah *et al.*, 2019). Disinfections with an electrostatic sprayer provided efficient and quick decontamination. This important application of electrostatic sprayers makes them useful, particularly during the recent coronavirus (COVID-19) epidemic [see Fig. 16(c)] (Cadnum *et al.*, 2020; Pendar and Páscoa, 2020b). Also, electrostatic powder coating techniques are increasingly used in the pharmaceutical industry due to the higher film quality on tablets, replacing previous technologies (Yang *et al.*, 2017; Yang *et al.*, 2020). The formed film coats provide drugs physical or chemical protection from moisture, light, mechanical stress, taste masking, gastrointestinal tract irritation, and aid easier identification of patients [see Fig. 16(d)] (Fernandes *et al.*, 2019). The wraparound effect of the charged droplets minimizes off-target deposition and improves spray efficiency in the application mentioned above.

The usage of the electrostatic spraying technique as a fundamental and crucial application in the automotive industry [see Fig. 16(a)] will be discussed in the following.

Here, in order to enhance the readability and improve connectivity in the narration of the story, we introduce the main stated concept of each subsection of the present section. The idea, advantages, employment mechanisms, and applications in other areas of the electrostatic spraying method are addressed at the outset of this section. In Subsection V A, overall literature consideration on electrostatic coating with a focus on three key aspects, including (a) droplet formation, disintegration, and transportation, (b) electrical charging process, and (c) droplet size distribution of spray, is implemented. In Subsection V B, the ERBSs design and corresponded formed spray using various bell size and rim patterns (smooth or serrations), hybrid shaping air nozzle combination and angles, and the external electrode structures are described. Also, an automotive spray booth (an enclosure area for

electrostatic spray coating implementation) is characterized. Then, in Subsection V C, the strategy of various force interactions on sprayed droplets and their influence on the complicated turbulence airflow is reviewed. Furthermore, detection of airflow patterns, constructed vortical structures, and paint droplet path is analyzed. The presence of different designs of the external conductor is assessed. In Subsection V D, an examination of the produced spray size distribution effect on the paint film quality is accomplished. The most influential parameters on the droplet size distribution range are introduced. Explanation of liquid droplets traveling process and the paint disintegration stages (criteria for the film, ligaments, and droplet formation) in electrostatic spraying is covered in Subsection V D 1. Subsection V D 2. summarizes various experimental approaches for particle size assessment, e.g., shadowgraphy, and infrared thermography, for particle size assessment. Different data processing methods used for the experimental spraying are also introduced. The breakup process after disintegration and its various detection modes, besides the sprayed droplets evaporation process, are considered in Subsection V D 3. The ionization and charging mechanisms of droplets during the electrostatic spraying are explained in Subsection V E. Finally, various electric charging methodologies and external electric field manipulation are described in Subsection V E 1.

A. Literature review of electrostatic coating by rotary sprayers

Deep literature analysis of studies about coating processes during the spray painting by using the electrostatic rotary bell sprayers (ERBSs) is mandatory to enhance their TE and reduce material cost. ERBSs usage in the automotive and aerospace have been rapidly developed in recent years because of their exceptional atomization performance and high TE, up to 90% in ideal conditions (Pendar and Páscoa, 2019a). New complex designs of the ERBS due to the production of the uniform film with appropriate spatial atomization characteristics are broadly used in the automotive coating industries. Using them leads to a significant material cost and environmental hazard reduction (Akafuah *et al.*, 2016). These rotary sprayers are rarely used in a powder industry and spray drying (Kuhnhenn *et al.*, 2018).

Here, the theoretical, numerical, and experimental investigations about the electrostatic rotary bell atomizers have been described. These investigations mainly focus on three main areas of (I) droplet formation, disintegration, and transportation (Ellwood and Braslaw, 1998; Viti *et al.*, 2010; Pendar and Páscoa, 2020a; and Guettler *et al.*, 2020), (II) electrical charging process (O'Rourke and Amsden, 2000; Viti *et al.*, 2010; and Gödeke *et al.*, 2021), and (III) droplet size distribution of spray (Frost, 1981; Liu *et al.*, 1998; Wilson *et al.*, 2018; Darwish Ahmad *et al.*, 2018; 2019; and Oswald *et al.*, 2019).

Hines (1966) measured the sizes and specific charges of the atomized droplets via single-jet rotating cups during the electrostatic spraying process at the Ford company. His findings were the basis of a qualitative understanding of various operational parameters on the quality of the obtained paint film. Bell and Hochberg (1981) implemented the first major complicated examination of metallic electrostatic painting. They correlated a power-law relation for the mean droplet size as a function of the rotational speed, bell cup voltage, liquid viscosity and flow rate. Ellwood and Braslaw (1998) used a two-phase flow model to simulate external electrostatic spraying. They concluded that the electric field and charge-to-mass ratio play an important role in droplets' atomization, trajectory, and deposition rate.

Im (1999; 2001; 2004) investigated the technical challenges of the ERBSs. They reported the size and velocity of the atomized water-borne paint droplets in various operational parameters, including liquid and shaping air flow rate, bell cup rotational speed, and high-voltage setting. Their results illustrate that the bell cup rotational speed is a dominant parameter, and increasing it produces finer droplets and reduces the spray cone diameter. The spray pattern was also strongly influenced by the paint flow rate and high voltage setting. Higher electric voltage resulted in denser and more uniform dispersion in the spray cone core. The higher values of liquid and shaping air flow rate caused widening and narrowing of the formed spray cone pattern, respectively. Figure 17 confirms the effects of mentioned key operating parameters on the overall spray pattern generated by the ERBS (Behr Eco-bell 55 mm diameter, a serrated edge, designated 55S), which were photographed with the SLR camera with an exposure period of 33.3 ms (Im *et al.* 2001). In Im *et al.* (2001; 2004) research team studies, although the electrical charging process, especially the effect of implementing the external charging electrodes to provide a reliable electric field were considered precisely (see Fig. 17), the breakup and coalescence of droplets and their interaction with air remain ambiguous.

Bell and Hochberg (1981) developed an empirical relationship between the main influential operational parameter and the mean droplet size ($\bar{D}_p$) during the spraying by the ERBS to establish a mean droplet diameter,

$$\bar{D}_p = f\left(V_{Cup},\, \omega,\, \dot{V}_L,\, \mu_L\right) = C V_{Cup}^{-0.2} \omega^{-0.7} \dot{V}_L^{0.4} \mu_L^{-0.2}. \tag{1}$$

This empirical relationship is founded on the bell voltage (V_{Cup}), bell cup rotary speed (ω), fluid flow rate ($\dot{V}_L$), and viscosity of the spray material (μ_L), as key factors mentioned in Fig. 17. The constant (C) relies on the employed bell cup geometry (Colbert, 2007).

A detailed list of the available empirical correlations related to the effective parameters on the mean droplet size produced by the rotating disk atomizers are presented in reference Ahmed and Youssef (2012). This information can be helpful for getting an in-depth understanding of the mentioned issues and redesigning the conventional apparatus. For instance, Kayano and Kamiya (1978) developed a correlation for the mean droplet sizes produced by a rotating disk as follows:

$$d_{32} = 2.0 D^{-0.69} \omega^{-0.79} \dot{V}_L^{0.32} \mu_L^{0.65} \sigma^{0.26} \rho^{-0.2}. \tag{2}$$

Ye *et al.* (2003; 2005), in their numerical simulation of the ERBS, evaluated the TE and paint film pattern on the target without taking into account the interaction among droplets. For particle size and trajectory measurement, they used particle sizer of Spraytec Fraunhofer-type. Domnick *et al.* (2005; 2010) used the CFD tool to examine the electrostatic spray painting with internal and external charging methods. Viti *et al.* (2010) applied the finite element method combined with the Lagrangian approach for analyzing paint droplet trajectory influenced by the electric fields. They concluded that the presence of a space charge affects the TE and paint film thicknesses. Then, Toljic (2010) three-dimensionally simulated the electrostatic spraying and found that increasing the average charge-to-mass ratio enhanced the TE. In a spray with a broader size distribution, larger droplets carried more charge, resulting in a higher TE.

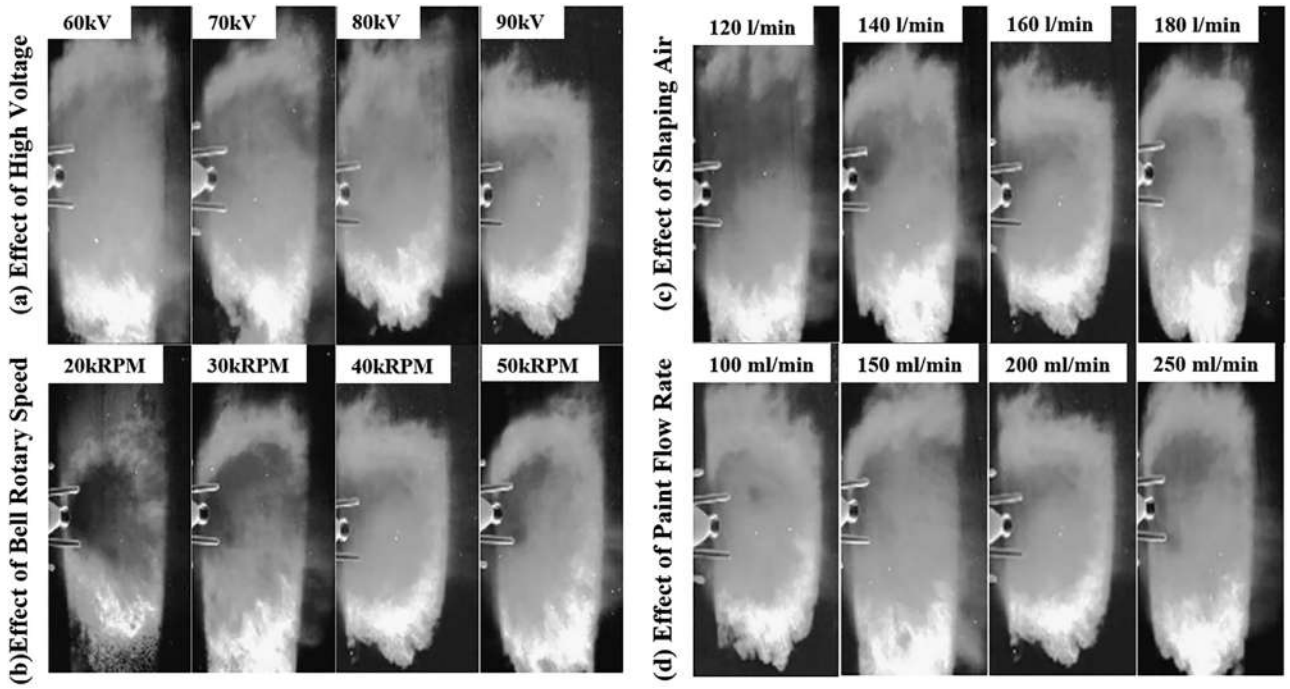

FIG. 17. Parametric analysis of four key operating factors on spray pattern produced by ERBS (Behr Eco-bell 55 mm diameter, serrated edge, designated 55S): (a) high voltage setting (60–90 kV), (b) bell rotational speed (20–50 kRPM), (c) shaping airflow rate (120–180 l/min), and (d) liquid flow rate (100–250 ml/min). Reproduced with permission from Im *et al.*, "Visualization and measurement of automotive electrostatic rotary-bell paint spray transfer processes," J. Fluids Eng. **123**, 237 (2001). Copyright 2001 ASME.

Inkpen and Melcher (1987), Fukuta *et al.* (1993), and Im *et al.* (2004), after investigating the factors that can be the reason for color change, stated that the aluminum flakes distortion with the paint during the pass to the target is the main reason. Using ERBSs with metallic paints facing with the apparent color changes problem. To minimize aluminum flake distortion, setting the optimal range of the bell cup rotational speed for producing fine droplet sizes with sufficient high air velocity to retain flake orientation is essential. Striking a balance between the metallic paints' color quality and the TE persists for ERBSs. Their TEs were around 65%, considerably lower than the TE of a normal ERBS's procedure 90% (Im, 1999). The traverse of the spray guns can be considered in the CFD simulation in two ways: using a dynamic mesh method (Toljic *et al.*, 2012; 2013) or static integration (Domnick *et al.*, 2006; Dominick and Thieme, 2006; and Toljic *et al.*, 2011). Toljic *et al.* (2012; 2013) determined the paint film thickness on the moving body during the electrostatic painting process using a commercial CFD solution. They revealed that higher film deposition uniformity in the moving body is obtained compared to stationary ones and strongly modified the TE values and the deposition profile. Colbert and Caircross (2005) reported that the accumulation on edge increased when a deposition at the flat body with a ring model was employed. During the electrostatic coating process, dynamic targets influenced the deposition processes, resulting in the formation of a boundary layer on the workpiece. Mark *et al.* (2013) simulated the electrocoating process for car fenders and plates as a dynamic target by coupling the airflow field, electric field, and droplet charging process. Zuzio *et al.* (2018) and Yu *et al.* (2017) developed an Eulerian–Lagrangian coupling model to have a more accurate transition between two phases. They examined the accuracy of spraying process simulation on a planar liquid sheet and diesel complex dynamics spray, respectively. Ray *et al.* (2019) developed a generic model for predicting droplet evaporation rate, fluid ligament diameter, and droplet size of water and clearcoat using a rotary bell atomizer. These models allowed for the development of the nozzle parameter and minimized the evaporation amount, following air pollution reduction as a desired goal.

Figure 18 illustrates the map of overall effective factors on the atomization and deposition rate in the electrostatic coating process by the high-speed rotary bell sprayer. In the electrostatic spray coating by rotary bell sprayers, five primary areas must be considered: geometric setup, paint liquid characteristics, electric field structure, bell cup rotational speed, and shaping air flow properties. Based on the investigation of literature, the parameters of bell rotary speed, shaping airflow rate, high voltage setting, and liquid flow rate, in order, are the four key operating factors (significantly manipulated the spray plum structure) while using the ERBSs (see Fig. 17), deeply considered in our paper. However, the efficient operation of the ERBSs depends on balance between several parameters like the geometric structure of the spray booth, workpiece, ERBS (e.g., bell cup diameter, angle and rim pattern, electrode structure) (see Fig. 18) and coating environmental conditions are vital in determining the TE, spray spatial distribution and formed film thickness, quality and uniformity.

The mathematical formulation for electrostatic spraying includes the Eulerian (airflow and electric field) and Lagrangian (paint droplets) models. The compressible Navier–Stokes equations are used for airflow field computing. The numerical modeling of the most critical

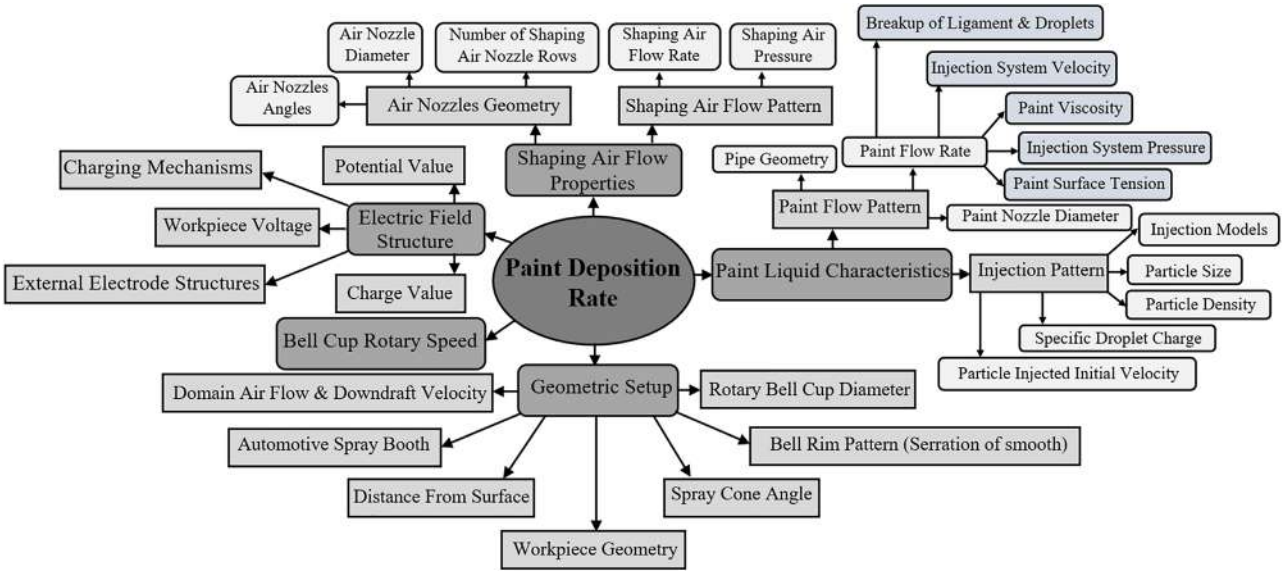

FIG. 18. Map of crucial factors influential on the electrostatic coating process efficiency, using high-speed ERBSs.

procedures of droplets traveling, evaporation and breakup processes description, electric field modeling and formed paint film construction have been described in this section.

B. Structure of ERBS and description of spray booth

The conventional designed ERBS that is commercialized by SAMES (SAMES Technology, 2019) (see Fig. 19), faced different modifications during recent decades. Some researchers looked at the ERBS design as a crucial effective parameter in coating quality and TE. The ERBSs are differentiated by a wide range of bell cup diameters, ranging from 20 to 70 mm, and a high rotational speed of up to 70 kRPM. Tanasawa *et al.* (1978), Panneton (2002), and Kazama (2003) compared the formed spray plume pattern and paint film quality via various atomizer structures that are operating under different conditions. Honma *et al.* (1999) investigated these shaping air nozzles design in the ERBS by examination of the number and size of the nozzles to redirect the path and velocities of disintegrated paint droplets. Then, Guettler *et al.* (2017) examined a hybrid bell atomizer consisting of 60 shaping air nozzles, half perpendicular to the bell edge and others with

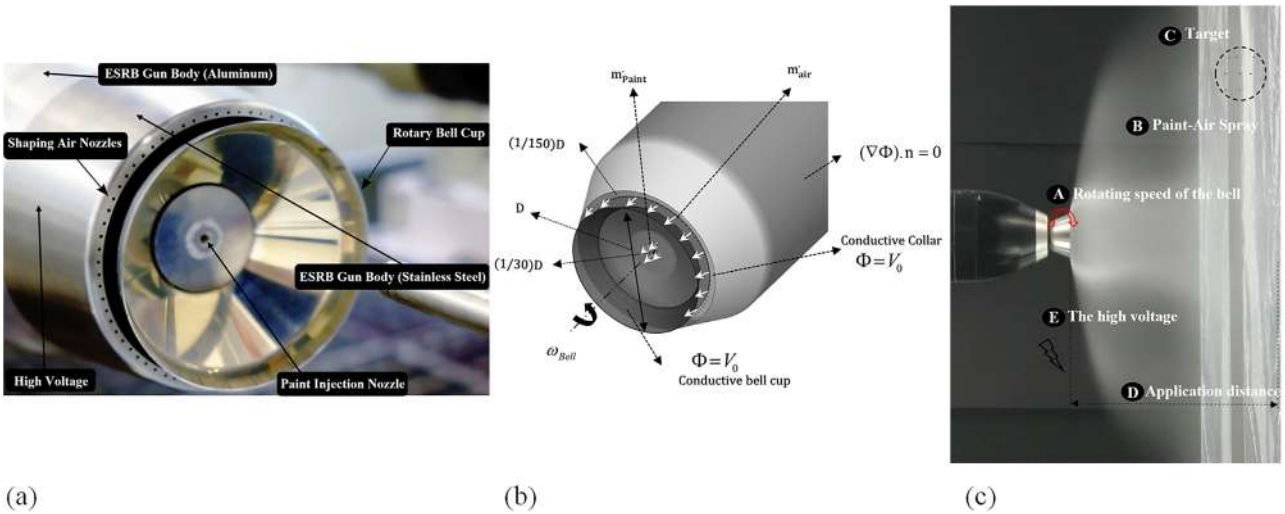

FIG. 19. (a) The PPH 308 model of the high-speed ERBS photograph is produced by SAMES-KREMLIN, (b) detailed visualization of the ERBS's dimension and boundary conditions, and (c) operation condition. Reproduced from Pendar, M. R. and Páscoa, J. C., "Numerical analysis of charged droplets size distribution in the electrostatic coating process: Effect of different operational conditions," Phys. Fluids **33**(3), 033317 (2021) with the permission of AIP Publishing LLC.

a given angle of 45°. Their numerical and experimental results demonstrated that the secondary shaping air nozzles (arranged at 45°) strongly impacted the airflow field around the sprayer. Toljic *et al.* (2010) visualized the electric field between the added planar electrode's structure and analyzed the dependency of the sprayed droplet size on their charge. Their findings also revealed that the radius in direct contact with the planar electrode had an exponent of two. Domnick (2010) analyzed the size distribution of paint droplets using bell geometries with cross-wise and straight serrations in various operational conditions. The term "serrations" refers to a machined line that extends ≈ 1–2 mm from the cup's outer edge and is intended to create ligaments when paint drips over the bell edge and prohibits it from escaping the bell cup as a film. Both of the mentioned serrated bell cups produced a bimodal distribution of droplet size with lower maximum size values than bell with no serrations. Pendar and Páscoa (2020a) examined droplet size distribution while changing the bell cup dimeter. They reported that enlarging the cup's diameter reduces the size distribution of the droplets. Pendar and Páscoa (2022a) added the high-voltage retractable blades or high-voltage adjustable control ring as a conductor to the ERBSs to manipulate the spray pattern. Their invention has advantages of higher coating transfer efficiency, reduction of losses of the liquid or mixture dispensed, and less environmental impact.

An automotive spray booth is an environmentally controlled enclosure area required during spray coating to improve the TE of the final coat. It includes handling systems for: (I) directing and removing float paint particles called overspray, (II) capturing VOCs, and (III) controlling humidity, temperature (monitoring through a tight operational window), and cleanliness (using dust and insect filters). As shown in Fig. 20, a typical automotive spray booth contains robot arms, sprayers (here, ERBSs are used), an intake air supplier and sliding rails in the portion above the floor grating. The part under the floor grating of the spray booth includes a water pond, air exhauster, return sluice and scrubber tube. A minimum downward air velocity in a booth's upper section of ≈0.5 m/s (100 fpm) is commonly used (Mitchell, 2020). The coating process in the modern spray booth designs is implemented using high-speed electrostatic rotary bell spray guns (ERBSs) or high-volume-low-pressure spray guns (HVLP). The ERBSs are mostly used for manual spraying for automatic painting with robot assistance, and the HVLP sprayers are commonly used for manual spraying.

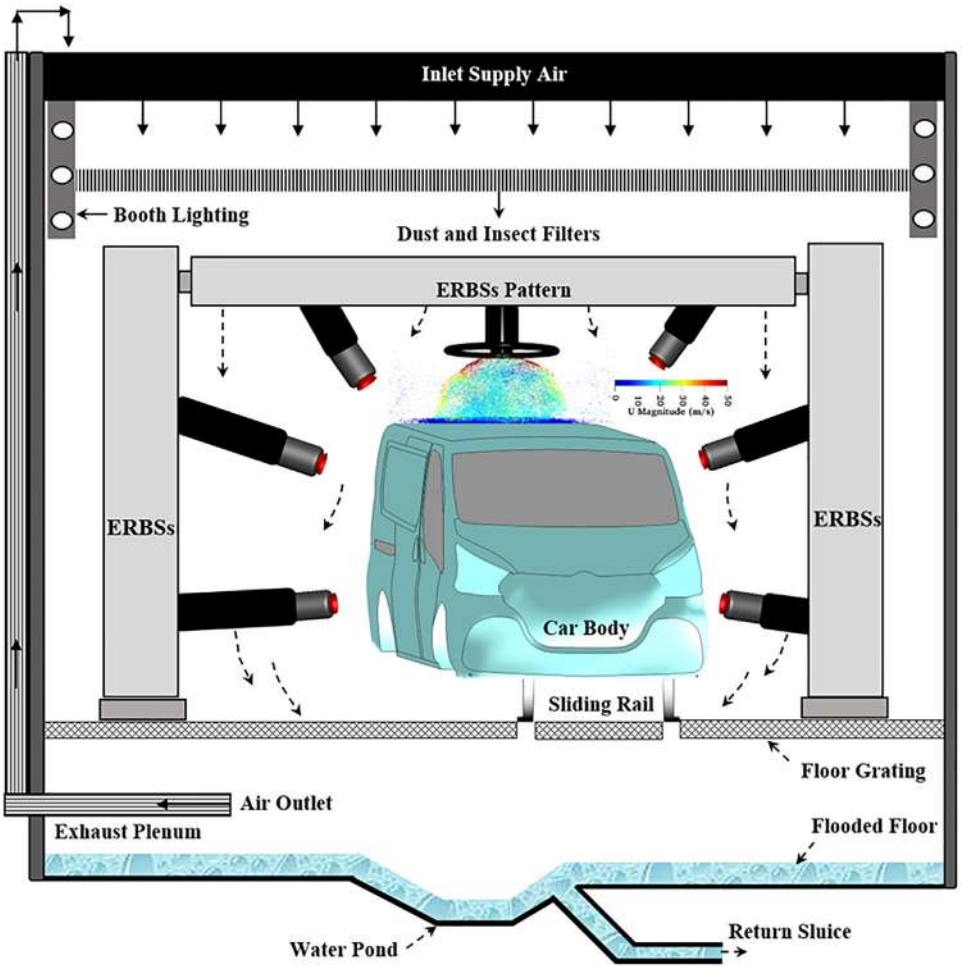

FIG. 20. Schematic representation of an automotive spray booth assembly.

C. Paint-air flow pattern and forces in ERBS

The influence of the force interaction on the paint droplets, the complicated airflow, and paint droplet trajectories pattern during the electrostatic spraying in the ERBS is a critical issue that needs to be considered. The schematic representation of these forces interaction on droplets is shown in Fig. 21.

The strategy of how various forces interact on the spraying paint droplets will be explained following. The distributed paint liquid sheet over the rotary bell cup surface is subjected to extreme centrifugal force due to high rotational speed and breakups into the smaller distribution of droplets after the formation of ligaments. Then the high-speed shaping airflow that exits from the nozzles, and the electric forces as dominant powers, alongside the other forces, e.g., gravity, Stokes drag and evaporation, manipulate and direct the paint droplets of spray plum cloud around the bell cup to reach the maximum TE. The air flow patterns trajectory constructed by the ERBSs operations (as shown in the left sub-frame of Fig. 21) are divided into four main behaviors of (a) shaping airflow stream, (b) outside toroid−shape air vortices, (c) inside toroid−shape air vortices, and (d) trapped air vortices. Paint droplets path are also divided into four primary categories of (e) paint droplet toroid-shape vortex, (f) larger size of paints droplet trajectory, (g) smaller sizes of paint droplet trajectory and (h) rebounded droplet from the body with the circular pattern. Recognizing the mentioned air-paint flow patterns and forces interaction is valuable for researchers and designers to project and introduce a more optimum version of ERBSs.

Due to the high-speed operating conditions of the ERBSs and resultant flow with high turbulence, the examination of the re-circulated vortical structures that play a vital role in the paint path is crucial (Pendar and Roohi, 2015). Yasumura *et al.* (2011a) considered the re-circulating flow around the ERBS during their numerical simulation. They showed that the inner re-circulation draws smaller droplets to the radial direction, preventing them from adhering to the body surface. The cross-sectional axial streamline patterns during the electrostatic spraying using various conductors are shown in Fig. 22 (Pendar and Páscoa, 2022a). In this figure, the line integral convolution (LIC) technique (Stalling and Hege, 1997) is implemented for better visualization. The high-voltage adjustable control ring [Fig. 22(b)] and retractable blades [Fig. 22(c)], which are added as a conductor to the ERBSs, manipulate and optimize the re-circulation airflow pattern around the sprayer's head compared to conventional ones. The airflow velocity decreased significantly in the blocked region inside the spray plum and accelerated close to the bell cup. Pendar and Páscoa (2022a) declared that the electric field, during the use of the same sprayer, does not have an influential effect on the vortical patterns. The inner (V_1) and outer (V_2) recirculation zones and vortical breakdown mechanisms are also represented. In the higher bell cup rotational speed, the length of the recirculation zone becomes more extensive, and the attachment position moves upstream (Stevenin *et al.*, 2015; Pendar and Páscoa, 2020). These evaluations provide helpful information about the airflow pattern for designing a new ERBS generation, which will be more efficient.

D. Spray size distribution produced by ERBS

The generated size distribution of droplets by operating the ERBSs has a considerable impact on the TE and formed paint film quality on the target surface. The smaller size of droplets produces

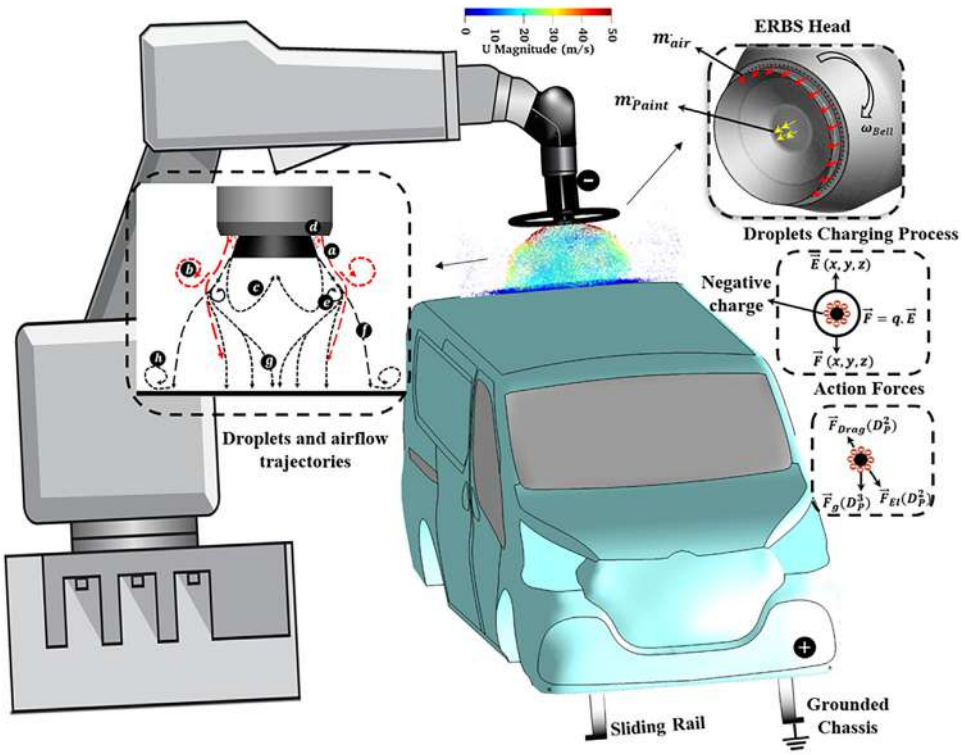

FIG. 21. Schematic representation of automotive electrostatic spray coating procedure using an ERBS system.

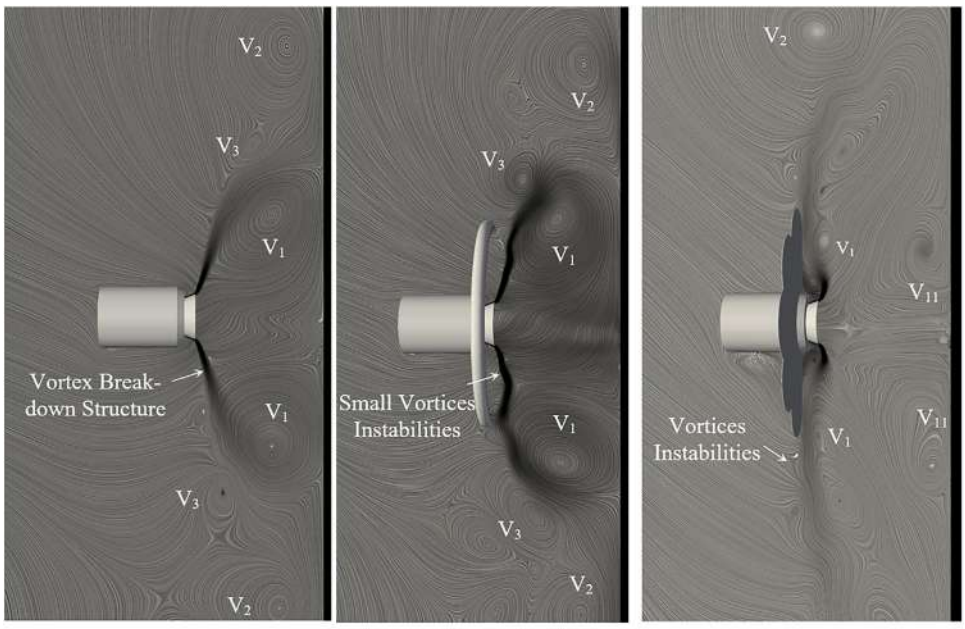

FIG. 22. Visualization of re-circulating flow around various ERBSs system, shown by the LIC method: (a) Conventional ERBS system, (b) ERBS with high-voltage adjustable control-ring and (c) ERBS with high-voltage retractable blades. Reproduced from Pendar, M. R. and Páscoa, J. C., "Numerical analysis of charged droplets size distribution in the electrostatic coating process: Effect of different operational conditions," Phys. Fluids **33**(3), 033317 (2021) with the permission of AIP Publishing LLC.

better finish quality with the lower TE due to the stronger effect of air drag forces on them, which disturb and deviates their paths. In other words, fine droplets are evolving a dry spray over time (Di Domenico and Henshaw, 2012). Flakes, which can be applied to paint formulations to improve the esthetic appearance and color flopping of a surface, are likewise incompatible with very fine droplets (Basu *et al.*, 2010). The droplet with larger sizes produces uneven and rough film thicknesses, usually with the higher TE due to higher momentum and lower drag forces of droplets. The droplet size distribution is mainly determined by atomization performance, which is controlled both the finish quality and the TE (Kwok, 1991). The most dominant parameters affecting the droplet size distribution while operating the rotary bell atomizer are the inlet liquid properties and flow rate, air inlet flow rate, cup or disk design configuration, and the bell cup rotational speed. Based on the published work, the inlet liquid flow rate and the rotational speed are the most influential parameters on the range of the droplet size distribution during atomization (Ray *et al.*, 2015).

In the following, the effect of mentioned factors on the spray size distribution brought in related references will be discussed. Some basic studies dealing with the ERBSs have considered the droplet size by changing the cup rotational speed and paint flow rate (Hinze and Milborn, 1950; Frost, 1981; Liu *et al.*, 1998; and Ellwood and Braslaw, 1998). They reliably confirmed the reduction of droplet size distribution by increasing the rotational speed while growth by enhancing the volumetric paint flow rate, albeit less pronounced. Growth in the paint viscosity generally raises the spray's SMD, contributing to a liquid flow rate decrement (Schick, 2006; Lefebvre and McDonell, 2017). Yasumura *et al.* (2011b), through numerical simulation of the ERBS, realized the impressive impact of electric voltage on the medium paint droplet size ($d_p \approx 10$–$40\ \mu$m) and shaping air on the small ($d_p < 10\ \mu$m) or large ($40\ \mu m < d_p$) size of the paint droplet. Ahmed and Youssef (2012) analyzed the effect of non-dimensional parameters of the Reynolds number, Weber number, and flow coefficient on the droplet size range, in other words, the SMD. Ahmed and Youssef (2014) presented a comprehensive evolution on the disk and cup geometrical optimization effect on the SMD and velocity of droplets. Many experimental research, such as those by Liu *et al.* (2012) and Ahmed and Youssef (2014), focused on the size of the droplets formed during the disintegration process and the transition between the film, ligament, and droplet modes. Ye and Domnick (2017) proposed a set of comparative results of the droplet dynamics impact of various atomizers, namely airless gun, pneumatic air spray gun and a high-speed rotary bell in terms of size distributions. In the case of the rotary bell atomizer, significantly finer droplets were obtained (average diameter of $\approx 15\ \mu$m), which deposited mainly near the spray pattern center, compared to the airless gun (average diameter of $\approx 310\ \mu$m). Wilson *et al.* (2018) experimentally visualized the formation of the ligament and droplets. They showed that the SMD and ligament sizes decrease around one quarter at a very high rotational speed. Darwish *et al.* (2019) examined the droplet size distribution by applying a 3D mapping style for a rotary bell sprayer and revealed that the size ranges increase by enlarging the lateral distance. Shen *et al.* (2019) investigated the non-Newtonian droplet disintegration phenomenon. Oswald *et al.* (2019) showed that the elongational resistance affected the disintegration process inside the bell cup atomizer. They mentioned that the complicated nature of droplet size prediction during numerical stimulation of spraying still needs more attention.

1. Droplets formation, transportation, and deposition in ERBS

The injected paint's travel in electrostatic spraying is divided into three stages: (I) inside the bell (film, ligament and droplet formation) (Fig. 23), (II) transport distance, and (III) target deposition. Inside and

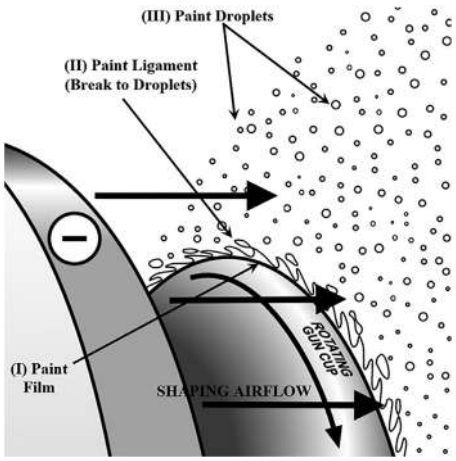

FIG. 23. Schematic view of the paint film, ligament, and droplet formation processes around the bell cup rim.

near the bell cup, three prominent phenomena of paint atomization, ionization and electrical charge occur. During the transport phase, the shaping-air interaction with turbulence flow, the electric field effect on the atomized droplet, and primary and secondary breakup processes are the main phenomenon (Im *et al.*, 2001). In numerical modeling of the ERBSs, the charged droplets' trajectory is described by solving a set of differential equations based on Newton's law to determine their velocity and position of them at each instant, detailed in Pendar and Páscoa (2020a). In the final stage, the downdraft flows that affect the droplets' position and paint film features are considered on the target body surface.

Inside the cup, the produced sheet disintegrated into the detached sheet fragment due to aerodynamic waves imposition. Under the influence of surface tension, these fragments transform into ligaments, which then breakup into droplets. Then, in the mechanism of second ligament production, liquid flows from a torus around the cup periphery in the form of elongate curved ligaments that disintegrate into the non-uniform droplets at a longer distance from the cup. Finally, the droplets hit the target and produce a uniform film on the body surface. Numerous studies have been devoted to determining criteria for film, ligament, and droplet formation mechanisms. Hinze and Milborn (1950) and Fraser *et al.* (1963) defined dominant mechanisms condition and reported empirical correlations to determine the transition point between them. Kamiya and Kayano (1972) obtained a relation for the maximum diameter of the droplet during sheet-type disintegration in a rotating disk. Dombrowski and Lloyd (1972) examined the effect of liquid viscosity on the droplet formation and size distribution over the rotary bell atomizer. Frost (1981) analyzed the ligament formation on the rotating disk and developed the available criteria for the ligament's construction. Kawase and De (1982) were the first who examine the mechanisms of the droplet formation on spinning disks while non-Newtonian liquids were consumed. Domnick and Thieme (2006) revealed that when the bell cup rotational speed increased, the fragment pattern became less consistent. Based on the experimental data, Liu *et al.* (2012) investigated ligament and droplet formation mechanisms and correlated an equation for droplet size over a broad range of operational conditions. Liu *et al.* (2013) implemented a mathematical model to predict the critical parameter of the wavelengths, the unstable growth rates, the breakup times, the film lengths, and the droplet sizes, which were validated by the experimental data. Shen *et al.* (2019), in their experiment, analyzed the evaluation of the wall film formation inside the rotary bell cup surface with a series of snapshots that were taken by a high-speed photographic camera (Fig. 24). Moore (2017) evaluated the transition disintegration process, from paint ligaments to droplets, during using of serrated and non-serrated rotary bell cups in various paint flow rates. They proved that in a high paint flow rate, the serrated bell cup retains regular spacing between the ligaments (frame II in Fig. 25), while the non-serrated shows more random spacing and irregular ligament length (frame V in Fig. 25). For both serrated and non-serrated cups, higher paint viscosity produces longer and more stable ligaments, which delays the disintegration into droplets (frames III and VI in Fig. 25).

2. Practical techniques for spray droplet size assessment

This part summarizes the available experimental approaches for assessing particle size distribution when atomizing by a rotary sprayer, e.g., shadowgraphy, infrared-thermography-based and high-speed imaging-phase Doppler interferometry techniques. The shadowgraphy technique utilizes a pulsed laser (freeze motion) to backlight the spray plume to take non-blurred images via synchronized cameras to obtain data on the size and velocity of sprayed droplets. Akafuah *et al.* (2010) developed the infrared-thermography-based method for qualitative characterization and visualization of the paint spray flow field and evaluated it during the operation of the high-speed rotary bell and HVLP sprayers. In this method, which is widely used in the recent works, e.g., Darwish Ahmad *et al.* (2018; 2019), a uniformly heated background acts as a thermal radiation source, and the infrared intensity is captured by an infrared camera as a receiver, proving the attenuation in the image as a result of the spray existence. Recently, Dhivyaraja *et al.* (2019) characterized the dynamical features of the sprays as well as the drop size and velocity spectra using high-speed imaging and phase Doppler interferometry method, respectively, in their experimental study of swirl atomizer.

In the following, an example of the implemented experiment for droplet size determination has been conveyed. The droplet size distributions histograms of a non-serrated rotary bell cup sprayer were

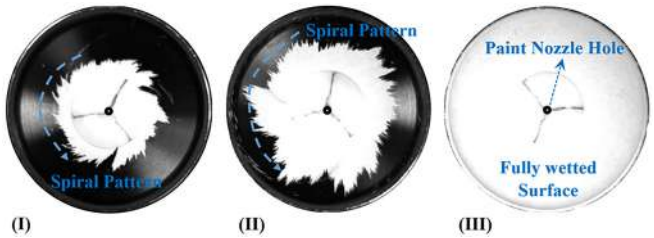

FIG. 24. Paint film propagation inside the rotary bell cup surface, a series experimental snapshot ($\omega_{bell} = 30kRPM$, $\dot{m}_{paint} = 400\text{ml/min}$). Reproduced with permission from Shen *et al.*, "Primary breakup of a non-Newtonian liquid using a high-speed rotary bell atomizer for spray-painting processes," J. Coat. Technol. Res. **16**, 1581–1596 (2019). Copyright 2019, Springer Nature.

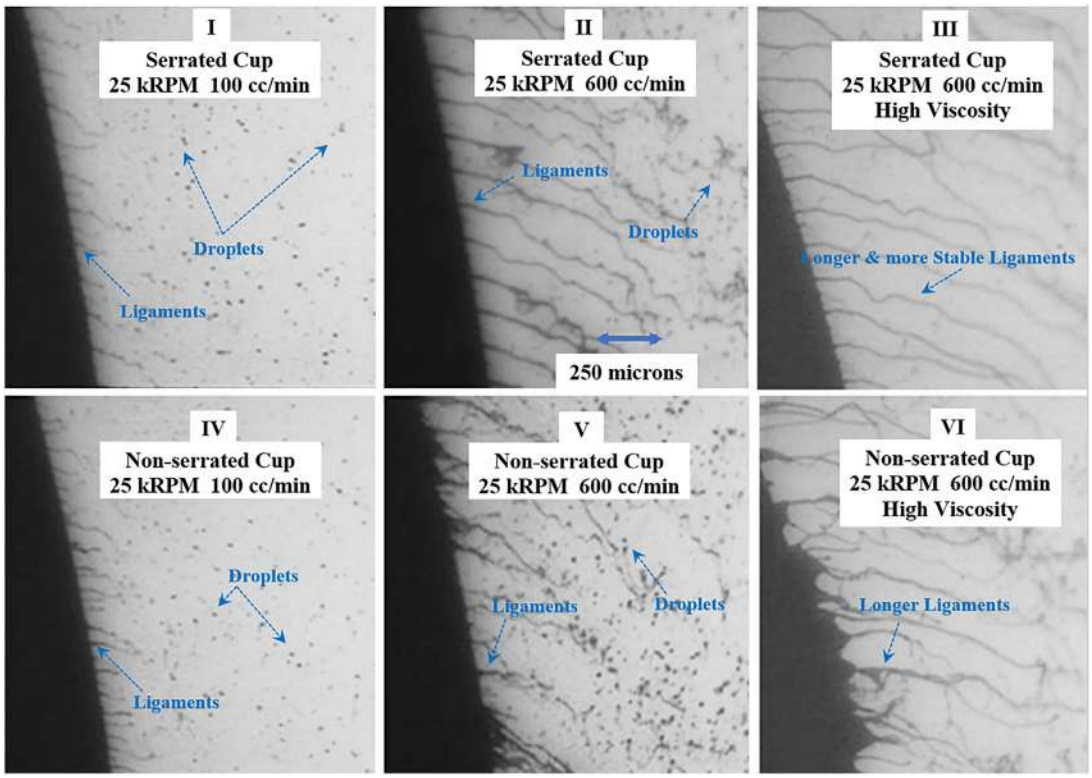

FIG. 25. Experimental shots of the transition disintegration process (ligament to droplets) for serrated and non-serrated bell cups. From Moore, J. R., *Protective Coatings*. Copyright 2017 Springer Nature. Reproduced with permission from Springer Nature.

compared with a standard pneumatic atomizer for an automotive basecoat in Fig. 26 (Moore, 2017). The results were obtained for the paint and airflow rate of 360 ml/min and 465 slpm, as well as bell cup with diameter and spinning of 65 mm and 20 kRPM. The shadowgraphy technique is used for obtaining the droplet size distribution (Berg *et al.*, 2006), which can be fitted precisely through gamma distribution (Keshavarz *et al.*, 2016). To simpler convey the information contained in the spray droplet size ranges, single metrics, such as the arithmetic mean diameter and Sauter mean diameter (SMD), are used. The polydisperse pattern distribution with the arithmetic mean

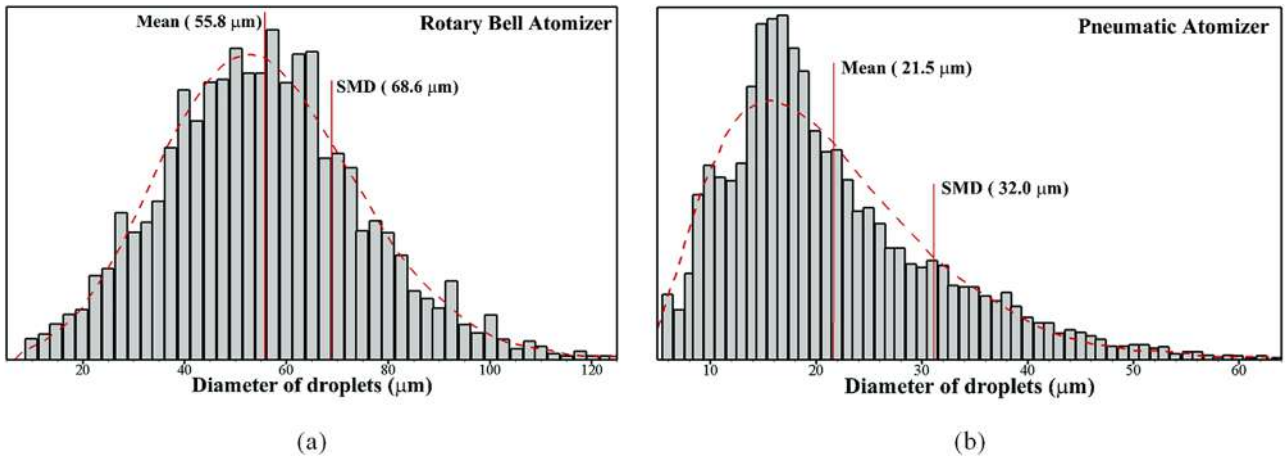

FIG. 26. Size distribution of paint droplets sprayed from typical automotive: (a) rotary bell atomizer and (b) pneumatic atomizer, implementing a gamma distribution to fit the data. From Moore, J. R., *Protective Coatings*. Copyright 2017 Springer Nature. Reproduced with permission from Springer Nature.

diameter of 21.5 μm was obtained for the pneumatic atomizer. While, for the rotary bell atomizer, the monomodal distribution with a mean diameter of 55.8 μm was reported (Moore, 2017). Domnick (2010) and Pendar and Páscoa (2020a) similarly observed a monomodal distribution of droplet size for a using non-serrated rotary bell cup sprayer, while Basu *et al.* (2010) and Domnick (2010) described bimodal distributions for serrated bell cup sprayer at the higher rotational speed.

Figure 27 compared the predicted SMD in various bell cup rotation speeds and paint flow rates using a smooth or serrated rotary bell cup sprayer (Moore, 2017; Domnick, 2010; and Pendar and Páscoa, 2020a). Domnick's results using viscoelastic paints produced larger droplet sizes than predicted by Tanasawa's Newtonian model in both cases. Nevertheless, all considered references agree that the rotational speed of the bell cup is the dominant parameter for the droplet size control. The results of Domnick's study contradict Tanasawa's prediction that serrated cups would generate smaller droplets than smooth bell cups. The difference in the atomization mode, summarized by Ahmed and Youssef (2012), can be considered the reason for this discrepancy. The rate of increase in SMD with increasing flow rate is identical when the result of Domnick (2012) for a smooth cup is plotted alongside Tanasawa's predicted values.

3. Droplets breakup and evaporation process

The breakup process during the operation of the rotary sprayer is one of the most important phenomena that must be considered. Inside the head of rotary bell cup, the ejected liquid paint is subjected to the extreme centrifugal force due to the rotational speed, breakups into the smaller droplet size distribution after film and ligaments formation. Generally, in spray modeling, the droplet breakup process is divided into primary and secondary modes. In primary breakup, the condition of droplets, like diameter and angle at the point, will start to be determined. In other words, in an aspect of the experiment, the breakup process inside the rotary cup is divided into droplet deformation, rim formation, rim expansion, and rim breakup (Jackiw and Ashgriz, 2021). During the transport phase of droplets from the bell cup to the target, the secondary breakup process is a prominent phenomenon (Im *et al.*, 2001). This process explains the decomposition of the big droplets via normal stresses (instability of Rayleigh–Taylor) and also by stripping of the very small particles (instability of Kelvin–Helmholtz). Recently, in an estimate for primary breakup during the electrostatic spray modeling, the Rosin–Rammler ($Y_d = \exp(-d/\bar{d})^n$) and Chi-squared approaches have been used broadly to model the distribution of the initially injected droplets during the electrostatic spray modeling (Pendar and Páscoa, 2020a). The Rosin–Rammler model generates a more acceptable droplet distribution that matches the experimental distribution (Pendar and Páscoa, 2020a). Many previous numerical studies for spraying, like Osman *et al.* (2015b), ignored using the primary breakup model and ejected different droplet size ranges from the presumed multiple injection points in the rotary bell sprayer by trial-and-error and then compared with experimental results. The capability and strength of different efficient secondary breakup models of the Reitz–KHRT Hybrid (Bellman and Pennington, 1954), Reitz–Diwakar (Reitz and Diwakar, 1986; 1987), Pilch–Erdman (Pilch and Erdman, 1987), Taylor analogy breakup (TAB) (Tanner, 1997) and modified TAB (Pendar and Páscoa, 2020a) are examined for breakup process during the electrostatic spraying in reference Pendar and Páscoa (2020a). They showed that the modified table model, which applied a non-linear turn to account for the large viscosity droplet, is in a better agreement with the experimental data. Pendar and Páscoa (2020a) proved that the secondary breakup model has a minimal effect on overall spray form but a more pronounced impact on the droplet size distribution and SMD.

Huang *et al.* (2000) modeled breakup procedures that the smaller size of droplets produced in a rotary cup atomizer. Saha *et al.* (2012) examined the breakup modes of liquid emitted from a hollow cone nozzle generated by the pressure-swirling vehicle. They were

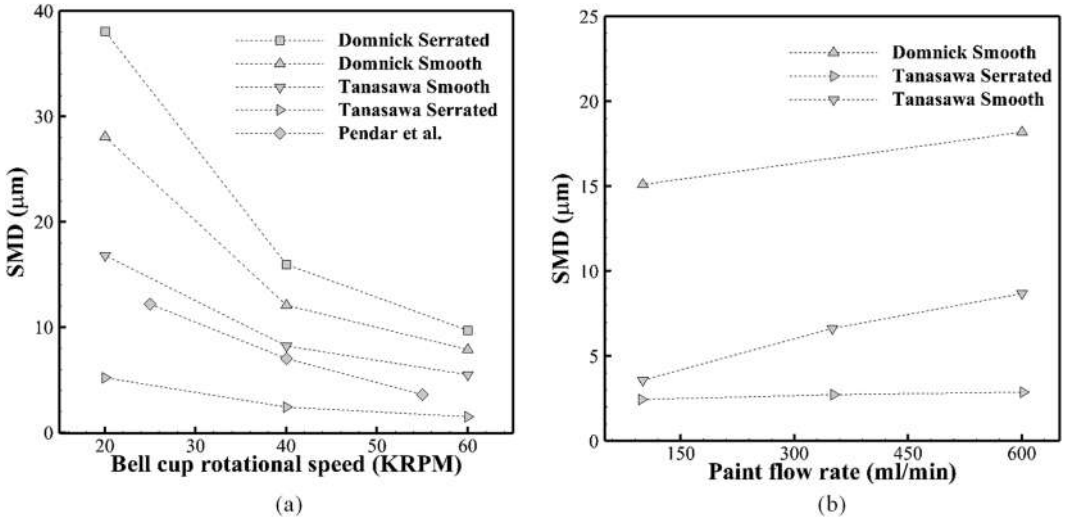

FIG. 27. SMD predictions for various (a) bell cup rotational speed and (b) paint flow rate. Adapted with permission from Pendar, M. R. and Páscoa, J. C., "Atomization and spray characteristics around an ERBS using various operational models and conditions: Numerical investigation," Int. J. Heat Mass Transfer **161**, 120243 (2020a). Copyright 2020 Elsevier.

considered the liquid primary and secondary breakup modes precisely. Andersson *et al.* (2013), as the main question in their research, considered whether the Taylor table model could be used in droplet size prediction during the spraying with a rotary bell sprayer. They found that the original table model can capture the overall shape of spray plume and the droplets size distribution, but with overestimation of viscous fluids breakup in higher rotational speed, resulting in so small particles. Shen *et al.* (2017) struggled with the primary liquid breakup process, film formation and propagation on the rotary bell inner surface while operating a high-speed rotary bell sprayer. Stefanitsis *et al.* (2019) and Kim *et al.* (2010) modified the breakup process by simulating the application of diesel spraying.

The lack of available studies focusing on the evaporation phenomenon in the ERBS's operation is evident. The droplet evaporation and heat transfer to the atmosphere during the electrostatic spraying is considered in studies of Shrimpton and Laoonual (2006) and Arumugham-Achari *et al.* (2015). Brentjes *et al.* (2020) investigated the implementation of the electric charge and its effect on the droplet's evaporation process. They reported a significant increment in the cooling rate and the TE, which becomes almost double. Droplet energy balance evolution for evaporation modeling during spraying is explained in reference Pendar and Páscoa (2021). Recently, Ranz and Marshall heat transfer approach (Ranz and Marshall, 1952) has been broadly employed to evaluate the droplet's mass due to the evaporation process. The temperature of the droplets is computed by solving energy and enthalpy equations, which are presented in detail in Dbouk and Drikakis (2020).

E. Electric field and droplets charging process

The proper performance of the droplet charging process and electric field creation and dispersion are key challenges in using the ERBSs. As recently published studies of electric field effect on the spray coating by the ERBSs, references Ye *et al.* (2005), Domnick *et al.* (2005), Colbert (2007), Toljic *et al.* (2011), and Pendar and Páscoa (2019a; 2019b; 2020a) can be mentioned.

The mechanisms of droplet charging as a primary factor in controlling the spray pattern are described in reference Ellwood and Braslaw (1998). Higashiyama *et al.* (1999) compared the spray pattern when charged and uncharged droplets were atomized from the airless nozzle. According to Im *et al.* (2001), proper electric field application greatly improves coating efficiency. During the spraying process, Ye *et al.* (2002) imposed a corona charge mechanism. Their findings reveal a significant dependence of the particle size on the space charge. Böttner and Sommerfeld (2002) coupled electric field with continuous airflow field in a two-dimensional static symmetric sprayer simulation.

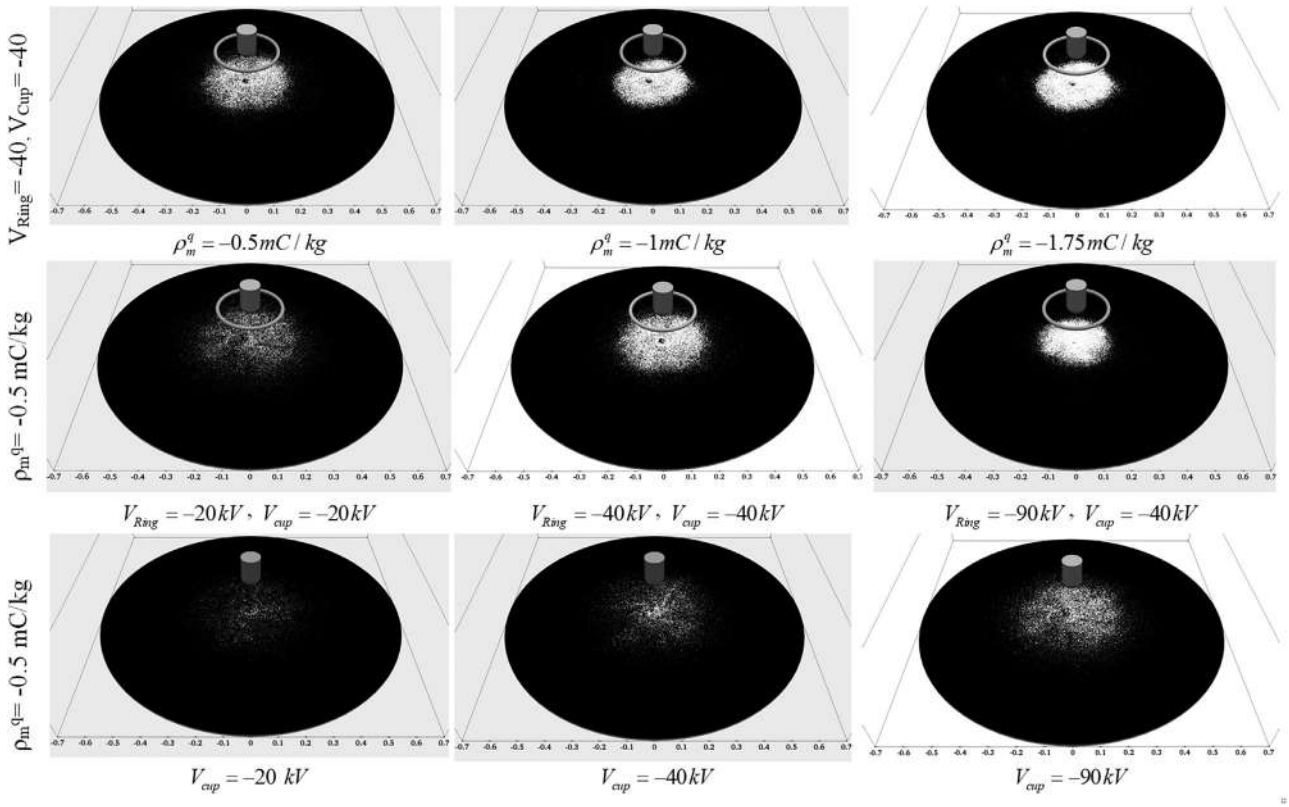

FIG. 28. Representation of deposited droplets pattern at various operating voltage and charge-to-mass ratio: ERBS combined with high-voltage control ring as an external conductor (two first row) and conventional ERBS (third row). Reproduced from Pendar, M. R. and Páscoa, J. C., "Numerical analysis of charged droplets size distribution in the electrostatic coating process: Effect of different operational conditions," Phys. Fluids **33**(3), 033317 (2021), with the permission of AIP Publishing LLC.

By analyzing the trajectory of particles, they discovered the significant impact of the electric space charge on them. Im *et al.* (2004) revealed that the pattern of spray plume is so sensitive to the charge-to-mass ratio and the electric force. They stated that the TE of the ERBS under the voltage of zero, −80 and −90 kV reaches about 44%, 90%, and 94%, respectively. They also showed that reaching very high values of shaping airflow rate (up to ≈300 l/min) or rotational speed (up to ≈50 kRPM) leads to a decrease in the TE value. Toljic *et al.* (2011) considered various charge-to-mass ratios of droplets with different sizes and found that they had a substantial impact on the produced film by increasing the TE. Osman *et al.* (2015a) ejected various droplet size ranges from multiple points that receive specific charge values. Dastourani *et al.* (2018) developed a mathematical approach for the electro-spraying procedure simulation in the cone jet using the OpenFOAM framework. The fundamental flow behavior of the spraying in the ERBS with the presence of an electric field and the positive impact of voltage setting was investigated by Pendar and Páscoa (2019a; 2020a). Figure 28 compared the constructed paint film of two cases of the conventional ERBS and in combination with a high-voltage ring conductor. Before the discussion, it must be mentioned that the mass, momentum and energy conservation, and thickness equation of the formed paint film during the numerical simulation of the ERBS operation were described in reference Pendar and Páscoa (2021). Pendar and Páscoa (2021) proved the significant effect of the charge-to-mass ratio, voltage, and appropriate external electric charge implementation (high-voltage ring) in droplet deposition rate. Adding a ring conductor around the ERBS increased the TE value by roughly 10%. Their results show that the moderate charge-to-mass ratio ($\rho_m^q \approx -1\, mC/kg$) obtained the maximum TE. Higher values of the charge-to-mass ratio have a negative impact on the TE.

1. Various electric charging methods

An external or internal methodology can accomplish the electric charging of paint droplets during the electrostatic coating process. In the internal (direct) approach [see Fig. 29(a)], the supplied high DC voltage to the applicator, in the range of −20 to −90 kV, charge the paint before atomizing. In the external (indirect) method [see Fig. 29(b)], the high voltage is applied to a forward-facing electrode series (Domnick and Scheibe, 2003; 2006) or control-ring (Pendar and Páscoa, 2021) or retractable blades (Pendar and Páscoa, 2022a) with a circular pattern around the sprayer. Here is the case around the rotary bell cup of the ERBS. The air around the bell cup ionized in this approach, which then charged the paint droplet passing through this region. The internal and external charging methods are ideal for solvent-based and water-based paints due to low and high conductivities (voltage leakage) of solvents, respectively. The internal method obtains higher TE values compared to the external ones. The following are the most recent patents on innovative charging methods that have been published. Domnick *et al.* (2006) manipulate the electric field pattern by adding external symmetric corona needles to the ERBS. They found that the implemented modification positively affects the TE and film deposition thickness on the curved object of the car's rear part. Wang *et al.* (2006) and after more than one-decade, Terebessy and Sumitomo Chemical Co Ltd. (2019) invented a spray gun combined with circular electrodes to produce and direct a uniform circular cone spray. Nolte *et al.* (2019) disclosed an electrodes assembly in an electrostatic atomizer that generates discharge currents flowing over a housing surface. Induction charging manner has been recognized as the most suitable way for enhancing deposition and coverage of charged atomized droplets, compared to charging by conduction, triboelectrification and corona methods (Appah *et al.*, 2019). Cooper and Es Product Development LLC (2021) invented a spray dispersal feature that decreases the paint cloud suspending time during the spraying process. Their system includes a nozzle for atomizing and charging the liquid. Brentjes *et al.* (2021) presented a novel approach for estimating the particle's charge in numerical modeling of high-flow rate charged sprays to reach balanced induction around the sprayer nozzle. Their geometry was selected based on the concept first released by (Ellwood and Braslaw, 1998), an electrostatic bell atomizer with a cylindrical induction tube around it.

VI. AUTOMOTIVE OVEN THERMAL CURING PROCEDURE INVESTIGATION

Over the years, with the increase in vehicle mass production, the need of faster paint curing time, as well as improved paint film quality in terms of corrosion and visual appearance durability, has grown (Streitberger and Dossel, 2008; Giampieri *et al.*, 2020). The final paint film quality is highly dependent on the paint curing process. However, automotive paint curing ovens are responsible for high energy consumption. Thus, it became significantly important to study and further optimize the automotive paint curing ovens, considering both potential energy savings and improved paint film quality (Despotovic and Babic, 2018). Taking it into account, this section of the present study focuses on automotive paint curing ovens and drying systems that need more attention. Curing ovens are widely used in various other applications, e.g., shortbread baking, coke, and baking bread (Buczynski *et al.*, 2016; Kokolj *et al.*, 2017). Rao and Gopinath (2013) concluded that paint curing ovens consume over 20% of the total energy used in the paint shop. When the oven is not curing vehicles, during the startup and setback, more than 25% of the energy is wasted. The management and recovery of thermal energy utilization in the automotive manufacturing industry is a powerful strategy for presenting a more efficient production process. Ovens, dryers, furnaces, and boilers are common heat waste sources that must be minimized (Giampieri *et al.*, 2020). Table III summarizes the temperature range of different mentioned heat sources during the automotive manufacturing process, which are classified based on various processes. The efficiency of the curing process in the automotive paint shop oven mainly depends on three factors of (I) curing time, (II) heat transfer rate, and (III) temperature distribution (Nazif, 2019). When a corrosion-protective paint film layer is exposed to heat below or above the prescribed temperature, it either remains crude or over-cures. Because of that, the main challenges in the paint curing oven process are controlling the curing temperature and optimizing the energy consumed in the process (Ajah and Ejiogu, 2019). To satisfy the requirements of the paint curing process for the newly released vehicle, the manufacturer attempts to modify, retrofit, or redesign the oven facilities (Yu, 2013; Svejda, 2011). In this scenario, considering the oven's performance under various operational conditions is critical to recognize its temperature distribution which directly impacts the final paint quality (Geipel and Stephan, 2005). The duty of ovens is to supply the required heat while maintaining the optimal oven length (Streitberger and Dossel, 2008). The automotive ovens are usually over fifty meters

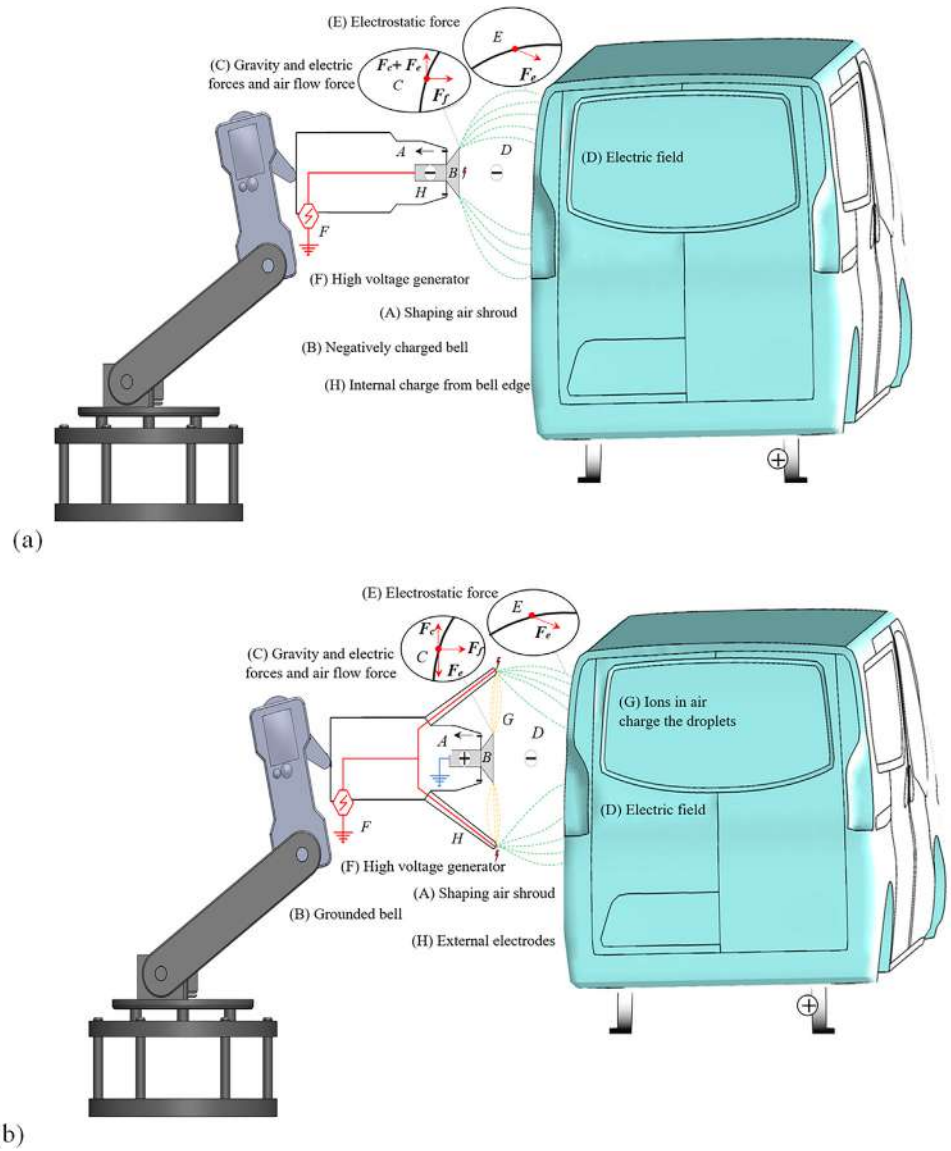

FIG. 29. Schematic representation of (a) internal and (b) external charging processes during the electrostatic coating.

long. A BiW is heated using convection, conduction, and radiation heat transfer modes through panels, nozzles, and hot air. The most prevalent forms of heat loss in the automotive oven are waste gas loss, wall loss, stored heat, and entrance radiation loss (Niamsuwan *et al.*, 2015), all of which can be controlled to reach the lowest values. The burners in the majority of automotive ovens consume fossil fuels like natural gas and liquefied petroleum gas (LPG) (Niamsuwan *et al.*, 2015; Despotovic and Babic, 2018).

A. Numerical modeling of curing oven

This part focuses on automotive paint ovens analysis in terms of numerical modeling. Automotive ovens are rarely studied numerically in the literature for the following reasons: (I) high computational costs of CFD simulation due to complicated geometry of vehicle and oven, (II) complex physical phenomena, (III) different scale of transient flows, and (IV) implementation of moving mesh with multiple bodies in the long oven (Rao and Teeparthi, 2011; Rao, 2013). A thorough numerical investigation of the turbulence flow behavior of thermo-fluid-solid coupling is essential to ensure the increment of the oven's efficiency and precise assessment of baked paint quality. Several authors simplified the process during the implementation of different numerical approaches in analyzing the automotive painting curing process. Ye *et al.* (2009) and Yu (2013) studied the automotive paint curing process in an oven by performing CFD simulations with the FLUENT commercial software. Ye *et al.* (2009) obtained results for the distribution of local temperature gradients on a vehicle body, which can be helpful for developing paint film predicting models, and Yu (2013) reported the instantaneous temperature of

TABLE III. Temperature range running in various heat sources inside automotive manufacturing plants.

Process	Temperature (°C)	Use	Potential recovery
Boiler exhaust	≈230–300 (Giampieri *et al.*, 2020)	Hot steam generation	• Economizer for boiler feed-water preheating. • Restoration of blowdown steam or hot water. • Combustion air preheating with heat wheel.
Regenerative thermal oxidizer	≈170–200 (Giampieri *et al.*, 2020)	Thermal oxidation	• Hot water generation for cooling and warming. • Combustion of air preheating with heat wheel.
Paint curing oven	≈130–180 (Streitberger and Dossel, 2008)	Paint curing after the coating process	• Hot water generation for heating and cooling. • Combustion air preheating with heat wheel. • Air heating for solid desiccant cooling.
Flash off drying booth	≈70–90 (Streitberger and Dossel, 2008)	Paint drying	• Hot water generation for heat pumps, absorption cooling and liquid desiccant. • Air heating for solid desiccant cooling and space heating.
Chilled water	≈40–45 (Giampieri *et al.*, 2020)	Air-conditioning for paint cooling process	• Warm water for liquid desiccant, space warming and heat pumps. • Air preheating for space warming.
Exhaust ventilation air	≈23–26 (Carel, 2017)	Air-conditioning for the painting process and building	• Air precooling or preheating.

the vehicle body surface at different heating and cooling zones for a preliminary oven design. The obtained validated results identified critical information and possible changes that should be implemented to optimize the oven design. By using a different approach, Zelder and Steinbeck-Behrens (2009) studied the automotive paint curing process using the virtual paint simulation (VPS) commercial software. They analyzed the time-dependent temperature and paint viscous behavior to plot an oven curve for each location or provide contour plots on the BiW surface. Posteriorly, Domnick *et al.* (2011) modeled the drying process of the automotive water-based paint films. They used a developed physical model of FLUENT software that treats mass and heat transfer of a ternary mixture on a substrate. On the other hand, Albiez *et al.* (2011) used Abaqus software to study the aluminum alloy thermomechanical characteristics changing during the coating and curing processes. They obtained the temperature field on the chassis surface for different instant times and analyzed the influence of the transient temperature on several chassis' mechanical parameters. To obtain an efficient simulation technique, Wu *et al.* (2013) presented a methodology based on approximating the transient convective field with intermittent steady-state solutions. They showed this method reduces the grid quality dependency and allows acceptable results in less computational time. An innovative and alternative approach was developed and applied by Rao and Teeparthi in 2011. They introduced a dual solver, semi-computational method and considered the arrangement and the position of nozzles in a distinct heat-up zone of the oven to obtain a steady-state profile and map of temperature over the full BiW during the transient heat transfer (Rao and Teeparthi, 2011). Then, Rao (2013) reconstructed the equations for automotive paint ovens exactly in the same manner as they performed in the heat exchangers. As the complex flow pattern in the oven is distributed in all directions, it would be tough to incorporate it into a basic exchanger assessment. In several articles (Shrivastava and Ameel, 2004; Bielski and Malinowski, 2005; Mishra *et al.*, 2008; and Rao, 2013), the transient behavior of three-stream or multi-stream heat exchangers are used in many applications, i.e., automotive, aerospace, and chemical industries during the curing oven simulation. Later, Vasudevan (2018) modeled the paint curing process in convective ovens and determined the heat transfer coefficients for the three-dimensional CFD simulations. To analyze which variables are more prevalent during the car paint oven operation, Despotovic and Babic (2018) presented a simple mathematical method for modeling energy flows in the curing oven. Their

simple model could determine which parameters, such as air or car body temperature, affect the operating conditions of the oven. The method had the ability to specify the desired temperature for redesigning the available oven. To simulate the heat-up zone of the car wax oven, Nazif (2019) used a simple turbulence model of realizable k-ε and compared the results with experimental measurements. As a result, they improved the oven's energy efficiency by up to 25% in measured air temperature by changing the geometry and optimizing the airflow circulation. A deep analysis of thermal management and energy efficiency was performed by Giampieri *et al.* (2020) to reduce energy consumption during the curing process of the automotive paint shop. In 2022, Pendar and Páscoa (2022b) conducted a comprehensive numerical evaluation of conjugate heat transfer in an automotive paint oven. They implemented an efficient algorithm under the framework of the OpenFOAM package using the large eddy simulation (LES) turbulence method (Pendar and Páscoa, 2022c) for modeling unsteady heated airflow behavior. They reported significant energy efficiency improvements by applying low-cost optimization of the intake hot flow rate and redesigning the oven's heat-up, holding, and cooling zones.

B. Experimental techniques for automotive curing oven analysis

The experimental analysis of the automotive curing oven in the operational mode is expensive, unpredictable, and time-consuming. Due to that, there is a lack in the literature of experimental works focusing on the automotive paint curing process inside an oven. As we will see, the experimental works reported in the literature just deal with simplified cases evaluating some characteristics of the paint curing/drying process. Okazaki *et al.* (1974) performed one of the pioneer practical works by conducting drying experiments on coated films using hot air. Gupta (1990) used dynamic mechanical-thermal analysis (DMA) to characterize the cured state of a coating on a steel substrate. Later, Saure *et al.* (1994; 1998) started using Fourier transform infrared (FTIR) spectroscopy techniques to experimentally analyze the drying behavior of polymeric coatings, a technique that later on kept being used by other researchers. In addition to using FTIR spectroscopy, Vessot *et al.* (1998) studied the air convective drying and curing of polyurethane-based paints by applying differential scanning calorimetry (DSC) and thermo-gravimetric analysis (TGA). In order to control the quality and drying time of a curing process, Schabel *et al.* (2004) proposed a new experimental technique for monitoring the progression of the concentration profiles within a paint film during the drying process. Geipel and Stephan (2005) studied the convective drying of coated paint layers on steel substrates by gravimetric experiments and FTIR measurements. Later on, Seubert and Nichols (2010) experimentally studied the curing of automotive epoxy clearcoats, and Brinckmann and Stephan (2011) performed laboratory-scale experiments to validate a software that simulates the drying process of automotive water-based paints. They monitored the temperature and weight of the paint film under different flow conditions and tracked the evaporation of the organic solvents. Posteriorly, Chen *et al.* (2014) experimentally studied the curing process of automotive paint by using the moving-window two-dimensional correlation spectroscopy (MW2DCS) method combined with the principal component analysis (PCA). However, due to the several difficulties in performing experiments in an oven, they considered a curing process without temperature effect and just let the paint dry. Choi *et al.* (2016) also performed experimental studies but on a combined near-infrared curing system with a convective oven to optimize the system's operation. The study of Vasudevan (2018) also focused on the paint curing process in convective ovens. They reported the values of transient residual weight and temperature that were achieved during the paint curing process at the top of the paint layer and the bottom of the metal substrate. Recently, Agha and Abu-Farha (2021) proposed an experimental method for capturing the curing-induced effects in adhesively bonded joints. Moreover, Sukhodolya *et al.* (2021) discussed the paint curing mechanisms through an analysis of thermomechanical curves.

C. Description of automotive convection oven

The paint drying process in an oven can be performed in two different ways: continuous or batch. Continuous ovens are more advantageous for large-scale production, like the automotive curing oven line, since they provide greater efficiency with lower operational costs per unit. In the continuous ovens, the produced car chassis are traversed through carriers with sleighs with a specific velocity. These carriers consume a significant part of the energy that is produced in the oven (Despotovic and Babic, 2018). This problem can be considered the main disadvantage of the continuous oven.

In the automotive industry, convection ovens, which employ heated air to warm the vehicle surface and, with thermal conduction, dry the paint film, are the prevailing choice for paint curing (Talbert, 2007). This type of oven, due to its operation principle, are capable of dealing with complicated vehicle configurations (Streitberger and Dossel, 2008). Proper ventilation, temperature and humidity adjustment in the curing oven as fundamental parameters play an essential role in the esthetic and physical quality of the final coated product (Gerini Romagnoli, 2016). The conveyor's speed is another critical parameter that significantly influences the final painting quality (Cavalcante *et al.*, 2020).

As demonstrated in Fig. 30, the oven includes three zones: (I) the heat-up zone, which is designed to heat the body, (II) the holding zones, which keep the body at a constant temperature, and (III) the cooling zone, where the vehicle body is cooled down. In the heat-up zone, heat is released to raise the temperature of the produced chassis, with the respective coating, to a temperature eligible for baking conditions (Nazif, 2019). This means that the vehicle body is heated to a temperature that leads to the vaporization of the paint solvent. The solid form bonds at the molecular level providing the paint curing. For heating the vehicle bodies, the heating zones either have heated walls to transfer heat to the body by radiation, or nozzles and panels, such as the ones demonstrated in Fig. 31, that blow hot air to the vehicle body (Rao and Teeparthi, 2011). In the heat-up zone, in the first instants of the paint curing process, the paint layers are still wet, and thus, it is necessary to use a transfer mechanism completely free of dust to ensure the high quality of the final painting (Ashrafizadeh *et al.*, 2009). After this step, the car passes over a holding zone in which the car chassis stands in order to complete the baking process that started in the previous stage. To finalize the process, the chassis of the vehicle moves to a cooling zone where it is cooled down to the environment temperature (Nazif, 2019; Rao and Teeparthi, 2011).

Figure 32 illustrates the map of the overall effective factors on the curing and drying process. In the curing, three primary areas must be

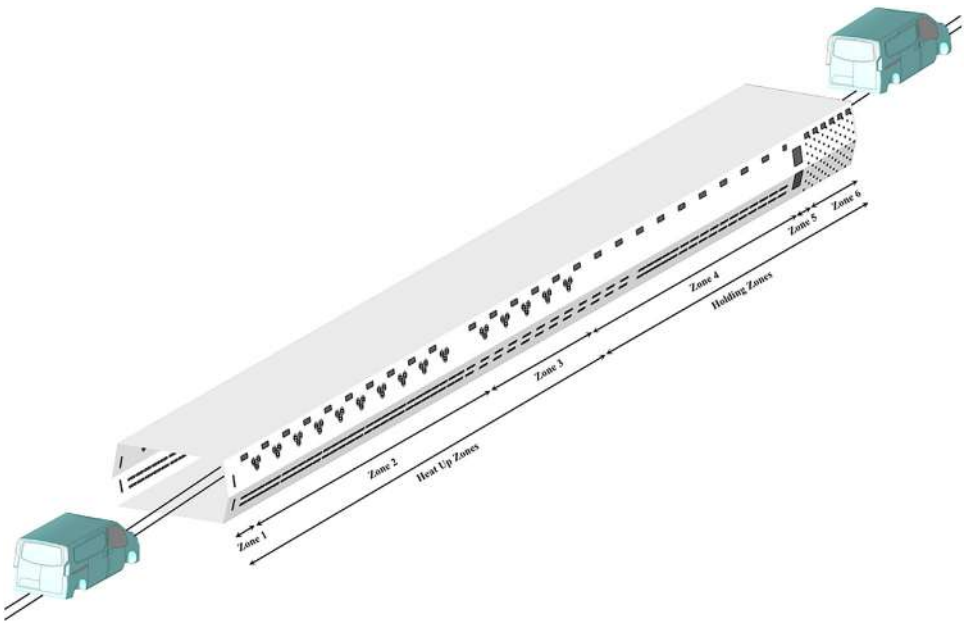

FIG. 30. Schematic representation of oven geometry configuration with all heat up, holding and cooling zones.

considered: (I) geometric setup, (II) thermal transformation, and (III) operational conditions (Niamsuwan *et al.*, 2015; Rao and Teeparthi, 2011; and Mehdipour *et al.*, 2010). The operational conditions are defined by air temperature, air velocity components, air flow rate, and BiW traverse speed. Typically, the conveyor speed is about 4–5 m/min (Mehdipour *et al.*, 2010), while the air temperature usually varies between 190 and 220 °C, with flow velocities ranging from 14 to 18 m/s (Rao, 2013). Usually, these are the conditions that can be changed and established in an easier way. On the other hand, the geometric setup includes the position of the supply air nozzles, air panels and aspiration air ducts, as well as their and the oven's dimensions (Nazif, 2019). Supply air nozzles are usually positioned on the walls of the oven (Rao and Teeparthi, 2011) but might also be placed on the floor (Rao, 2013) or the roof (Ye *et al.*, 2009). Besides that, automotive ovens usually present lengths of a few hundred meters (Yu, 2013; Rao and Teeparthi, 2011). Once the oven is fabricated, these positions cannot be modified and thus, must be studied and defined before the oven implementation. Furthermore, we

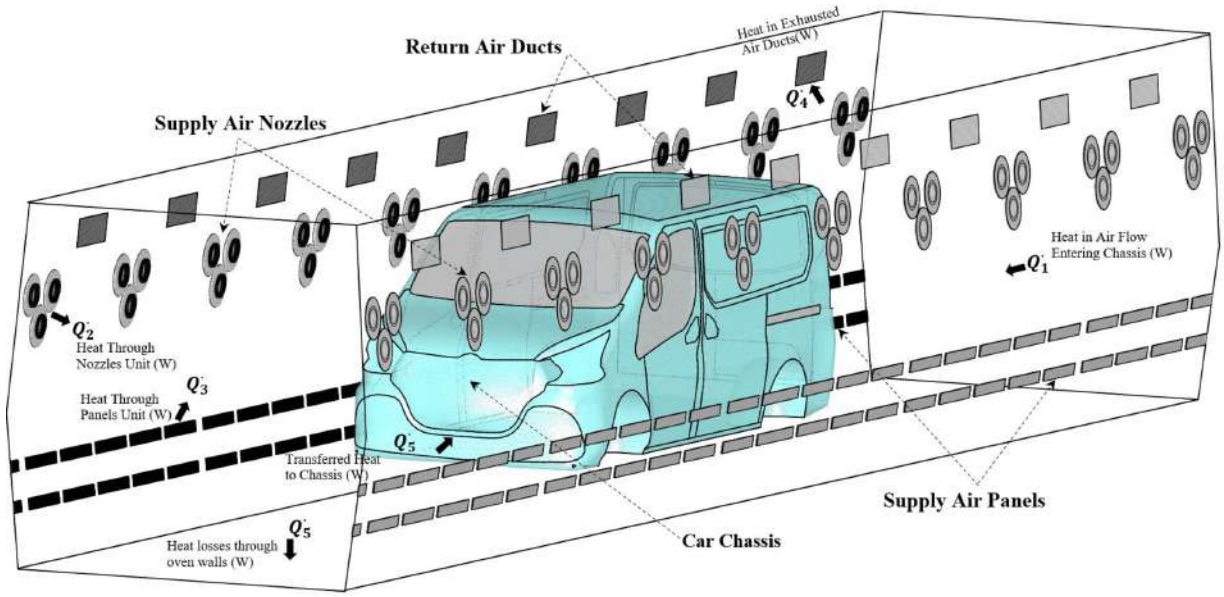

FIG. 31. Schematic representation of position of hot air nozzles' s components: base and wall.

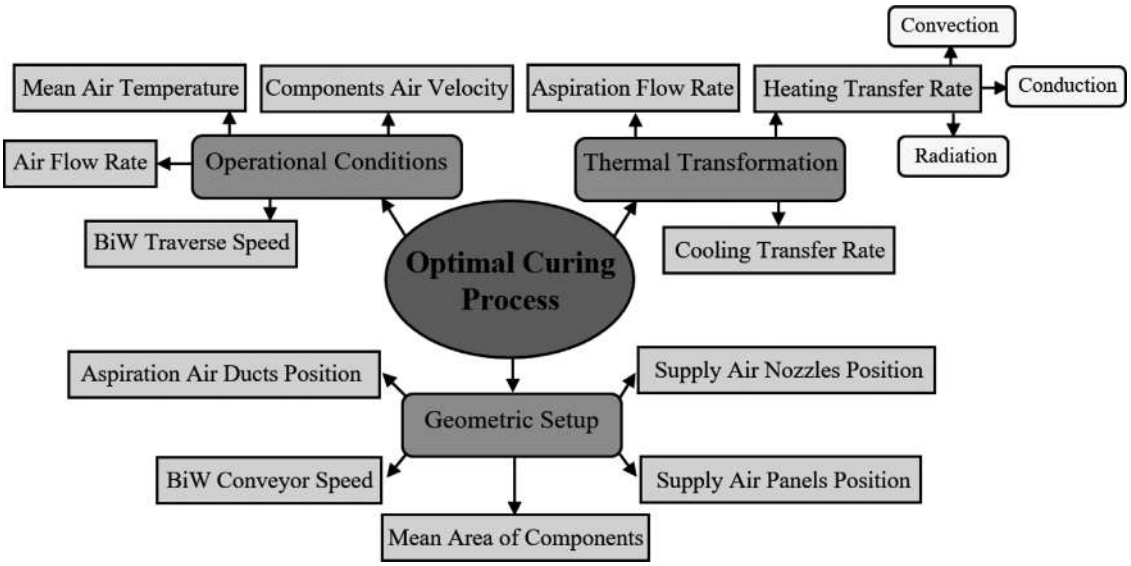

FIG. 32. Map of effective variation on the curing and drying process.

have the thermal transformation conditions, which include the heating transfer, cooling transfer rate, and aspiration flow rate, which will be highly influenced by the operational and geometric conditions (Ashrafizadeh *et al.*, 2009; Cavalcante *et al.*, 2020). For example, cooling times of 13.90 min in the cooler zone and 14.55 min in the building can be used to obtain an optimal cooling transfer rate (Yu, 2013).

D. Quality control of paint curing process

The heat transfer rate, temperature achievement, and heating time are crucial factors in the curing process of the continuous oven. Many deficiencies in the paint film quality are the consequence of the under-curing or over-curing phenomenon (Ashrafizadeh *et al.*, 2009). The consideration of the paint cure window (PCW), which is a helpful feature of the automotive paint curing process, is vital. Figure 33(a) represents a schematic of a typical PCW. The PCW defines the range of the temperatures for a determined heating time and these tolerances specify the desired curing temperature and time (Prendi *et al.*, 2015). In this frame, we also observe the transformed temperature (TT)-designed curve, which is the transformed temperature (TT) curve. The calculation of this curve and its analysis against the PCW is a common approach used to check the quality of the cured paint film

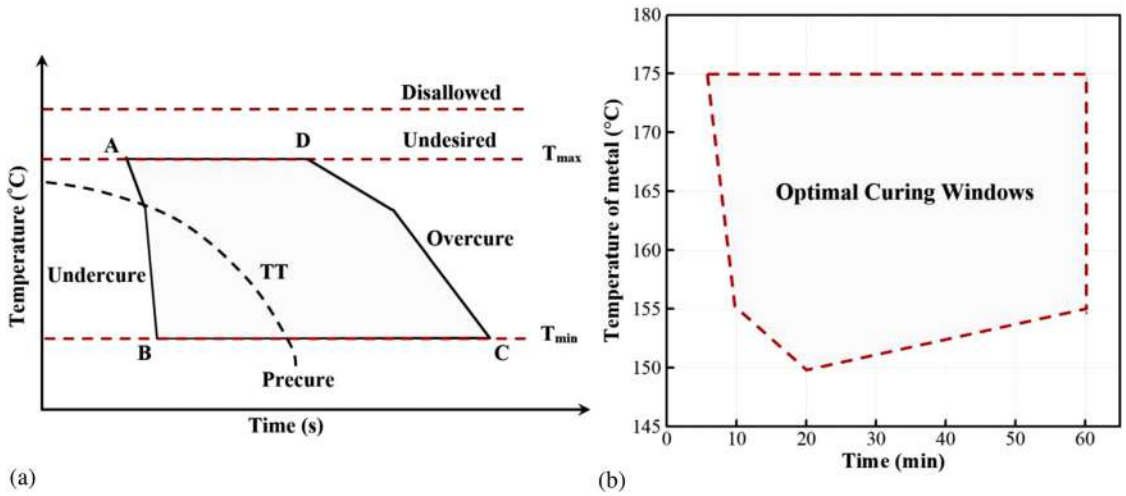

FIG. 33. Schematic representation of (a) a typical paint cure window (PCW), and (b) optimal curing operational conditions of primer coat layer. From Wonnemann, H., *Automotive Paints and Coatings*. Copyright 2008, John Wiley and Sons. Reproduced with permission from John Wiley and Sons.

(Mehdipour *et al.*, 2010). Primer, base, and clear coatings are applied one by one for various functions after sealing and underbody coating (Rivera and Reyes-Carrillo, 2014). Following the application of the primer coat, a curing procedure is carried out under ideal conditions, as shown in Fig. 33(b) (Wonnemann, 2008).

Usually, this curve is obtained by measuring the temperature history at critical points of the vehicle body. When the TT curve enters from the AB line side and exits from the BC line side, as represented in Fig. 33(a), the paint curing process is considered acceptable. On the other hand, for any other TT curve that does not pass through the PCW properly, the final paint quality will not be acceptable (Ashrafizadeh *et al.*, 2009). The PCW also defines the maximum and minimum temperature that may be applied to the paint film (Xiao *et al.*, 2006). If the paint film reaches a temperature above the maximum temperature, the paint film will be considered overbaked or "burned-out" independently of the curing time. On the other hand, if the paint film does not achieve a temperature higher than the minimum temperature, regardless of the curing time, the paint will be underbaked (Mehdipour *et al.*, 2010; Ashrafizadeh *et al.*, 2009). Therefore, to obtain a good paint quality, it is mandatory that the paint film reaches a temperature within the temperature range defined by the PCW (Giampieri *et al.*, 2020). However, if the time is not enough for the TT curve to cross the AB line, the paint film will reach an undercure state. On the other hand, if the cure time is excessive and the TT curve crosses the line CD, the paint film will be overcured (Ashrafizadeh *et al.*, 2009). Xiao *et al.* (2006) proposed a new cure window based proactive QC approach for car topcoat curing. Their methodology assessed film curing quality using dynamic process-product models.

VII. CONCLUSIONS AND SUGGESTIONS

The main objective of this work is to review available studies in the literature on the automotive electrostatic spray-painting process and thermal procedure in a curing oven, initiating a detailed consideration of the paint shop plant description, coating film layers recognition, and various paint spray applicators' technology characterization. The focus is on introducing ways to improve coating flow physics recognition, better thermal management of manufacturing processes, lower paint curing energy cost, higher coating transfer efficiency, and increase paint film uniformity, quality and aesthetic appeal in automotive paint shop plants. The following conclusions can be drawn:

1. The review clarified that the paint shop plant consumes the largest portion of energy during vehicle manufacturing operations. Due to energy saving and obtaining defects-free products, effectively controlling humidity and temperature of the air in the paint booths and ovens, which are two major energy consumers, is fundamental.
2. The basic concepts of paint atomization, coating layers composition, film formation processes, and film uniformity and thickness control have all been explored. The current paper provided an up-to-date review of innovative coating and curing techniques and technologies to be of value to industrial practitioners and researchers to improvements in manufacturing technologies and paints.
3. In the automotive paint shop's electrostatic painting application, the charged droplets' rebounding, off-target deposition, impinging, and drift inefficiencies have been reduced and spray efficiency enhanced due to the wraparound effect and substrate attraction.
4. The induction charging method has been identified as the most appropriate way for enhancing deposition and coverage of charged droplets, compared to charging by conduction, tribo-electrification, and corona manners.
5. Controlled delivery of charged paint droplets by using various surrounded conductors, in contrast to a conventional sprayer where the electrode material is embedded in a gun aperture to charge droplets, is one useful field of interest in the automated electrostatic coating system.
6. The deposition TE and the droplet size distribution of modern sprayer technologies and designs, as well as their potential for usage in the automotive coating in various terms, were discussed.
7. The optimum combination and accurate sets of parameters, as established by the researchers (discussed here), are essential for efficient electrostatic spraying and continuous curing operations.
8. The applications of electrostatic spraying in various fields, e.g., agriculture area, medical sector (disinfection), food processing, pharmaceutical, and automotive industries, were highlighted in this review.
9. From the review, among all operational parameters in the electrostatic coating by ERBSs, bell rotary speed, shaping airflow rate, high voltage setting, and liquid flow rate, in order to significantly manipulated the paint spray shape and the vortical airflow structure.
10. The paint film quality is highly dependent on the paint cure in the automotive oven. It is significantly influenced by the oven's operational conditions, thermal transformation, and geometric parameters. From the literature review, we conclude that the conveyor speed, inlet air temperature, airflow rate, and positioning of the inlet air nozzles are essential parameters for achieving an ideal and uniform surface temperature that will promote the proper paint cure. After attaining the desired uniform curing surface temperature, controlling the cooling transfer rate is vital to achieving an optimal final paint film quality.

The review provided in this paper is expected to improve comprehension of the entire coating and curing processes, which still require attention, resulted in new ideas for energy efficiency, heat recovery, saving materials, and renewable energy practices. The four issues of a systematic validation for the realistic geometries and dynamic targets, experimental methods, fundamental understanding of the interaction among the effective parameters, and standardized methods to achieve realistic deposition TEs all deserve investigation in future research. Future works could also focus on deploying smart coatings, superior coating techniques, and devices to reach desired paint film properties or functionalities, e.g., superhydrophobicity, sound-proofing, vibration damping, self-healing, self-sensing, high gloss, durability to corrosion, UV light exposure and abrasion.

ACKNOWLEDGMENTS

This work was supported by Project "MOSIPO," Project Grant No. POCI-01–0247-FEDER-072621. The research was also partly supported by CMAST Center for Mechanical and Aerospace Science and Technology, Research Unit No. 151 (Project No. UID/00151/2020) from Fundacao para a Ciencia e Tecnologia (Portugal).

AUTHOR DECLARATIONS

Conflict of Interest

The authors have no conflicts to disclose.

Author Contributions

Mohammad Pendar: Conceptualization (lead); Data curation (lead); Formal analysis (lead); Investigation (lead); Methodology (lead); Supervision (lead); Validation (lead); Visualization (lead); Writing – original draft (lead); Writing – review & editing (lead). **Frederico Freire Rodrigues:** Investigation (equal); Methodology (equal); Writing – original draft (supporting); Writing – review & editing (supporting). **José Páscoa:** Funding acquisition (equal); Project administration (lead); Supervision (lead); Writing – review & editing (supporting). **Rui Lima:** Funding acquisition (supporting); Project administration (supporting); Writing – review & editing (supporting).

DATA AVAILABILITY

The data that support the findings of this study are available on request from the authors.

REFERENCES

Adornato, A. V., "Effect of heating and ionization of four atomizing gases on the spray characteristics of a high volume low pressure spray atomizer," Master's thesis (University of Kentucky, 2015).

Agha, A., and Abu-Farha, F., "Experimental methods to capture curing induced effects in adhesive bonded joints," Int. J. Adhes. Adhes. **104**, 102735 (2021).

Ahmed, M., and Youssef, M. S., "Characteristics of mean droplet size produced by spinning disk atomizers," J. Fluids Eng. **134**(7), 071103 (2012).

Ahmed, M., and Youssef, M. S., "Influence of spinning cup and disk atomizer configurations on droplet size and velocity characteristics," Chem. Eng. Sci. **107**, 149–157 (2014).

Ajah, V., and Ejiogu, E., "Solar thermal/electricity paint curing oven," in *2019 IEEE International Conference on Sustainable Energy Technologies and Systems (ICSETS)* (IEEE, 2019), pp. 075–080.

Akafuah, N. K., "Automotive paint spray characterization and visualization," in *Automotive Painting Technology* (Springer, Dordrecht, 2013), pp. 121–165.

Akafuah, N. K., Poozesh, S., Salaimeh, A., Patrick, G., Lawler, K., and Saito, K., "Evolution of the automotive body coating process—A review," Coatings **6**(2), 24 (2016).

Akafuah, N. K., Salazar, A. J., and Saito, K., "Infrared visualization of automotive paint spray transfer process," in *Fluids Engineering Division Summer Meeting* (ASME, 2009), Vol. 43727, pp. 759–765.

Akafuah, N. K., Salazar, A. J., and Saito, K., "Infrared thermography-based visualization of droplet transport in liquid sprays," Infrared Phys. Technol. **53**(3), 218–226 (2010).

Albiez, C., Liewald, M., Görres, A., and Regensburger, J., "Numerical prediction of thermal panel distortion incorporating thermal material properties of 6016 aluminum alloy," in Proceedings of European Aluminium Congress (2011), pp. 11–23.

AMS, see https://automotivemanufacturingsolutions.com/process-materials/economicalalternative for "Economical Alternative" (last accessed 20 August 2018).

Ansdell, D., "Painting of plastic body components for cars," Ind. Prod. Eng. (3), 30–35 (1980).

Andersson, B., Golovitchev, V., Jakobsson, S., Mark, A., Edelvik, F., Davidson, L., and Carlson, J. S., "A modified TAB model for simulation of atomization in rotary bell spray painting," J. Mech. Eng. Autom. **3**(2), 54–61 (2013).

Andrade, R. D., Skurtys, O., and Osorio, F. A., "Atomizing spray systems for application of edible coatings," Compr. Rev. Food Sci. Food Saf. **11**(3), 323–337 (2012).

Appah, S., Wang, P., Ou, M., Gong, C., and Jia, W., "Review of electrostatic system parameters, charged droplets characteristics and substrate impact behavior from pesticides spraying," Int. J. Agric. Biol. Eng. **12**(2), 1–9 (2019).

Arikan, M. S., and Balkan, T., "Modeling of paint flow rate flux for elliptical paint sprays by using experimental paint thickness distributions," Ind. Rob. **33**, 60 (2006).

Arumugham-Achari, A. K., Grifoll, J., and Rosell-Llompart, J., "A comprehensive framework for the numerical simulation of evaporating electrosprays," Aerosol. Sci. Technol. **49**(6), 436–448 (2015).

Ashrafizadeh, A., Mehdipour, R., and Rezvani, M., "An efficient and accurate numerical simulation method for the paint curing process in auto industries," in Proceedings of International Conference on Applications and Design in Mechanical Engineering (ICADME), Penang, Malaysia, 2009.

Basu, S. K., Zhou, J., Harding, A., Moncier, A., Williams, C., Baker, L., and McCreight, K., "Effect of atomization and rheology control additives on particle size and appearance of automotive coatings," in Proceedings of the 15th International Coating Science and Technology Symposium, St. Paul, MN, 12–15 September, 2010.

Bell, G. C., and Hochberg, J., "Mechanics of electrostatic atomization, transport, and depositions of coatings," in Proceedings of the 7th International Conference in Organic Science and Technology (1981), pp. 59–115.

Bellman, R., and Pennington, R. H., "Effects of surface tension and viscosity on Taylor instability," Q. Appl. Math. **12**(2), 151–162 (1954).

Bensalah, W., Loukil, N., Wery, M., and Ayedi, H. F., "Assessment of automotive coatings used on different metallic substrates," Int. J. Corros. **2014**, 838054.

Berg, T., Deppe, J., Michaelis, D., Voges, H., and Wissel, S., "Comparison of particle size and velocity investigations in sprays carried out by means of different measurement techniques," in ICLASS'06, Kyoto, Japan, 2006.

Besra, L., and Liu, M., "A review on fundamentals and applications of electrophoretic deposition (EPD)," Prog. Mater. Sci. **52**(1), 1–61 (2007).

Bielski, S., and Malinowski, L., "An analytical method for determining transient temperature field in a parallel-flow three-fluid heat exchanger," Int. Commun. Heat Mass Transfer **32**(8), 1034–1044 (2005).

Bienduga, T. J., and Wagner Systems, Inc., "Apparatus for electrostatic spray painting," U.S. patent 5,443,642 (22 August 1995).

BMW, "To use hydropower to manufacture Megacity electric car" (2010) (last accessed 20 December 2018), available from https://www.zdnet.com/article/bmw-to-usehydropower-to-manufacture-megacity-electric-car/.

Böttner, C. U., and Sommerfeld, M., "Numerical calculation of electrostatic powder painting using the Euler/Lagrange approach," Powder Technol. **125**(2–3), 206–216 (2002).

Brentjes, A., Pozarlik, A. K., and Brem, G., "Numerical simulation of evaporating charged sprays in spray chilling," J. Electrostatics **107**, 103471 (2020).

Brentjes, A., Pozarlik, A. K., and Brem, G., "Estimating droplet charge in numerical simulations of charged sprays," J. Electrost. **112**, 103591 (2021).

Brinckmann, F., and Stephan, P., "Experimental investigation of the drying process of water-based paints used in automotive industry," Chem. Eng. Process.: Process Intensif. **50**(5–6), 489–494 (2011).

Broumand, M., Khan, M. S., Kuppili, H., Yun, S., Hong, Z., and Thomson, M. J., "The effect of preheating of a viscous and non-Newtonian bioliquid on its internally mixed twin-fluid atomization," Int. J. Multiphase Flow **147**, 103910 (2022).

Buczynski, R., Weber, R., Kim, R., and Schwöppe, P., "One-dimensional model of heat-recovery, non-recovery coke ovens. IV: Numerical simulations of the industrial plant," Fuel **181**, 1151–1161 (2016).

Cadnum, J. L., Jencson, A. L., Livingston, S. H., Li, D. F., Redmond, S. N., Pearlmutter, B., Wilson, B. M., and Donskey, C. J., "Evaluation of an electrostatic spray disinfectant technology for rapid decontamination of portable equipment and large open areas in the era of SARS-CoV-2," Am. J. Infect. Control **48**(8), 951–954 (2020).

CAREL, "Air humidity in paint booths," in *Sustainable Solutions for Correct Application of Paints* (CAREL, 2017).
Cavalcante, E. S., Gonzaga, L., Vasconcelos, S., de Farias Neto, G. W., Ramos, W. B., and Brito, R. P., "Automotive painting process: Minimizing energy consumption by using adjusted convective heat transfer coefficients," Prog. Org. Coat. **140**, 105479 (2020).
Chang, L. P., "Analysis of the influence of car body structure on the pretreatment and electrophoresis process," Shanghai Coat. **8**, 27–28 (2011).
Chen, J. B., Sun, S. Q., Yu, J., and Zhou, Q., "Tracking the curing process of automotive paint by moving-window two-dimensional infrared correlation spectroscopy and principal component analysis," J. Mol. Struct. **1069**, 112–117 (2014).
Chen, Y., Hu, J., Chen, W., Zhang, G., Zhou, S., and Li, B., "Simulation research on characteristics of paint deposition on spherical surface," IOP Conf. Ser.: Mater. Sci. Eng. **542**(1), 012024 (2019).
Chiara, F., and Canova, M., "A review of energy consumption, management, and recovery in automotive systems, with considerations of future trends," Proc. Inst. Mech. Eng., Part D **227**(6), 914–936 (2013).
Choi, J. W., Chun, W. P., Oh, S. H., Lee, K. J., and Kim, S. I., "Experimental studies on a combined near infrared (NIR) curing system with a convective oven," Prog. Org. Coat. **91**, 39–49 (2016).
Clément, Z., Fredrik, E., Andreas, M., and Oliver, H., "Efficient numerical simulation of spray painting processes in automotive manufacturing," SAE Technical Paper No. 2014-360418, 2014.
Colbert, S. A., "Numerical simulations of droplet trajectories from an electrostatic rotary-bell atomizer," Doctoral dissertation (Drexel University, 2007).
Colbert, S. A., and Caircross, R. A., "A computer simulation for predicting electrostatic spray coating patterns," Powder Technol. **151**, 77–86 (2005).
Cooper, S. C., and Es Product Development LLC, "Electrostatic fluid sprayer with active fluid cloud dispersal feature and method of electrostatic spraying," U.S. patent 10,894,262 (18 January 2021).
Corbeels, P. L., Senser, D. W., and Lefebvre, A. H., "Atomization characteristics of a highspeed rotary-bell paint applicator," Atomization Sprays **2**(2), 87 (1992).
Corber, P. A., "The performance of a pressure atomizer with a flow obstruction upstream of the nozzle," Doctoral dissertation (University of Ottawa, 2009).
Darroch, J. B., "HVLP revolution: Basics buying HVLP spray equipment," Furniture Des. Manuf. **69**, 100–106 (1997).
Darwish Ahmad, A., Abubaker, A. M., Salaimeh, A. A., and Akafuah, N. K., "Schlieren visualization of shaping air during operation of an electrostatic rotary bell sprayer: Impact of shaping air on droplet atomization and transport," Coatings **8**(8), 279 (2018).
Darwish Ahmad, A., Singh, B. B., Doerre, M., Abubaker, A. M., Arabghahestani, M., Salaimeh, A. A., and Akafuah, N. K., "Spatial positioning and operating parameters of a rotary bell sprayer: 3D mapping of droplet size distributions," Fluids **4**(3), 165 (2019).
Dastourani, H., Jahannama, M. R., and Eslami-Majd, A., "A physical insight into electrospray process in cone-jet mode: Role of operating parameters," Int. J. Heat Fluid Flow **70**, 315–335 (2018).
Dbouk, T., and Drikakis, D., "On coughing and airborne droplet transmission to humans," Phys. Fluids **32**(5), 053310 (2020).
Demeter, J., and Villamos Automatika Intezet, "Electrostatic spray gun," U.S. patent 3,504,851 (7 April 1970).
Despotovic, M., and Babic, M., "Analysis of different scenarios of car paint oven redesign to achieve desired indoor air temperature," Energy Effic. **11**(4), 877–891 (2018).
Dhivyaraja, K., Gaddes, D., Freeman, E., Tadigadapa, S., and Panchagnula, M. V., "Dynamical similarity and universality of drop size and velocity spectra in sprays," J. Fluid Mech. **860**, 510–543 (2019).
Di Domenico, J., and Henshaw, P., "The effects of basecoat bell application parameters on elements of appearance for an automotive coatings process," J. Coat. Technol. Res. **9**(6), 675–686 (2012).
Dombrowski, N., and Lloyd, T. L., "The spread of liquid on a rotating vane," Chem. Eng. Sci. **27**(5), 1003–1012 (1972).
Domnick, J., " Effect of bell geometry in high-speed rotary bell atomization," in *Proceedings of the 23rd Annual Conference on Liquid Atomization and Spray Systems*, Brno, Czech Republic, 6–8 September 2010.
Domnick, J., "High-speed rotary bell atomization of Newtonian and non-Newtonian fluids," in *12th International Conference on Liquid Atomization and Spray Systems*, Heidelberg, Germany, 2–6 September 2012.
Domnick, J., Gruseck, D., Pulli, K., Scheibe, A., Ye, Q., and Brinckmann, F., "Investigations of the drying process of a water based paint film for automotive applications," Chem. Eng. Process.: Process Intensif. **50**(5–6), 495–502 (2011).
Domnick, J., Lindenthal, A., Tropea, C., and Xu, T. H., "Application of phase Doppler anemometry in paint sprays," Atomization Sprays **4**(4), 437 (1994).
Domnick, J., Scheibe, A., and Ye, Q., "The electrostatic spray painting process with high-speed rotary bell atomizers: Influences of operating conditions and target geometries," in Conference on Liquid Atomization and Spray Systems, 2003.
Domnick, J., Scheibe, A., and Ye, Q., "The simulation of the electrostatic spray painting process with high-speed rotary bell atomizers," Part. Part. Syst. Charact. **22**(2), 141–150 (2005).
Domnick, J., Scheibe, A., and Ye, Q., "The simulation of electrostatic spray painting process with high-speed rotary bell atomizers," Part. Part. Syst. Charact. **23**(5), 408–416 (2006).
Domnick, J., and Thieme, M., "Atomization characteristics of high-speed rotary bell atomizers," Atomization Sprays **16**, 857–874 (2006).
Doerre, M., Hibbitts, L., Patrick, G., and Akafuah, N. K., "Advances in automotive conversion coatings during pretreatment of the body structure: A review," Coatings **8**(11), 405 (2018).
Dutt, W., King, J. G., and Axalta Coating Systems IP Co. LLC, "Method of producing a polished metal effect finish on a vehicle," U.S. patent 8,512,802 (20 August 2013).
Dürr, "Dürr's Tailor-Made Solutions for Dry Paint Overspray Separation" (2018), http://www.motorindiaonline.in/corporate/durrstailor-made-solutions-for-dry-paint-overspray-separation/ for (last accessed 15 October 2018).
Ellwood, K. R., and Braslaw, J., "A finite-element model for an electrostatic bell sprayer," J. Electrostatics **45**(1), 1–23 (1998).
Felstein, S., and Lum, J., "An air-assisted 'airless,' conformal coating process," Surf. Mount Technol. **7**, 27–27 (1993).
Feng, L., "Manufacturing system energy modeling and optimization," Ph.D. thesis (Clemson University, 2019).
Feng, L., Mears, L., and Schulte, J., "Key variable analysis and identification on energy consumption of automotive manufacturing plant," in *2016 IEEE Conference on Technologies for Sustainability (SusTech)* (IEEE, 2016), pp. 162–168.
Fernandes, E. C., Rondolfo, N., Beraldo-de-Araújo, V., and Oliveira-Nascimento, L., "Quality deviation handling on the polymeric coating of pharmaceutical tablets," J. Pharm. Innov. **14**(4), 332–340 (2019).
Fettis, G., *Automotive Paints and Coatings* (VCH, Weinheim, 1995).
Flynn, M. R., Gatano, B. L., Mckernan, J. L., Dunn, K. H., Blazicko, B. A., and Carlton, G. N., "Modeling breathing-zone concentrations of airborne contaminants generated during compressed air spray painting," Ann. Occup. Hyg. **43**(1), 67–76 (1999).
Flynn, M. R., and Sills, E. D., "Numerical simulation of human exposure to aerosols generated during compressed air spray-painting in cross-flow ventilated booths," J. Fluids Eng. **123**(1), 64–70 (2001).
Fogliati, M., Fontana, D., Garbero, M., Vanni, M., Baldi, G., and Donde, R., "CFD simulation of paint deposition in an air spray process," J. Coat. Technol. Res. **3**(2), 117–125 (2006).
Fraser, R. P., Dombrowski, N., and Routley, J. H., "The production of uniform liquid sheets from spinning cups," Chem. Eng. Sci. **18**(6), 315–321 (1963).
Frost, A. R., "Rotary atomization in the ligament formation mode," J. Agric. Eng. Res. **26**(1), 63–78 (1981).
Fukuta, K., Murate, M., Ohashi, Y., and Toda, K., "New rotary bell for metallic paint application," Met. Finish. **91**, 39–39 (1993).
Galitsky, C., and Worrell, E., "Energy efficiency improvement and cost saving opportunities for the vehicle assembly industry: An energy star guide for energy and plant managers," Report No. LBNL-50939, Lawrence Berkeley National Laboratory (LBNL), Berkeley, CA, 2008.
Gatano, B. L., "Determining the transfer efficiency of a HVLP spray gun," Master's thesis (University of North Carolina, 1997).
Geipel, C., and Stephan, P., "Experimental investigation of the drying process of automotive base paints," Appl. Therm. Eng. **25**(16), 2578–2590 (2005).

Gerini Romagnoli, M., "Simulation of energy savings in automotive coatings processes," Master's thesis (University of Windsor, 2016).
Gerlock, J. L., Kucherov, A. V., and Smith, C. A., "Determination of active HALS in automotive paint systems II: HALS distribution in weathered clearcoat/base-coat paint systems," Polym. Degrad.n Stab. **73**(2), 201–210 (2001).
Giampieri, A., Ling-Chin, J., Ma, Z., Smallbone, A., and Roskilly, A. P., "A review of the current automotive manufacturing practice from an energy perspective," Appl. Energy **261**, 114074 (2020).
Gödeke, L., Oswald, W., Willenbacher, N., and Ehrhard, P., "Dimensional analysis of droplet size and ligament length during high-speed rotary bell atomization," J. Coat. Technol. Res. **18**, 75–77 (2021).
Guerrero, C. A., Wang, J., Li, J., Arinez, J., Biller, S., Huang, N., and Xiao, G., "Production system design to achieve energy savings in an automotive paint shop," Int. J. Prod. Res. **49**(22), 6769–6785 (2011).
Guettler, N., Knee, P., Ye, Q., and Tiedje, O., "Initial droplet conditions in numerical spray painting by electrostatic rotary bell sprayers," J. Coat. Technol. Res. **17**(5), 1091–1104 (2020).
Guettler, N., Paustian, S., Ye, Q., and Tiedje, O., July. "Numerical and experimental investigations on rotary bell atomizers with predominant air flow rates," in *28th European Conference on Liquid Atomization and Spray Systems, ILASS Europe* (Editorial Universitat Politècnica de València, 2017), pp. 114–121.
Gupta, M. K., "Dynamic mechanical analysis of automotive coatings on a metal substrate," Thermochim. Acta **166**, 157–167 (1990).
Hayati, I., Bailey, A. I., and Tadros, T. F., "Investigations into the mechanisms of electrohydrodynamic spraying of liquids. I. Effect of electric field and the environment on pendant drops and factors affecting the formation of stable jets and atomization," J. Colloid Interface Sci. **117**(1), 205–221 (1987).
Heitbrink, W. A., Verb, R. H., Fischbach, T. J., and Wallace, M. E., "A comparison of conventional and high volume-low pressure spray-painting guns," Am. Ind. Hyg. Assoc. J. **57**(3), 304–310 (1996).
Hicks, P. G., "Drop transport in air paint sprays," Ph.D. thesis (Purdue University, 1995).
Hicks, P. G., and Senser, D. W., "Simulation of paint transfer in an air spray process," J. Fluids Eng. **117**, 713 (1995).
Higashiyama, Y., Tanaka, S. I., Sugimoto, T., and Asano, K., "Size distribution of the charged droplets in an axisymmetric shower," J. Electrost. **47**(3), 183–195 (1999).
Hines, R. L., "Electrostatic atomization and spray painting," J. Appl. Phys. **37**(7), 2730–2736 (1966).
Hinze, J. O., and Milborn, H., "Atomization of liquids by means of a rotating cup," Trans ASME, J Appl. Mech. **17**, 145–153 (1950).
Honma, K., Yamasaki, I., and Toyota Motor Corp., "Rotary atomizing electrostatic coating apparatus and method," U.S. patent 5,980,994 (9 November 1999).
Huang, H., Lai, M. C., and Meredith, M., "Simulation of spray transport from rotary cup atomizer using KIVA-3V," in 10th International KIVA User's Group Meeting, 2000.
Iglauer, O., and Zahler, C., "A new solar combined heat and power system for sustainable automobile manufacturing," Energy Procedia **48**, 1181–1187 (2014).
Im, K. S., *An Experimental and Numerical Study of the Spray Transfer Processes in An Electrostaic Rotating Bell Spray* (Wayne State University. 1999).
Im, K. S., Lai, M. C., Liu, Y., Sankagiri, N., Loch, T., and Nivi, H., "Visualization and measurement of automotive electrostatic rotary-bell paint spray transfer processes," J. Fluids Eng. **123**(2), 237–245 (2001).
Im, K. S., Lai, M. C., Yu, S.-T. J., and Matheson, R. R., Jr., "Simulation of spray transfer processes in electrostatic rotary bell sprayer," J. Fluids Eng. **126**(3), 449–456 (2004).
Inkpen, S. L., and Melcher, J. R., "Dominant mechanisms for color differences in the mechanical and the electrostatic spraying of metallic paints," Ind. Eng. Chem. Res. **26**(8), 1645–1653 (1987).
Jackiw, I. M., and Ashgriz, N., "On aerodynamic droplet breakup," J. Fluid Mech. **913**, A33 (2021).
Janna, W. S., "Drop-size distributions of sprays produced by fan-jet pressure nozzles," Ph.D. thesis (University of Toledo, 1976).
Jaworek, A., "Micro-and nanoparticle production by electrospraying," Powder Technol. **176**(1), 18–35 (2007).
Jaworek, A., and Krupa, A., "Jet and drops formation in electrohydrodynamic spraying of liquids. A systematic approach," Exp. Fluids **27**(1), 43–52 (1999).
Joseph, R., "Painting problem solver: Tips for eliminating 'orange peel' when using HVLP spray guns," Met. Finish. **107**(6), 60–62 (2009).
Kamiya, T., and Kayano, A., "Film-type disintegration by rotating disk," J. Chem. Eng. Jpn. **5**(2), 174–182 (1972).
Kawase, Y., and De, A., "Ligament-type disintegration of non-Newtonian fluid in spinning disk atomization," J. Non-Newtonian Fluid Mech. **10**(3–4), 367–371 (1982).
Kayano, A., and Kamiya, T., "Calculation of the mean size of droplets purged from the rotating disc," in *Proceedings of 1st International Conference on Liquid Atomization-Spray Systems* (Fuel Society of Japan, 1978), pp. 133–138.
Kazama, S., "Steady-state paint flow under high centrifugal force: Atomization in spray painting," JSAE Rev. **24**, 489–494 (2003).
Kelly, A. J., "On the statistical, quantum and practical mechanics of electrostatic atomization," J. Aerosol Sci. **25**(6), 1159–1177 (1994).
Keshavarz, B., Houze, E. C., Moore, J. R., Koerner, M. R., and McKinley, G. H., "Ligament mediated fragmentation of viscoelastic liquids," Phys. Rev. Lett. **117**(15), 154502 (2016).
Khanna, A. S., *High-Performance Organic Coatings* (Elsevier, 2008).
Khatir, Z., Paton, J., Thompson, H., Kapur, N., and Toropov, V., "Optimisation of the energy efficiency of bread-baking ovens using a combined experimental and computational approach," Appl. Energy **112**, 918–927 (2013).
Kiliç, F. Ç., Eyidoğan, M., and Sapmaz, S., "Bir otomobil montaj işletmesinde enerji verimliliği artırıcı çözümlerin irdelenmesi," Gazi Univ. J. Sci. Part C: Des. Technol. **6**(1), 149–162 (2018).
Kim, B. R., "VOC emissions from automotive painting and their control: A review," Environ. Eng. Res. **16**(1), 1–9 (2011).
Kim, K. Y., and Marshall, W. R., Jr., "Drop-size distributions from pneumatic atomizers," AIChE J. **17**(3), 575–584 (1971).
Kim, S., Hwang, J. W., and Lee, C. S., "Experiments and modeling on droplet motion and atomization of diesel and bio-diesel fuels in a cross-flowed air stream," Int. J. Heat Fluid Flow **31**(4), 667–679 (2010).
Kokolj, U., Škerget, L., and Ravnik, J., "A numerical model of the shortbread baking process in a forced convection oven," Appl. Therm. Eng. **111**, 1304–1311 (2017).
Koronis, G., Silva, A., and Fontul, M., "Green composites: A review of adequate materials for automotive applications," Composites, Part B **44**(1), 120–127 (2013).
Kuhnhenn, M., Luh, M. F., Joensen, T. V., Reck, M., Roisman, I. V., and Tropea, C., "Modelling of the breakup process of viscous fluids by a high-speed rotary atomizer," Exp. Fluids **59**, 117 (2018).
Kumar, R., and Lakshmi Prasod, K. S., "Studies on pneumatic atomization," Ind. Eng. Chem. Proc. Des. Dev. **10**(3), 357–365 (1971).
Kumar, V., and Sutherland, J. W., "Sustainability of the automotive recycling infrastructure: Review of current research and identification of future challenges," Int. J. Surf. Min. **1**(1), 145–167 (2008).
Kwok, K. C., "A fundamental study of air spray painting," Ph.D. thesis (University of Minnesota, 1991).
Learner, T., "A review of synthetic binding media in twentieth-century paints," Conservator **24**(1), 96–103 (2000).
Lee, I., Kim, D., and Koo, J., "Liquid jet breakup structure and transfer efficiency of a two-stage air-blast injector," Atomization Sprays **22**(7), 561 (2012).
Lefebvre, A. H., *Atomization and Sprays* (Hemisphere Publishing Corporation, New York, 1989).
Lefebvre, A. H., "Energy considerations in twin-fluid atomization," ASME J. Eng. Gas Turbines Power **114**(1), 89–96 (1992).
Lefebvre, A. H., and McDonell, V. G., *Atomization and Sprays* (CRC Press, 2017).
Li, J., Uttarwar, R. G., and Huang, Y., "CFD-based modeling and design for energy-efficient VOC emission reduction in surface coating systems," Clean Technol. Environ. Policy **15**(6), 1023–1032 (2013).
Li, W., Qian, L., Song, S., and Zhong, X., "Numerical study on the influence of shaping air holes on atomization performance in pneumatic atomizers," Coatings **9**(7), 410 (2019).
Liu, J., Yu, Q., and Guo, Q., "Experimental investigation of liquid disintegration by rotary cups," Chem. Eng. Sci. **73**, 44–50 (2012).

Liu, J. X., Yu, Q. B., and Qin, Q., "Numerical study on film disintegration by centrifugal atomisation using rotating cup," Powder Metall. **56**(4), 288–294 (2013).
Liu, L. S., "Experimental and theoretical investigation on the characteristics and two-phase spray flow field of effervescent atomizers," Ph.D. thesis (Tianjing University, 2001).
Liu, Y., Lai, M. C., Im, K. S., Sankagiri, N., Loch, T., and Nivi, H., "An experimental investigation of spray transfer processes in an electrostatic rotating bell applicator," J. Mater. Manufac. **107**, 1235–1243 (1998).
Liu, Y., Sparer, J., Woskie, S. R., Cullen, M. R., Chung, J. S., Holm, C. T., and Redlich, C. A., "Qualitative assessment of isocyanate skin exposure in auto body shops: A pilot study," Am. J. Ind. Med. **37**(3), 265–274 (2000).
Loop, F. M., "Cathodic automotive electrodeposition (paint)," Report No. SAE 780189, 1978.
Love, J. C., Smith, G. F., Pharaoh, M., and Coates, R., "Orange peel: Who cares?," Proc. Inst. Mech. Eng., Part D **215**(12), 1241–1244 (2001).
Luangkularb, S., Prombanpong, S., and Tangwarodomnukun, V., "Material consumption and dry film thickness in spray coating process," Procedia CIRP **17**, 789–794 (2014).
Mark, A., Andersson, B., Tafuri, S., Engstrom, K., Sorod, H., Edelvik, F., and Carlson, J. S., "Simulation of electrostatic rotary bell spray painting in automotive paint shops," Atomization Sprays **23**(1), 25 (2013).
Martin, D. E., and Latheef, M. A., "Aerial electrostatic spray deposition and canopy penetration in cotton," J. Electrost. **90**, 38–44 (2017).
Mayyas, A., Qattawi, A., Omar, M., and Shan, D., "Design for sustainability in automotive industry: A comprehensive review," Renewable Sustainable Energy Rev. **16**(4), 1845–1862 (2012).
McMinn, B. W., Newman, C. R., McCrillis, R. C., and Kosusko, M., "VOC prevention options for surface coating," in *Proceedings of the World Clean Air Congress* (U.S. Environmental Protection Agency, 1993), Vol. 1, p. IU-6B.
Mehdipour, R., Ashrafizadeh, A., Daun, K. J., and Aghanajafi, C., "Dynamic optimization of a radiation paint cure oven using the nominal cure point criterion," Drying Technol. **28**(12), 1405–1415 (2010).
Michalos, G., Makris, S., Papakostas, N., Mourtzis, D., and Chryssolouris, G., "Automotive assembly technologies review: Challenges and outlook for a flexible and adaptive approach," CIRP J. Manuf. Sci. Technol. **2**(2), 81–91 (2010).
Misev, T. V., and Van der Linde, R., "Powder coatings technology: New developments at the turn of the century," Prog. Org. Coat. **34**(1–4), 160–168 (1998).
Mishra, M., Das, P. K., and Sarangi, S., "Dynamic behavior of three-fluid cross-flow heat exchangers," J. Heat Transfer **130**(1), 011801 (2008).
Mitchell, A. H., "Occupational Safety and Health Administration (OSHA) regulatory compliance," in *Preventing Occupational Exposures to Infectious Disease in Health Care* (Springer, Cham, 2020), pp. 51–66.
Moore, J. R., "Automotive paint application," in *Protective Coatings* (Springer, 2017), pp. 465–496.
Morikita, H., and Taylor, A. M., "Application of shadow Doppler velocimetry to paint spray: Potential and limitations in sizing optically inhomogeneous droplets," Meas. Sci. Technol. **9**(2), 221 (1998).
Movahednejad, E., Ommi, F., and Hosseinalipour, S. M., "Prediction of droplet size and velocity distribution in droplet formation region of liquid spray," Entropy **12**(6), 1484–1498 (2010).
Nazif, H. R., "Improving the thermal efficiency of a car wax oven using CFD simulation and measurement," Int. J. Modell. Simul. **39**(2), 125–134 (2019).
Niamsuwan, S., Kittisupakorn, P., and Suwatthikul, A., "Enhancement of energy efficiency in a paint curing oven via CFD approach: Case study in an air-conditioning plant," Appl. Energy **156**, 465–477 (2015).
Nichols, M., and Tardiff, J., "Automotive coatings," in *Active Protective Coatings* (Springer, Dordrecht, 2016), pp. 373–384.
Noh, S. M., Lee, J. W., Nam, J. H., Byun, K. H., Park, J. M., and Jung, H. W., "Dual-curing behavior and scratch characteristics of hydroxyl functionalized urethane methacrylate oligomer for automotive clearcoats," Prog. Org. Coat. **74**(1), 257–269 (2012).
Nolte, H. J., Fischer, A., Marquardt, P., Berkowitsch, J., Schneider, J., and Duerr Systems, GMBH, "Electrode assembly for an electrostatic atomizer," U.S. patent 10,464,084 (27 February 2019).
Nukiyama, S., and Tanasawa, Y., "An experiment on the atomization of liquid: 4th report—The effect of the properties of liquid on the size of drops," Jpn. Soc. Mech. Eng. Trans. **5**, 136–143 (1939).
Ochowiak, M., Matuszak, M., Włodarczak, S., Krupińska, A., Markowska, M., Gościniak, A., and Szulc, T., "The concept design and study of twin-fluid effervescent atomizer with air stone aerator," Chem. Eng. Process.: Process Intensif. **124**, 24–28 (2018).
Oh, S. C., and Hildreth, A. J., *Analytics for Smart Energy Management* (Springer International Publishing, 2016).
Okazaki, M., Shioda, K., Masuda, K., and Toei, R., "Drying mechanism of coated film of polymer solution," J. Chem. Eng. Jpn. **7**(2), 99–105 (1974).
Okuda, H., and Kelly, A. J., "Electrostatic atomization—Experiment, theory and industrial applications," Phys. Plasmas **3**(5), 2191–2196 (1996).
O'Rourke, P. J., and Amsden, A. A., "A spray/wall interaction submodel for the KIVA-3 wall film model," SAE Technical Paper No. 2000-01-0271, 2000.
Orsato, R. J., and Wells, P., "U-turn: The rise and demise of the automobile industry," J. Cleaner Prod. **15**(11–12), 994–1006 (2007).
Osman, H., Adamiak, K., Castle, G. S., Fan, H. T. C., and Simmer, J., "Comparison between the numerical and experimental deposition patterns for an electrostatic rotary bell sprayer," in *ASME 2015 International Mechanical Engineering Congress and Exposition* (ASME, 2015a).
Osman, H., Ghazian, O., Adamiak, K., Castle, G. P., Fan, H. T., and Simmer, J., "Charging level of a ligament-droplet system atomized in a uniform electric field," IEEE Trans. Ind. Appl. **52**(2), 1814–1822 (2015b).
Oswald, W., Gödeke, L., Ehrhard, P., and Willenbacher, N., "Influence of the elongational flow resistance and pigmentation of coating fluids on high-speed rotary bell atomization," Atomization Sprays **29**(10), 913 (2019).
Panneton, B., "Geometry and performance of a rotary cup atomizer," Am. Soc. Agric. Eng. **18**, 435–441 (2002).
Patel, M. K., "Technological improvements in electrostatic spraying and its impact to agriculture during the last decade and future research perspectives—A review," Eng. Agric., Environ. Food **9**(1), 92–100 (2016).
Patel, M. K., Sahoo, H. K., Nayak, M. K., Kumar, A., Ghanshyam, C., and Kumar, A., "Electrostatic nozzle: New trends in agricultural pesticides spraying," SSRG Int. J. Electr. Electron. Eng. 6–11 (2015).
Pendar, M. R., and Páscoa, J. C., "Numerical modeling of electrostatic spray painting transfer processes in rotary bell cup for automotive painting," Int. J. Heat Fluid Flow **80**, 108499 (2019a).
Pendar, M. R., and Pascoa, J., "Numerical investigation of electrostatic spray painting transfer processes for vehicle coating," SAE Int. J. Adv. Curr. Pract. Mobility **2**, 747–754 (2019b).
Pendar, M. R., and Páscoa, J. C., "Atomization and spray characteristics around an ERBS using various operational models and conditions: Numerical investigation," Int. J. Heat Mass Transfer **161**, 120243 (2020a).
Pendar, M. R., and Páscoa, J. C., "Numerical modeling of the distribution of virus carrying saliva droplets during sneeze and cough," Phys. Fluids **32**(8), 083305 (2020b).
Pendar, M. R., and Páscoa, J. C., "Numerical analysis of charged droplets size distribution in the electrostatic coating process: Effect of different operational conditions," Phys. Fluids **33**(3), 033317 (2021).
Pendar, M. R., and Páscoa, J. C., "Electrostatic painting process: Impact of using connected high-voltage embodiments with rotary bell atomizers on droplets transport and deposition," Report No. FEDSMs2022-88033, 2022a.
Pendar, M. R., and Páscoa, J. C., "Numerical investigation of automotive paint oven for improving the thermal efficiency," Report No. FEDSMs2022-88044, 2022b.
Pendar, M. R., and Páscoa, J. C., "Numerical investigation of plasma actuator effects on flow control over a three-dimensional airfoil with a sinusoidal leading edge," J. Fluids Eng. **144**(8), 081208 (2022c).
Pendar, M. R., and Roohi, E., "Detailed investigation of cavitation and supercavitation around different geometries using various turbulence and mass transfer models," J. Phys.: Conf. Ser. **656**, 012070 (2015).
Pfaff, G., *Special Effect Pigments: Technical Basics and Applications* (Vincentz Network GmbH & Co. KG, 2008).
Pilch, M., and Erdman, C. A., "Use of breakup time data and velocity history data to predict the maximum size of stable fragments for acceleration-induced breakup of a liquid drop," Int. J. Multiphase Flow **13**(6), 741–757 (1987).
Plesniak, M. W., Sojka, P. E., and Singh, A. K., "Transfer efficiency for airless painting systems," J. Coat. Technol. Res. **1**(2), 137–145 (2004).

Poozesh, S., Akafuah, N., and Saito, K., "Effects of automotive paint spray technology on the paint transfer efficiency—A review," Proc. Inst. Mech. Eng., Part D **232**(2), 282–301 (2017).
Poth, U., *Automotive Coatings Formulation: Chemistry, Physics Und Practices* (Vincentz Network GmbH & Co. KG, 2008).
Prendi, L., Mills, M., Bastien, J., and Henshaw, P., "Thermosetting powder coatings: Finish appearance and durability at cure window corner points," Prog. Organic Coat. **78**, 411–418 (2015).
Prieto, J., "Painting the future green," Eur. Coat. J. **4**, 20–25 (2010).
Qian, L., Song, S., and Li, X., "A new spray approach to produce uniform ultrafine coatings," J. Nanotechnol. **2018**, 8978541.
Ranz, W. E., and Marshall, W. R., "Evaporation from drops," Chem. Eng. Prog. **48**(3), 141–146 (1952).
Rao, P., and Teeparthi, S., "A semi–computational method to predict body temperatures in an automotive paint bake oven," in *ASME International Mechanical Engineering Congress and Exposition* (ASME, 2011). Paper No. 54891, pp. 85–95.
Rao, P. P., "A heat exchanger analogy of automotive paint ovens," Appl. Therm. Eng. **61**(2), 381–392 (2013).
Rao, P. P., and Gopinath, A., "Energy savings in automotive paint ovens: A new concept of shroud on the carriers," J. Manuf. Sci. Eng. **135**(4), 045001 (2013).
Ray, R., Henshaw, P., and Biswas, N., "Characteristics of spray atomization for liquid droplets formed using a rotary bell atomizer," J. Fluids Eng. **141**(8), 081303 (2019).
Ray, R., Henshaw, P., Biswas, N., and Sak, C., "Effects of bell speed and flow rate on evaporation of water spray from a rotary bell atomizer," Coatings **5**(2), 186–194 (2015).
Reitz, R. D., and Diwakar, R., "Effect of drop breakup on fuel sprays," SAE Technical Paper No. 860469, 1986.
Reitz, R. D., and Diwakar, R., "Structure of high-pressure fuel sprays," SAE Technical Paper No. 870598, 1987.
Rivera, J. L., and Reyes-Carrillo, T., "A framework for environmental and energy analysis of the automobile painting process," Procedia CIRP **15**, 171–175 (2014).
Rivera, J. L., and Reyes-Carrillo, T., "A life cycle assessment framework for the evaluation of automobile paint shops," J. Cleaner Prod. **115**, 75–87 (2016).
Roelant, G. J., Kemppainen, A. J., and Shonnard, D. R., "Assessment of the automobile assembly paint process for energy, environmental, and economic improvement," J. Ind. Ecol. **8**(1-2), 173–191 (2008).
Roger, P. M. A., and Sames Machines Electrostatiques, "Rotating heads for electrostatic atomizing and spraying apparatus," U.S. patent 3,063,642 (13 November 1962).
Saha, A., Lee, J. D., Basu, S., and Kumar, R., "Breakup and coalescence characteristics of a hollow cone swirling spray," Phys. Fluids **24**(12), 124103 (2012).
Salazar, A. J., McDonough, J. M., and Saito, K., "Computational fluid dynamics simulation of the automotive spray painting process," Comput. Model. Simul. Eng. **2**(2), 131–144 (1997).
Salazar, A. J., Saito, K., Alloo, R. P., Tanaka, N., and University of Kentucky Research Foundation, Toyota Motor Engineering and Manufacturing North America, Inc., "Wet scrubber and paint spray booth including the wet scrubber," U.S. patent 6,093,250 (26 January 2000).
Salonitis, K., Pandremenos, J., Paralikas, J., and Chryssolouris, G., "Multifunctional materials used in automotive industry: A critical review," in *Engineering Against Fracture* (Springer, 2009), pp. 59–70.
SAMES Technology (2019), http://www.sames-kremlin.co (last accessed 15 September 2019).
Sankara Narayanan, T. S. N., "Surface pretreatment by phosphate conversion coatings—A review," Rev. Adv. Mater. Sci. **9**, 130–177 (2005).
Saure, R., and Gnielinski, V., "Moisture measurement by FT-IR-spectroscopy," Drying Technol. **12**(6), 1427–1444 (1994).
Saure, R., Wagner, G. R., and Schlünder, E. U., "Drying of solvent-borne polymeric coatings. II. Experimental results using FTIR spectroscopy," Surf. Coat. Technol. **99**(3), 257–265 (1998).
Schabel, W., Ludwig, I., and Kind, M., "Measurements of concentration profiles in polymeric solvent coatings by means of an inverse confocal micro Raman spectrometer—Initial results," Drying Technol. **22**(1–2), 285–294 (2004).
Schick, R. J., *Spray Technology Reference Guide: Understanding Drop Size* (Spray Analysis and Research Services, Eldersburg, Maryland, 2006).
Settles, G. S., "A flow visualization study of airless spray painting," in Proceedings of the 10th Annual Conference on Liquid Atomization and Spray Systems, ILASS-Americas (1997), Vol. 97, pp. 145–149.
Seubert, C. M., and Nichols, M. E., "Epoxy thiol photolatent base clearcoats: Curing and formulation," J. Coat. Technol. Res. **7**(5), 615–622 (2010).
SEAT al Sol (2018), available from https://www.trinasolar.com/en-uk/resources/success-stories/seat-al-sol (last accessed 20 December 2018).
Shen, B., Ye, Q., Guettler, N., Tiedje, O., and Domnick, J., "Primary breakup of a non-Newtonian liquid using a high-speed rotary bell atomizer for spray-painting processes," J. Coat. Technol. Res. **16**(6), 1581–1596 (2019).
Shen, B., Ye, Q., Tiedje, O., and Domnick, J., "Primary breakup of liquids using a high-speed rotary bell atomizer for spray painting processes," in *28th European Conference on Liquid Atomization and Spray Systems, ILASS Europe* (Editorial Universitat Politècnica de València, 2017), pp. 355–361.
Shilton, M. G., Miles, P., Robinson, G. W., and Robinson, J. V., "Spray gun with common control of fluid and air valve," U.S. patent 6,425,533 (30 July 2002).
Shrimpton, J. S., and Laoonual, Y., "Dynamics of electrically charged transient evaporating sprays," Int. J. Numer. Methods Eng. **67**(8), 1063–1081 (2006).
Shrivastava, D., and Ameel, T. A., "Three-fluid heat exchangers with three thermal communications. Part A: General mathematical model," Int. J. Heat Mass Transfer **47**(17–18), 3855–3865 (2004).
Spang, P., "Applying paints with nitrogen," Int. Surf. Technol. **7**(1), 15–15 (2014).
Stalling, D., and Hege, H.-C., "LIC on surfaces," in *Texture Synthesis with Line Integral Convolution* (1997), pp. 51–64.
Standeven, H., "The development of decorative gloss paints in Britain and the United States C. 1910–1960," J. Am. Inst. Conserv. **45**(1), 51–65 (2006).
Stefanitsis, D., Strotos, G., Nikolopoulos, N., Kakaras, E., and Gavaises, M., "Improved droplet breakup models for spray applications," Int. J. Heat Fluid Flow **76**, 274–286 (2019).
Stevenin, C., Bereaux, Y., Charmeau, J. Y., and Balcaen, J., "Shaping air flow characteristics of a high-speed rotary-bell sprayer for automotive painting processes," J. Fluids Eng. **137**(11), 111304 (2015).
Streitberger, H. J., and Dossel, K. F., *Automotive Paints and Coatings* (John Wiley & Sons, 2008).
Sukhodolya, A., Cherepnina, T., Kostyuk, I., and Klimenko, V., "Investigation of the paint curing mechanism," Transp. Res. Procedia **57**, 667–671 (2021).
Svejda, P., "Designing an automotive paint shop for optimal flexibility and efficiency," Met. Finish. **109**(109), 23–26 (2011).
Swoboda, W., Hihn, E., and Eisenmann, SE, "Device for separating paint overspray," U.S. patent 8,974,579 (10 March 2015).
Taikisha, G., "ELENE oven" (2018) available from https://geicotaikisha.com/solutions/pretrattamento-e-catoforesi/ (last accessed 1 November 2018).
Tan, Y. M., *The Impact of Transfer Efficiency on Worker Exposure during Spray Painting* (The University of North Carolina at Chapel Hill, 2001).
Tanner, F. X., "Liquid jet atomization and droplet breakup modeling of non-evaporating diesel fuel sprays," SAE Technical Paper No. 970050, 1997.
Talbert, R., *Paint Technology Handbook* (CRC Press, 2007).
Tanasawa, Y., Miyasaka, Y., and Umehara, M., "Effect of shape of rotating disks and cups on liquid atomization," in Proceedings of the 1st International Congress on Liquid Atomization and Spray Systems (1978), pp. 165–172.
Terebessy, T., and Sumitomo Chemical Co Ltd., "Electrostatic atomizer, and method for electrostatically atomizing by use of the same," U.S. patent 10,179,338 (15 January 2019).
Tilney, R., "Electrostatic coating processes," Br. J. Appl. Phys. **4**(S2), S51 (1953).
Toda, K., Salazar, A., and Saito, K., *Automotive Painting Technology: A Monozukuri-Hitozukuri Perspective* (Springer Science & Business Media, 2012).
Toljic, N., "Estimation of charge to mass ratio distribution in particles charged by conduction," Ph.D. thesis (University of Western Ontario, 2012).
Toljic, N., Adamiak, K., Castle, G. S. P., Kuo, H. H., and Fan, H. T., "Three-dimensional numerical studies on the effect of the particle charge to mass ratio distribution in the electrostatic coating process," J. Electrost. **69**(3), 189–194 (2011).
Toljic, N., Adamiak, K., Castle, G. S. P., Kuo, H. H., and Fan, H. T., "3D numerical model of the electrostatic coating process with moving objects using a moving mesh," J. Electrost. **70**, 499–504 (2012).

Toljic, N., Adamiak, K., Castle, G. S. P., Kuo, H. H., and Fan, H. T., "A full 3D numerical model of the industrial electrostatic coating process for moving targets," J. Electrost. **71**, 299–304 (2013).
Toljic, N., Castle, G. S. P., and Adamiak, K., "Charge to radius dependency for conductive particles charged by induction," J. Electrost. **68**, 57–63 (2010).
Tomalino, M., and Bianchini, G., "Heat-expandable microspheres for car protection production," Prog. Org. Coat. **32**(1–4), 17–24 (1997).
Tricou, C., and Knasiak, K., "Development of a high transfer efficiency painting technology using effervescent atomization," in *Annual Conference on Liquid Atomization and Spray Systems*, Irvine, California, 18 May 2005.
Trinh, Q. H., and Mok, Y. S., "Environmental plasma-catalysis for the energy-efficient treatment of volatile organic compounds," Korean J. Chem. Eng. **33**(3), 735–748 (2016).
U.S. Department of Energy, *Technology Roadmap for Energy Reduction in Automotive Manufacturing* (U.S. Department of Energy, 2008).
Vasudevan, M., "Numerical modelling of paint curing in convective ovens," Master's thesis (Chalmers University of Technology, 2018).
Vessot, S., Andrieu, J., Laurent, P., Galy, J., and Gérard, J. F., "Air convective drying and curing of polyurethane-based paints on sheet molding compound surfaces," J. Coat. Technol. **70**(882), 67–76 (1998).
Viti, V., Kulkarni, J., and Watve, A., "Computational fluid dynamics analysis of the electrostatic spray painting process with a rotating bell cup," Atomization Sprays **20**(1), 1 (2010).
Wang, S., Golden, J., Kocher, C. G., and Clean Earth Technologies LLC, "Method and apparatus for electrostatic spray," U.S. patent 7,150,412 (22 September 2006).
Wang, Y. A., Xie, X. P., and Lu, X. H., "Design of a double-nozzle air spray gun and numerical research in the interference spray flow field," Coatings **10**(5), 475 (2020).
Wilson, J., Grib, S., Darwish Ahmad, A., Renfro, M., Adams, S., and Salaimeh, A., "Study of near-cup droplet breakup of an automotive electrostatic rotary bell (ESRB) atomizer using high-speed shadowgraph imaging," Coatings **8**(5), 174 (2018).
Wonnemann, H., "Primer surfacer," in *Automotive Paints and Coatings* (Wiley, 2008), pp. 129–174.
Wu, Y. H., Srinivasan, K., Patterson, S., and Bot, E., "Transient thermal analysis for the automotive underhood and underbody components," in *Heat Transfer Summer Conference* (American Society of Mechanical Engineers, 2013), Vol. 55508, p. V004T14A028.
Wu, Y. H., Surapaneni, S., Srinivasan, K., and Stibich, P., "Automotive vehicle body temperature prediction in a paint oven," SAE Technical Paper No. 2014-01-0644, 2014.
Xiao, J., Li, J., Lou, H. H., and Huang, Y., "Cure-window-based proactive quality control in topcoat curing," Ind. Eng. Chem. Res. **45**(7), 2351–2360 (2006).
Xing, L., Glass, J. E., and Fernando, R. H., "Parameters influencing the spray behavior of water boron coatings," in Annual Meeting of the Federation of Societies for Coatings Technology, 1998.
Yang, Q., Ma, Y., Zhu, J., Chow, K., and Shi, K., "An update on electrostatic powder coating for pharmaceuticals," Particuology **31**, 1–7 (2017).
Yang, Q., Yuan, F., Ma, Y., Shi, K., Yang, G., and Zhu, J., "Electrostatic powder coated osmotic pump tablets: Influence factors of coating powder adhesion and film formation," Powder Technol. **360**, 444–451 (2020).
Yano, A., Oe, T., Takaishi, K., and Amagai, K., "Visualization of the paint film formation process during spray coating," Adv. Exp. Mech. **4**, 43–48 (2019).
Yasumura, K., Saito, Y., Shoji, M., Matsushita, Y., Aoki, H., Miura, T., Ogasawara, S., Daikoku, M., Shirota, M., and Inamura, T., "A numerical investigation of the factor decreasing transfer efficiency in a high-speed rotary bell-cup atomizer," Kagaku Kogaku Ronbunshu **37**, 251–260 (2011a).
Yasumura, K., Saito, Y., Shoji, M., Matsushita, Y., Aoki, H., Miura, T., Ogasawara, S., Daikoku, M., Shirota, M., and Inamura, T., "Development of quantitative evaluation method for droplet behavior with high speed rotary bell-cup atomizer," Kagaku Kogaku Ronbunshu **37**, 296–304 (2011b).
Ye, Q., and Domnick, J., "Analysis of droplet impingement of different atomizers used in spray coating processes," J. Coat. Technol. Res. **14**(2), 467–476 (2017).
Ye, Q., Domnick, J., and Khalifa, E., "Simulation of the spray coating process using a pneumatic atomizer," in ILASS-Europe, 9–11 September 2002.
Ye, Q., Domnick, J., and Scheibe, A., "Numerical simulation of spray painting in the automotive industry," in Proceedings of the 1st European Automotive CFD Conference, Bingen, Germany, 2003.
Ye, Q., Domnick, J., Scheibe, A., and Pulli, K., "Numerical simulation of electrostatic spray-painting processes in the automotive industry," in *High Performance Computing in Science and Engineering'04* (Springer, Berlin, Heidelberg, 2005), pp. 261–275.
Ye, Q., and Pulli, K., "Numerical and experimental investigation on the spray coating process using a pneumatic atomizer: Influences of operating conditions and target geometries," Coatings **7**(1), 13 (2017).
Ye, Q., Pulli, K., Scheibe, A., Domnick, J., and Gruseck, D., "Numerical simulation of turbulent heat transfer in industrial drying processes," in *Proceeding of the 4th EASC 2009, European Automotive Simulation Conference*, 2009.
Ye, Q., Shen, B., Tiedje, O., Bauernhansl, T., and Domnick, J., "Numerical and experimental study of spray coating using air-assisted high-pressure atomizers," Atomization Sprays **25**(8), 643 (2015).
Ye, Q., Shen, B., Tiedje, O., and Domnick, J., "Investigations of spray painting processes using an airless spray gun," J. Energy Power Eng. **7**, 74–81 (2013).
Ye, Q., Steigleder, T., Scheibe, A., and Domnick, J., "Numerical simulation of the electrostatic powder coating process with a corona spray gun," J. Electrost. **54**(2), 189–205 (2002).
Yu, G., "Simulation of automotive paint curing process in an oven," Met. Finish. **111**(2), 18–22 (2013).
Yu, H., Goldsworthy, L., Ghiji, M., Brandner, P. A., and Garaniya, V., "A parallel volume of fluid-Lagrangian parcel tracking coupling procedure for diesel spray modelling," Comput. Fluids **150**, 46–65 (2017).
Zahler, C., and Iglauer, O., "Solar process heat for sustainable automobile manufacturing," Energy Procedia **30**, 775–782 (2012).
Zelder, G., and Steinbeck-Behrens, C., "Simulation on car body painting processes," in 4th European Automotive Simulation Conference (2009), pp. 2–7.
Zuzio, D., Estivalezes, J.-L., and Dipierro, B., "An improved multiscale Eulerian–Lagrangian method for simulation of atomization process," Comput. Fluids **176**(4), 285–301 (2018).